Nonequilibrium dynamics of exactly solvable one-dimensional many-body Bose systems

Jukić, Dario

Doctoral thesis / Disertacija

2012

Degree Grantor / Ustanova koja je dodijelila akademski / stručni stupanj: **University of Zagreb, Faculty of Science / Sveučilište u Zagrebu, Prirodoslovno-matematički fakultet**

Permanent link / Trajna poveznica: https://urn.nsk.hr/urn:nbn:hr:217:183458

Rights / Prava: In copyright/Zaštićeno autorskim pravom.

Download date / Datum preuzimanja: **2025-04-01**

Dario Jukić

Nonequilibrium dynamics of exactly solvable one-dimensional many-body Bose systems

Dario Jukić

Neravnotežna dinamika egzaktno rješivih jednodimenzionalnih višečestičnih bozonskih sustava

University of Zagreb   Doctoral Thesis

Faculty of Science

Department of Physics

Nonequilibrium dynamics of exactly solvable one-dimensional many-body Bose systems

Dario Jukić

Faculty of Science, University of Zagreb

Nonequilibrium dynamics of interacting many-body systems is extremely interesting in the context of one-dimensional (1D) bosonic gases for many reasons: (i) these systems are experimentally realized with atoms trapped in 1D atomic waveguides, (ii) models which describe such systems, e.g. the Lieb-Liniger model, are exactly solvable in some non-equilibrium situations, and (iii) quantum effects are enhanced in systems of reduced dimensionality. Our aim is to describe dynamics of a many-body system by employing exact methods, which is of particular importance when the system approaches strongly correlated regime, when the usual mean-field treatment is not applicable. We have studied nonequilibrium dynamics within the framework of the Lieb-Liniger model, where interaction strength varies from weakly to strongly interacting regime, using an exact approach, originally introduced by Gaudin. Furthermore, in the strongly interacting limit of the Tonks-Girardeau gas we have studied the phenomenon of Anderson localization.

(111 pages, 119 references, original in English)

Supervisor:	Prof. Dr. sc. H. Buljan
Reviewers:	Prof. Dr. sc. D. Veža
	Prof. Dr. sc. H. Buljan
	Doc. Dr. sc. R. Pezer
	Prof. Dr. sc. M. Mileković
	Prof. Dr. rer. nat. T. Gasenzer
Thesis accepted:	2012.

Sveučilište u Zagrebu   Doktorska disertacija
Prirodoslovno-matematički fakultet
Fizički odsjek

Neravnotežna dinamika egzaktno rješivih jednodimenzionalnih višečestičnih bozonskih sustava

Dario Jukić

Prirodoslovno-matematički fakultet, Sveučilište u Zagrebu

Neravnotežna dinamika međudjelujućih višečestičnih sustava zanimljiva je u kontekstu jednodimenzionalnih bozonskih plinova iz više razloga: (i) ovi su sustavi eksperimentalno realizirani, (ii) modeli kojima opisujemo ovakve sustave, npr. Lieb-Liniger model, egzaktno su rješivi u nekim slučajevima i (iii) kvantni efekti pojačani su u sustavima reduciranih dimenzija. Naš je cilj opis neravnotežne dinamike korištenjem egzaktnih metoda što je od posebnog značaja kada se sustav približava jako koreliranom režimu. U okviru Lieb-Liniger modela, gdje jakost interakcije varira od slabo do jako interagirajućeg režima, koristimo metodu koja daje egzaktna vremenski ovisna višečestična rješenja, a izvorno ju je uveo Gaudin. Također, u jako interagirajućem limesu Tonks-Girardeau plina proučili smo pojavu Andersonove lokalizacije.

(111 stranica, 119 literaturnih navoda, jezik izvornika engleski)

Acknowledgements

The work in this thesis was made under the supervision of Prof. Dr. Hrvoje Buljan. I thank him for his constant guidance and great enthusiasm which he put into our projects. His ideas and vision were of immeasurable value. Patient comments helped me throughout the whole research process. I am also grateful to him for making my stay in the group very enjoyable.

There are several more colleagues I wish to mention here. I thank Doc. Dr. Robert Pezer, Prof. Dr. Thomas Gasenzer, Juraj Radić, Karlo Lelas, Bruno Klajn and Stipe Galić for the effort and the time they invested in preparing our papers.

At the end, a personal note. For all their support and care, I thank my family and Marija.

The work presented in this thesis has been published in several articles. The reference for each chapter is given below.

Chapter 3:
D. Jukić, R. Pezer, T. Gasenzer, and H. Buljan,
Free expansion of a Lieb-Liniger gas: Asymptotic form of the wave functions,
Phys. Rev. A **78**, 053602 (2008).

D. Jukić, B. Klajn, and H. Buljan,
Momentum distribution of a freely expanding Lieb-Liniger gas,
Phys. Rev. A **79**, 033612 (2009).

Chapter 4:
D. Jukić and H. Buljan,
Reflection of a Lieb-Liniger wave packet from the hard-wall potential,
New J. Phys. **12**, 055010 (2010).

Chapter 5:
D. Jukić, S. Galić, R. Pezer, and H. Buljan,
Lieb-Liniger gas in a constant-force potential,
Phys. Rev. A **82**, 023606 (2010).

Chapter 6:
J. Radić, V. Bačić, D. Jukić, M. Segev, and H. Buljan,
Anderson localization of a Tonks-Girardeau gas in potentials with controlled disorder,
Phys. Rev. A **81**, 063639 (2010).

Contents

Chapter 1

Introduction

Recent years have witnessed a growing interest in studies of theoretical 1D models, first introduced by Lieb and Liniger [1] and Girardeau [2]. This has been largely inspired by experimental progress in realizing these models with ultracold atomic gases [3, 4, 5, 6, 7, 8, 9]. In experiments, an effectively one-dimensional system is achieved in elongated and transversely tight atomic wave guides, loaded with ultracold atoms, where transverse excitations are strongly suppressed [3, 4, 5, 6, 7, 8, 9]. These atomic gases are well described by the Lieb-Liniger model [1] - a system of identical Bose particles in 1D which interact via δ-function interactions of strength c. In the limit of infinite interaction strength ($c \to \infty$), the Bose particles are described by the Tonks-Girardeau model [2], describing an "impenetrable" Bose gas. This regime occurs when effective interactions are strong, whereas temperatures and linear densities are low [10, 11, 12].

1.1 Experimental realization

Let us briefly review the experimental techniques which enable realization of low-dimensional models in ultracold atomic systems. This field advanced thanks to the development of methods for cooling and trapping of atomic vapors. These techniques are based on manipulating neutral atoms with various optical (laser) and magnetic fields [13]. The gases were cooled even down to the temperatures in the nano-kelvin regime. A great breakthrough came in 1995 with the achievement of Bose-Einstein condensates (BECs) in three-

dimensional (3D) systems of ultracold atoms [14, 15, 16].

By manipulating the geometry of atomic traps, one- and two-dimensional (2D) systems became available. The standard way to change the dimensionality is by means of creating an optical potential [4, 17, 18, 19]. Consider the potential created by superimposing two counter-propagating laser beams. Their interference produces a standing wave pattern of light intensity with periodicity determined by the wavelength of light. When placed in an electric field, neutral atoms acquire dipole moments which are determined by their polarizability. Due to the coupling of this dipole and the electric field, the dipole force on atoms arises. In a simple two level model, it can be shown that the force on atoms is attractive (atoms are pushed towards intensity maxima) if the laser frequency is red-detuned, that is, laser frequency is smaller then the resonant frequency of a two-level transition. The dipole force is repulsive in the case of a blue-detuned laser, that is, when the laser frequency is above the resonant frequency of a two-level transition. Because of that, the interference between two counter-propagating beams will create a periodic potential for atoms.

If the amplitude of this potential is large enough, so that the hopping of atoms from one minumum of the periodic potential to the neighbouring one is unlikely, the three-dimensional gas of atoms turns into a system of many decoupled two-dimensional sheets of gas. By superimposing two orthogonal standing waves, a large number of one-dimensional tubes can be formed [see Fig. 1.1 (a)]. Evenmore, three orthogonal standing waves produce a three-dimensional optical lattice for atoms [see Fig. 1.1 (b)]. In the explanation above, we have not mentioned the dissipative term in the light force which is a consequence of spontaneous emission: in experiments, it can be diminished by using detunings which are much greater then the spontaneous emision rates [20]. Also, due to the Gaussian profile of the light beam an additional (small) harmonic confinement is present.

Another efficient technique for trapping atoms utilizes so-called atom chip traps [21, 22]. Here, atoms are trapped close to the surface (chip) by magnetic fields. Microfabricated structure of the chip consists of tiny wires carrying electric currents which produce a magnetic field. An external uniform field perpendicular to the wire axis is superimposed in order to create local minimum of the total magnetic field along the line parallel to the wire. Because
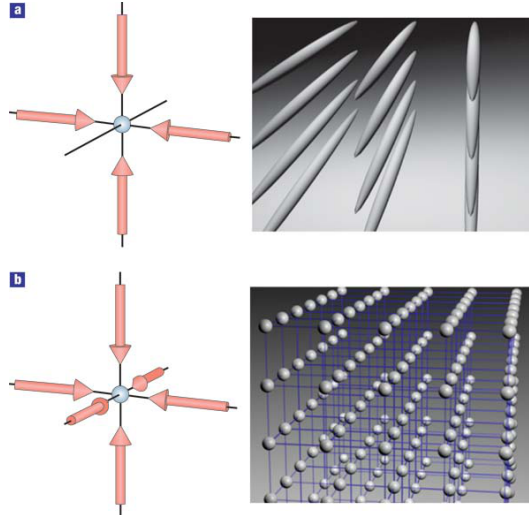
Figure 1.1: Optical lattice potentials are created by superimposing orthogonal standing waves. (a) The atoms are confined to an array of tightly confining 1D potential tubes if a 2D optical lattice is formed. (b) For a three-dimensional (3D) lattice, the potential can be approximated by a 3D simple cubic array of tightly confining harmonic oscillator potentials at each lattice site. Reprinted by permission from Macmillan Publishers Ltd: Nature Phys. [19], ©2005.

of the coupling between atoms with spin and the magnetic field, the field minimum traps atoms in states with spin antiparallel to the magnetic field (low-field seeking spin states). An experimental difficulty here is to prevent nonadiabatic spin-flipping in the region of zero magnetic field and effective loss of the particles. This is done by adding another magnetic field (parallel to the wire) [21, 22].

The essential feature which makes ultracold atomic systems highly interesting in physics nowadays is the possibility to control various parameters of the system. Besides trapping (optical and magnetic) potentials discussed above, interatomic interactions can be tuned as well. In general, collisions in ultracold regime take place in the channel with lowest angular momentum. Therefore, the s-wave scattering dominates for bosons. The interatomic potential is described by a pseudopotential with delta function (in 3D, this delta potential has to be regularized [20]). The strength of the interaction is determined by the s-wave scattering length a. Again, in 3D, the potential is repulsive (attractive) for $a > 0 (a < 0)$. It is important to point out that the scattering length

can be tuned by applying an external magnetic field. This effect is known as the Feshbach resonance [23, 13]. Two particles undergo collision in the allowed (open) channel, determined by quantum numbers of the initial and final state. If the coupling between open and closed (forbidden) channel is present, the scattering process in the open channel can change. This happens if the energy of the scattering particles in the open channel is close to some bound state in the closed channel. The scattering length is modified depending on energy distance from the bound state. As channels usually describe different spin states, their relative position in energy can be manipulated by the magnetic field. In summary, the external field can drive the system through various interaction regimes.

In addition to this, in one dimension effective interaction depends also on the strength of transversal confinement which holds atoms in effectively 1D geometry (see Ref. [10] and the discussion in Section 1.2). Therefore, by merely changing geometry of the system, one can modify the strength (and the sign) of the interaction. In literature, this is known as the confinement induced resonance [10].

1.2 Theoretical models

The Lieb-Liniger model describes N identical bosons in one spatial dimension, which interact via a δ-function potential of strength c. The model can be represented in terms of the Schrödinger equation:

$$i\frac{\partial \psi}{\partial t} = -\sum_{i=1}^{N} \frac{\partial^2 \psi}{\partial x_i^2} + \sum_{1 \le i < j \le N} 2c\,\delta(x_i - x_j)\psi + \sum_{i=1}^{N} V(x_i)\psi(x_1, \ldots, x_N, t). \quad (1.1)$$

The spatial and temporal coordinates (x and t, respectively), as well as the external one-body potential $V(x)$ will be dimensionless in this thesis. Their connection to physical units is as follows: $x = X/X_0$, $t = T/T_0$, and $V(x) = U(X)/E_0$, where X, T and $U(X)$ are space, time, and energy variables in physical units. Given the mass of the atoms m, the choice of an arbitrary length scale X_0 sets the time scale $T_0 = 2mX_0^2/\hbar$, and energy scale $E_0 = \hbar^2/(2mX_0^2)$. Suppose that the transverse confinement of the atomic waveguide is described by a harmonic oscillator with frequency $\omega_\perp$. The interaction parameter c is

proportional to the effective 1D coupling strength g_{1D} [10], $2c = g_{1D}/(X_0 E_0) = g_{1D} \, 2mX_0/\hbar^2$, which is related to the 1D scattering length a_{1D} via $g_{1D} = -2\hbar^2/ma_{1D}$; the 1D scattering length $a_{1D} = -(l_\perp^2/a)(1 - Ca/\sqrt{2}l_\perp)$ depends on three-dimensional scattering length a and the transverse oscillator width $l_\perp = \sqrt{\hbar/m\omega_\perp}$ (the constant $C = 1.4603\ldots$) [10].

We illustrate connection to physical units with the following example. If we consider a system of ^{87}Rb atoms, then the ratio $X_0^2/T_0 \approx 3.65 \times 10^{-10}\text{m}^2/\text{s}$ is fixed. By choosing for example $X_0 \approx 1.35\,\mu\text{m}$ for the spatial scale, the temporal scale is set to $T_0 = 5$ ms. The 3D scattering length is $a = 5.3$ nm. The interaction parameter c can be varied by changing the width of transversal confinement $l_\perp$; for example, the values of $c = 0.25$ up to $c = 10$, can be obtained by varying $l_\perp$ from 242 nm down to $l_\perp \approx 41$ nm, respectively. Of course, for a different choice of temporal and spatial scales, transversal confinements $l_\perp$ would have different values. Also, for the choice of scales in our example, the longitudinal energy E_0 is less then the transverse energy spacing $\hbar\omega_\perp$, a condition needed for freezing the radial degrees of freedom.

Experiments are even capable of exploring nonequilibrium quantum dynamics of these 1D many-body systems [7, 8], which may occur after some sudden change in the system's parameters. These ultracold atomic assemblies are well isolated from the environment, that is, their quantum coherence stays preserved for long times [8]. Therefore, they may serve as a playground to investigate relaxation of isolated quantum many-body systems, which is one of the most interesting questions in theoretical physics (e.g. see Refs. [24, 25, 26, 27, 28, 29, 30, 31] and references therein). Subsequent relaxation of 1D gases via collisions is greatly determined by the reduced dimensionality and the integrability of the underlying models. We are motivated to study the time-dependent Lieb-Liniger model because (i) today's experiments can explore fundamental physical questions in these systems [7, 8], and (ii) one can construct exact solutions of some relevant problems for all interaction strengths (from the mean field regime up to the strongly correlated regime) [32, 33, 34, 35].

The eigenstates of the Lieb-Liniger model (without an external potential present), which were constructed by employing the Bethe ansatz [1], are determined by a set of quasimomenta; when periodic [1] boundary conditions are imposed, the quasimomenta must obey a set of transcendental Bethe equations

[1]. The Lieb-Liniger eigenstates in the presence of the hard-wall (i.e., on the semi-infinite line) can be constructed via superposition of free space eigenstates [36]; again, if the quasimomenta should obey a particular set of transcendental equations [36], this superposition yields eigenstates in an infinitely deep box [36]. Recent years have witnessed an increasing interest in exact solutions of these models (e.g., see [37, 38, 39, 40, 41, 42, 43] and references therein), most of which are focused on the properties of the ground and excited eigenstates (see also Refs. [44, 45]). Unfortunately, the Lieb-Liniger model does not reveal exact solutions in the presence of some smooth external trapping potential $V(x)$ (the only exception to the best of our knowledge is the linear potential).

In the Tonks-Girardeau limit $c \to \infty$, the methods for finding eigenstates [2], time-dependent solutions [46], as well as observables (e.g., see Ref. [47] for the system of hard-core bosons on the lattice and [48] for the continuous Tonks-Girardeau model) are much simpler due to the Fermi-Bose mapping, which in a simple fashion maps a fermionic wave function describing spinless noninteracting fermions onto a Tonks-Girardeau wave function [2, 46]. It is important to emphasize that these methods are valid for any external potential. Perhaps the simplicity of the methods and phenomenological relevance of the model [7] have lead to increasing interest in quantum many-body dynamics of Tonks-Girardeau gases. Some of these studies include dynamics during free expansion [47, 49, 50, 51], dynamics of dark soliton-like states [46], and reflections from a periodic potential [48].

In the case of finite interaction strength c, it is far more difficult to calculate exact many-body wave functions and/or observables describing dynamics of time-dependent Lieb-Liniger wave packets. Without attempting to provide a review, let us mention a few approaches utilized to study nonequilibrium dynamics of 1D interacting Bose gases. The hydrodynamic formalism [12] (the local density approximation) can be formulated in terms of the Nonlinear Schrödinger like equation with variable nonlinearity [52]; this approach reduces to the Gross-Pitaevskii theory in the weakly interacting limit [12, 52]. More sophisticated numerical approaches include the time-evolving block decimation algorithm [53], which has recently been utilized to study relaxation following a quench in a 1D Bose gas [54], the twoparticle irreducible (2PI) effective action approach [55, 56], the multiconfigurational time-dependent Hartree method for bosons (MCTDHB) [57] (the MCTDHB method is numerically exact when

sufficiently many time-dependent orbitals are taken into account), and the multiconfigurational time-dependent Hartree method (e.g., see Ref. [58] and references therein). Reference [35] provides a discussion of several methods which can be used to describe nonequilibrium dynamics of Lieb-Liniger gases with greater focus on the form-factor approach [35], which has been recently utilized to calculate equilibrium correlation functions of a 1D Bose gas (see [59] and references therein). A broader review discussing many-body physics with ultracold gases can be found in Ref. [20]. The physics of 1D interacting Bose gases is reviewed in Ref. [60]. We also mention a recent review on quantum transients [61].

1.3 Objectives and results

The objective of this research is the study of nonequilibrium dynamics of many-body quantum systems by using exact methods. In this context we have studied the Lieb-Liniger model [1] which describes one-dimensional Bose particles with point-like interactions. Whether or not is it possible to use an exact approach to study out-of-equilibrium dynamics in the Lieb-Liniger model depends on the external potential $V(x)$. The eigenstates of the Lieb-Liniger model have so far been found only for certain potentials $V(x)$, or should we say mainly in the absence of it. The eigenstates are known for homogeneous system (on an infinite line and with periodic boundary conditions [1]), on a semi-infinite line [36] and in an infinitely deep box [36].

Exact time-dependent solutions of the Lieb-Liniger model were not studied until recently [34]. One approach in attempting to find new exact time-dependent solutions is by using the Gaudin's Fermi-Bose mapping operator [32]. The method of Gaudin has been shown to be valid in the absence of any external potential (i.e., on an infinite line [32, 34]). There one can apply it to find both time-dependent and stationary Lieb-Liniger wave functions.

Gaudin's Fermi-Bose transformation has been used in Ref. [34] to study time evolution of the Lieb-Liniger system on a particular family of time-dependent wave functions. We would like to emphasize that, to the best of our knowledge, apart from the aforementioned study this idea has not been utilized in the literature. In this thesis, we find that for some specific cases, exact time-

dependent solution of the Lieb-Liniger model can be obtained by calculating an N-dimensional Fourier transform. Our analysis includes dynamics during free expansion (i.e. on an infinite line) which corresponds to the time-of-flight experiments. Next, we present reflection of the Lieb-Liniger wave packet from the the hard-wall potential, and finally evolution in the field of constant force. The analysis of these cases represents the main findings of this thesis.

The thesis is organized into chapters as follows. In Chapter 2 we review the Tonks-Girardeau and the Lieb-Liniger model. We describe Fermi-Bose mapping techniques by which these models can be solved. In Chapter 3 we study free expansion of the Lieb-Liniger gas from a localized initial many-body wave packet. We explore both the transient and the asymptotic regime. The time-dependent wave function for this problem can be calculated via an N-dimensional Fourier transform, where N is the number of particles in a wave packet. Interestingly, in Chapter 4 we show that this approach can also be utilized for Lieb-Liniger gas reflecting from the hard-wall potential. We will use Gaudin's operator for construction of the Lieb-Liniger eigenstates in linear external potential in Chapter 5; the time dynamics is in this case also found by computing an N-dimensional Fourier transform.

In Chapter 6 we use the Tonks-Girardeau model to study the phenomenon of Anderson localization [62]. In the limit of the Tonks-Girardeau gas, $c \to \infty$, the Fermi-Bose mapping (which was discovered in 1960 [2]) can be utilized for any external potential [2] and for time-dependent problems [46]. Motivation for investigation of Anderson localization in atomic gases is prompted by recent experiments in Bose-Einstein condensates [63, 64]. Starting from an initially trapped gas with controlled disorder, we explore correlations in the expanding system when the confining potential is suddenly turned off but disorder is present at all times. Finally, in Chapter 7 we summarize.

Chapter 2

Fermi-Bose mapping techniques for Tonks-Girardeau and Lieb-Liniger gases

Exact solutions for 1D Bose gases can be constructed by using the Fermi-Bose mapping techniques [2, 32, 46, 65]. In 1960 Girardeau discovered that the wave function of a spinless noninteracting 1D Fermi gas can be symmetrized such that it describes an impenetrable-core 1D Bose gas [2]. This mapping is valid for arbitrary external potentials [2], for time-dependent problems [46], and in the context of statistical mechanics [65]. In fact, fermion-boson duality in 1D exists for arbitrary interaction strengths [66, 67]. Furthermore, a time-dependent antisymmetric wave function describing a 1D system of noninteracting fermions can be transformed, by using a differential Fermi-Bose mapping operator, to an exact time-dependent solution for a Lieb-Liniger gas, as outlined by Gaudin [32]. This method is applicable in the absence of external potentials and other boundary conditions. Therefore, it is particularly useful to study free expansion of Lieb-Liniger gases from an initially localized state. In the following two sections we present the techniques utilized to exactly solve (time-dependent) Tonks-Girardeau and Lieb-Liniger models.

2.1 Tonks-Girardeau model

In this section we review the Tonks-Girardeau model which describes "impenetrable - core" 1D Bose gas [2, 46]. We study a system of N identical Bose particles in 1D geometry, which experience an external potential $V(x)$. The bosons interact with impenetrable pointlike interactions [2], which means that the wave function describing the bosons vanishes whenever the two particles are in contact, that is,

$$\psi_B(x_1, x_2, \ldots, x_N, t) = 0 \text{ if } x_i = x_j, 1 \leq i < j \leq N. \quad (2.1)$$

In addition to this constraint, the wave function ψ_B must obey the Schrödinger equation

$$i\frac{\partial \psi_B}{\partial t} = \sum_{j=1}^{N} \left[-\frac{\partial^2}{\partial x_j^2} + V(x_j) \right] \psi_B. \quad (2.2)$$

The solution of this system may be written in compact form via the famous Fermi-Bose mapping, which relates the Tonks-Girardeau bosonic wave function ψ_B to an antisymmetric many-body wave function ψ_F describing a system of noninteracting spinless fermions in 1D [2, 46]. Let $\psi_F(x_1, x_2, \ldots, x_N, t)$ be a solution of Eq. (2.2) which is antisymmetric with respect to exchange of any two coordinates x_i and x_j. Let us also define an antisymmetric unit function

$$A(x_1, x_2, \ldots, x_N) = \Pi_{1 \leq i < j \leq N} \text{sgn}(x_i - x_j), \quad (2.3)$$

where $\text{sgn}(x)$ is the sign function, $+1(-1)$ for $x > 0$ $(x < 0)$. Then, the wave function

$$\psi_B(x_1, x_2, \ldots, x_N, t) = A(x_1, x_2, \ldots, x_N)\psi_F(x_1, x_2, \ldots, x_N, t) \quad (2.4)$$

is a solution of Eq. (2.2), it posseses Bose symmetry under exchange of x_i and x_j, and satisfies hard-core constraint (2.1) [2, 46]. Thus, it is a solution of the Tonks-Girardeau model in arbitrary external potential $V(x)$.

To verify this, an N-dimensional configuration space is divided into $N!$ disjoint sectors by hyperplanes $x_i = x_j$. For example, the fundamental permutation sector is defined as $R_1 : x_1 < x_2 < \ldots < x_N$. In each permutation sector the function A has constant value, which is either 1 or -1. Therefore,

ψ_B is a solution of Eq. (2.2) in every sector because ψ_F obeys it. In addition, the boundary condition (2.1) is met because of the Pauli principle imposed on ψ_F. The Bose symmetry of ψ_B is ensured by an antisymmetric function A: both A and ψ_F are antisymmetric in particle coordinates, and as a result ψ_B is symmetric.

In many physically relevant situations, the fermionic wave function ψ_F can be written in a form of the Slater determinant,

$$\psi_F(x_1, \ldots, x_N, t) = \frac{1}{\sqrt{N!}} \det_{m,j=1}^{N} [\psi_m(x_j, t)], \qquad (2.5)$$

where $\psi_m(x, t)$ denote N orthonormal single-particle wave functions obeying a set of uncoupled single-particle Schrödinger equations

$$i\frac{\partial \psi_m}{\partial t} = \left[-\frac{\partial^2}{\partial x^2} + V(x) \right] \psi_m(x, t), \ m = 1, \ldots, N. \qquad (2.6)$$

Therefore, due to the Fermi-Bose mapping the many-body problem of strongly interacting bosons in one dimension is reduced to solving the single-particle equations (2.6). We note here that generalization of the Fermi-Bose mapping to higher dimensions is restricted by the fact that we cannot construct generalization of the function A in more then one dimension [2]: we cannot divide the configuration space into disjoint sectors by hyperplanes $x_i = x_j$.

The Fermi-Bose mapping (2.4) described here also applies to the eigenvalue equation:

$$\sum_{j=1}^{N} \left[-\frac{\partial^2}{\partial x_j^2} + V(x_j) \right] \psi_B = E\psi_B, \qquad (2.7)$$

where E is energy of an eigenstate. That is, all eigenstates of noninteracting spinless fermions in 1D are mapped onto the Tonks-Girardeau model by (2.4). The spectra of energies of two systems are identical.

So far we have outlined the construction of the many-body wave function describing the Tonks-Girardeau gas in an external potential $V(x)$, which is valid both in the static [2] and the time-dependent case [46]. For the discrete system of impenetrable-core bosons (i.e. on the lattice), the Jordan-Wigner transformation can be applied to find exact solutions [47, 68]. Equivalence of this transformation and the Fermi-Bose mapping is discussed in Ref. [69].

The calculation of observables and correlation functions for interacting many-body state is, in general, very difficult task. However, from the Fermi-Bose mapping it is clear that the density correlations of Tonks-Girardeau gas will be the same as in the case of noninteracting fermions. The conclusion follows because for density correlations the product of sign factors in (2.4) equals to one. This statement is not valid for one-particle correlations, where sign factors are present and the calculation is not trivial. Yet, an efficient and exact algorithm to compute these correlations was presented in Ref. [48].

Given the wave function ψ_B, we can straightforwardly calculate all one-body observables furnished by the reduced single-particle density matrix (RSPDM),

$$
\begin{aligned}
\rho_B(x, y, t) &= N \int dx_2 \ldots dx_N \, \psi_B(x, x_2, \ldots, x_N, t)^* \\
&\times \psi_B(y, x_2, \ldots, x_N, t).
\end{aligned}
\tag{2.8}
$$

If the RSPDM is expressed in terms of the single-particle wave functions ψ_m as

$$
\rho_B(x, y, t) = \sum_{i,j=1}^{N} \psi_i^*(x, t) A_{ij}(x, y, t) \psi_j(y, t),
\tag{2.9}
$$

it can be shown that the $N \times N$ matrix $\mathbf{A}(x, y, t) = \{A_{ij}(x, y, t)\}$ has the form

$$
\mathbf{A}(x, y, t) = (\mathbf{P}^{-1})^T \det \mathbf{P},
\tag{2.10}
$$

where the entries of the matrix $\mathbf{P}$ are $P_{ij}(x, y, t) = \delta_{ij} - 2 \int_x^y dx' \psi_i^*(x', t) \psi_j(x', t)$ ($x < y$ without loss of generality) [48].

2.2 Lieb-Liniger model

A system of N identical δ-interacting bosons in one spatial dimension and in external potential $V(x)$ is described by the many-body Schrödinger equation [1]

$$
i \frac{\partial \psi_B}{\partial t} = -\sum_{i=1}^{N} \frac{\partial^2 \psi_B}{\partial x_i^2} + \sum_{1 \le i < j \le N} 2c \, \delta(x_i - x_j) \psi_B + \sum_{i=1}^{N} V(x_i) \psi(x_1, \ldots, x_N, t).
\tag{2.11}
$$

Here, $\psi_B(x_1, \ldots, x_N, t)$ is the time-dependent wave function, and c is the strength of the interaction. This model was first introduced by Lieb and Liniger in 1963 [1]. Due to the finite strength of the coupling c the set of exact solutions, both time-dependent and stationary, is limited only to some specific external potentials $V(x)$. The stationary states were found via Bethe ansatz when there is no external potential present [1]. As mentioned in the Introduction, they are determined by a set of quasimomenta. If we impose periodic boundary conditions, the quasimomenta satisfy transcendental Bethe equations [1]. Also, the Lieb-Liniger model on a semi-infinite line (and in the hard-wall box) can be solved by superimposing free-space eigenstates [36].

In order to address the Lieb-Liniger model, let us divide an N-dimensional configuration space again into $N!$ different sectors separated by hyperplanes $x_i = x_j$. The Schödinger equation in each sector reduces to the one for non-interacting particles, that is, Eq. (2.2). Finite interactions between Bose particles can be expressed as a boundary condition at surfaces $x_i = x_j$. The condition for Lieb-Liniger gas relates the value of the wave function and its derivative at the boundary. At the borders of the fundamental permutation sector R_1 this can be expressed as [1]:

$$\left[1 - \frac{1}{c}\left(\frac{\partial}{\partial x_{j+1}} - \frac{\partial}{\partial x_j}\right)\right]_{x_{j+1}=x_j} \psi_B = 0. \tag{2.12}$$

In other words, the δ-interactions create a cusp in the wave function when two particles touch. The wave function remains continuous at the border of R_1, and discontinuity of its derivative is determined by c. Equation (2.12) can be obtained by integrating Schrödinger equation (2.11) over the surface $x_j = x_{j+1}$. These boundary conditions can easily be rewritten for any permutation sector. In the Tonks-Girardeau limit, i.e., for $c \to \infty$, the cusp condition implies that the wave function vanishes when two particles are in contact: $\psi_B(x_1, \ldots, x_j, x_{j+1}, \ldots, x_N, t)|_{x_{j+1}=x_j} = 0$ [2, 46].

We now present the Fermi-Bose transformation for the Lieb-Liniger model which was first suggested by Gaudin [32] to study time evolution in free space. In what follows, we set external potential in (2.11) to zero,

$$V(x) = 0.$$

Here the spatial dimension is infinite $x_j \in (-\infty, \infty)$, i.e., we do not impose any boundary conditions.

Due to the Bose symmetry of the wave function, it is sufficient to express it in the fundamental sector of the configuration space, $R_1 : x_1 < x_2 < \ldots < x_N$, where ψ_B obeys

$$i\frac{\partial \psi_B}{\partial t} = -\sum_{i=1}^{N} \frac{\partial^2 \psi_B}{\partial x_i^2}. \tag{2.13}$$

In particular, the eigenvalue problem can be formulated as an N-dimensional Helmholtz equation in the sector R_1 with additional boundary condition (2.12) at its borders.

Exact solutions of the time-dependent Schrödinger equation (2.11) can be obtained by using a Fermi-Bose mapping operator [32, 34] acting on fermionic wave functions: If $\psi_F(x_1, \ldots, x_N, t)$ is an antisymmetric (fermionic) wave function, which obeys the Schrödinger equation for a noninteracting Fermi gas,

$$i\frac{\partial \psi_F}{\partial t} = -\sum_{i=1}^{N} \frac{\partial^2 \psi_F}{\partial x_i^2}, \tag{2.14}$$

then the wave function

$$\psi_{B,c} = \mathcal{N}_c \hat{O}_c \psi_F, \tag{2.15}$$

where

$$\hat{O}_c = \prod_{1 \le i < j \le N} \left[\mathrm{sgn}(x_j - x_i) + \frac{1}{c}\left(\frac{\partial}{\partial x_j} - \frac{\partial}{\partial x_i} \right) \right], \tag{2.16}$$

is the differential Fermi-Bose mapping operator, and $\mathcal{N}_c$ is a normalization constant, obeys Eq. (2.11) with $V(x) = 0$ [32].

In Appendix A, we present a detailed proof of this statement. In brief, without loss of generality, we restrict ourselves to the fundamental sector R_1. First we show that the wave function (2.15) obeys the cusp condition (2.12) imposed by the interactions (see Appendix A). Next, it is straightforward to see that the Schrödinger equation (2.13) is satisfied. This is due to the commutators

$$\left[\frac{\partial^2}{\partial x_i^2}, \hat{O}_c \right] = 0 \text{ and } \left[i\frac{\partial}{\partial t}, \hat{O}_c \right] = 0,$$

and the fact that ψ_F obeys Eq. (2.14), which concludes the proof.

By using the Fermi-Bose mapping operator we are not able to address the

14

Lieb-Liniger problem in some general external potential $V(x)$. This idea is limited by nonvanishing commutation relations between $\hat{O}_c$ and $V(x)$, i.e. in general we have

$$\left[\hat{O}_c, \sum_j V(x_j)\right] \neq 0.$$

We will consider this issue in more details in Chapter 5. There we will use the Gaudin's operator $\hat{O}_c$ to construct exact solutions of the Lieb-Liniger model in the linear potential $V(x) = \alpha x$, where α is a constant force. As a final remark, we note that in the strongly correlated regime a $1/c$ expansion can be applied for a general potential $V(x)$ [70].

Chapter 3

Free expansion of a Lieb-Liniger gas

Free expansion of interacting Bose gases has recently attracted considerable attention. It has been utilized in experiments to deduce information on the initial state (see, e.g., Ref. [20] and references therein), and can be considered as a quantum-quench-type problem which provides insight into the relaxation of quantum systems (see, e.g., Refs. [24, 29] and references therein). Free expansion of a Lieb-Liniger (LL) gas has been analyzed in Ref. [52] by employing the hydrodynamic formalism [12]; it was shown that the density of the gas does not follow self-similar evolution [52]. However, in 1D Bose systems, most exact many-body solutions are given for the Tonks-Girardeau (TG) gas [52, 47, 49, 50, 51]. An important result is that the momentum distribution of the freely expanding TG gas asymptotically approaches the momentum distribution of free fermions [47, 49]. Recently, a particular family of exact solutions describing a LL gas freely expanding from a localized initial density distribution has been constructed [34]. It was shown that for any interaction strength, the wave functions asymptotically (as $t \to \infty$) assume TG form. Even though it is generally accepted that 1D Bose gases become less ideal with decreasing density, this intuition is mainly based on the studies of a LL gas in equilibrium ground states [1]. Thus, a more rigorous analysis of the expanding LL gas, which leads to more dilute system, but out of equilibrium, is desirable. In particular, it is interesting to study the dependence of the asymptotic wave functions on the initial state, and to see how are the initial conditions imprinted

in the asymptotic states.

Here we study the asymptotic form of the wave function describing a freely expanding Lieb-Liniger gas, which can be constructed via the Fermi-Bose transformation and the stationary phase approximation. In Section 3.1 we demonstrate that the asymptotic wave functions have Tonks-Girardeau structure, that is, they vanish when any of the two particle coordinates coincide. The dependence of the asymptotic state on the initial state is discussed. We illustrate that the properties of the asymptotic wave functions can significantly differ from the properties of a TG gas in the ground state of some external potential. This study generalizes and adds upon the previous result from Ref. [34], as the initial conditions studied here encompass ground states for generic external potentials and various interaction strengths. From the next-to-leading order term in the asymptotic regime, we deduce that the interaction energy of the LL gas decays as a universal power law in time $E_{\text{int}} \propto t^{-3}$. This is illustrated on a particular example in Section 3.2, where we provide further analysis of the particular family of time-dependent LL wave functions studied in Ref. [34]. In Section 3.3 we define one-body observables of interest. Explicit expressions for the asymptotic form of the single-particle density are provided in Section 3.4. In Section 3.5 we calculate the asymptotic single-particle density for free expansion of a LL gas from an infinitely deep box potential. We compare our exact calculation with the hydrodynamic approximation introduced in Ref. [12], and employed in Ref. [52] in the context of free expansion, obtaining good agreement for all values of the interaction strength.

In Section 3.6 we derive analytically (by using the stationary phase approximation) the formula which connects the asymptotic shape of the momentum distribution and the initial state. For sufficiently large times the momentum distribution coincides (up to a simple scaling transformation) with the shape of the real-space single-particle density, reflecting the fact that the expansion is asymptotically ballistic. The relation between the asymptotic expansion velocity of the LL cloud, and the overall energy stored in the system is derived.

Furthermore, in Section 3.7 we numerically study free expansion of a few Lieb-Liniger bosons, which are initially in the ground state of an infinitely deep hard-wall trap. The numerical calculation is carried out by employing a standard Fourier transform, as follows from the Fermi-Bose transformation for a time-dependent Lieb-Liniger gas [32, 34]. We focus on dynamics of one-

18

body observables of the system, in particular the momentum distribution, the occupancies of natural orbitals, and also the real-space single-particle density. Our numerical calculation allows us to explore the behavior of these observables in the transient regime of the expansion, where they are non-trivially affected by the particle interactions. Our analytical and numerical results are in good agreement.

3.1 Free expansion: Asymptotics

In this section we study the asymptotic form of time-dependent LL wave functions $\psi_{B,c}$ which are obtained by the Fermi-Bose transformation (2.15). All information on the initial condition $\psi_{B,c}(x_1, \ldots, x_N, t = 0)$ is contained in the initial fermionic wave function $\psi_F(x_1, \ldots, x_N, t = 0)$:

$$\psi_{B,c}(x_1, \ldots, x_N, 0) = \mathcal{N}_c \hat{O}_c \psi_F(x_1, \ldots, x_N, 0). \tag{3.1}$$

The initial bosonic wave function $\psi_{B,c}$, which can be expressed in this way, is assumed to describe a LL gas in its ground state when trapped in some external potential $V(x)$, e.g., in a harmonic oscillator potential, or some other trapping potential used in experiments. We consider the evolution from this initial state after the trapping potential has been suddenly turned off, as studied in experiments to deduce information on the initial state [20].

The time-dependent fermionic wave function $\psi_F(x_1, \ldots, x_N, t)$, which freely expands from the initial condition $\psi_F(x_1, \ldots, x_N, 0)$, can be expressed in terms of its Fourier transform,

$$\psi_F(x_1, \ldots, x_N, t) = \int dk_1 \cdots dk_N \; \tilde{\psi}_F(k_1, \ldots, k_N) e^{i \sum_{j=1}^{N} [k_j x_j - \omega(k_j) t]}, \tag{3.2}$$

where $\omega(k) = k^2$, and

$$\tilde{\psi}_F(k_1, \ldots, k_N) = \frac{1}{(2\pi)^N} \int dx_1 \cdots dx_N$$
$$\times \; \psi_F(x_1, \ldots, x_N, t = 0) e^{-i \sum_{j=1}^{N} k_j x_j}. \tag{3.3}$$

By using the Fermi-Bose transformation, the time-dependent bosonic wave function describing the freely expanding LL gas can be expressed as

$$\psi_{B,c} = \int dk_1 \cdots dk_N \ G(k_1, \ldots, k_N) e^{i \sum_{j=1}^{N} [k_j x_j - \omega(k_j)t]}, \qquad (3.4)$$

where the function $G(k_1, \ldots, k_N)$ is defined as

$$G(k_1, \ldots, k_N) = \mathcal{N}_c \tilde{\psi}_F(k_1, \ldots, k_N) \prod_{1 \le i < j \le N} [\text{sgn}(x_j - x_i) + \frac{i}{c}(k_j - k_i)]. \quad (3.5)$$

It should be noted that $G(k_1, \ldots, k_N)$ is *not* the Fourier transform of $\psi_{B,c}$ because it depends on x_j through the $\text{sgn}(x_j - x_i)$ terms. However, if we calculate G in the fundamental sector R_1, its Fourier transform will give us with the wave function $\psi_{B,c}$ in R_1. From this, due to the bosonic symmetry, we obtain the time-dependent wave function ih the whole coordinate space.

The asymptotic form of the wave function (3.4) can be obtained by evaluating the integral with the stationary phase approximation. The phase $\phi = \sum_{j=1}^{N} [k_j x_j - \omega(k_j)t]$ is stationary when $\partial \phi / \partial k_j = 0$. Let $\{k'_j\}$ denote the k_j-values for which

$$\left. \frac{\partial \phi}{\partial k_j} \right|_{k'_j} = x_j - 2k'_j t = 0,$$

that is, $k'_j = x_j/2t$. The phase can be rewritten as

$$\phi(\{k\}) = \phi(\{k'\}) - t \sum_{j=1}^{N} (k_j - k'_j)^2.$$

The leading term of the integral in Eq. (3.4), as well as the next-to-leading term, can be evaluated by expanding $G(k_1, \ldots, k_N) \equiv G(\{k\})$ in a Taylor series

20

around the stationary phase point $\{k'\}$:

$$
\begin{aligned}
\psi_{B,c} = {} & e^{i\phi(\{k'\})} \Big[G(\{k'\}) \int dk_1 \cdots dk_N e^{-it\sum_{j=1}^{N}(k_j-k_j')^2} \\
& + \sum_{i=1}^{N} \frac{\partial G(\{k\})}{\partial k_i}\bigg|_{\{k'\}} \int dk_1 \cdots dk_N (k_i - k_i') e^{-it\sum_{j=1}^{N}(k_j-k_j')^2} \\
& + \frac{1}{2!} \sum_{i,j=1}^{N} \frac{\partial^2 G(\{k\})}{\partial k_i \partial k_j}\bigg|_{\{k'\}} \\
& \times \int dk_1 \cdots dk_N (k_i - k_i')(k_j - k_j') e^{-it\sum_{l=1}^{N}(k_l-k_l')^2} + \dots \Big]. \quad (3.6)
\end{aligned}
$$

The remaining integrals in the three terms written out in this expansion can be calculated analytically. The second term involving the first derivatives of $G(\{k\})$ vanishes. The third term is nonvanishing only for $i = j$. Thus Eq. (3.6) reduces to

$$
\psi_{B,c} = e^{i\phi(\{k'\})} \left(\sqrt{\frac{\pi}{t}} e^{-i\pi/4} \right)^N \left[G(\{k'\}) - \frac{i}{4t} \sum_{i=1}^{N} \frac{\partial^2 G(\{k\})}{\partial k_i^2}\bigg|_{\{k'\}} + \dots \right]. \quad (3.7)
$$

From Eq. (3.7) we obtain in leading order the asymptotic wave function

$$
\begin{aligned}
\psi_\infty \propto {} & t^{-N/2} \prod_{1 \le i < j \le N} \left[\operatorname{sgn}(x_j - x_i) + \frac{i}{c}(k_j' - k_i') \right] \\
& \times \tilde{\psi}_F(k_1', \dots, k_N') e^{i\sum_{j=1}^{N}[k_j' x_j - \omega(k_j')t]}, \quad (3.8)
\end{aligned}
$$

which is written in a more convenient form in terms of the variables $\xi_j = x_j/t$:

$$
\begin{aligned}
\psi_\infty \propto {} & t^{-N/2} \prod_{1 \le i < j \le N} \left[\operatorname{sgn}(\xi_j - \xi_i) + \frac{i}{2c}(\xi_j - \xi_i) \right] \\
& \times \tilde{\psi}_F(\xi_1/2, \dots, \xi_N/2) \, e^{\frac{i}{4}\sum_{j=1}^{N}\xi_j^2 t}. \quad (3.9)
\end{aligned}
$$

Equation (3.9) is the main result of this section. Evidently the asymptotic form of the LL wave function ψ_∞ has TG form. Namely, the Fourier transform of a fermionic wave function $\tilde{\psi}_F(\xi_1/2, \dots, \xi_N/2)$ is antisymmetric, which implies that ψ_∞ is zero whenever $\xi_i = \xi_j$ $(i \ne j)$. Furthermore, ψ_∞ is symmetric under the exchange of any two coordinates ξ_i and ξ_j. This clearly shows that a localized LL wave function during free expansion asymptotically approaches

a wave function with the TG structure. However, it should be emphasized that the properties of the asymptotic state are not necessarily similar to the wave function describing TG gas in equilibrium, in the ground state of some external potential. The connection between the initial and the asymptotic state is illustrated below.

In the derivation of Eq. (3.9) we have analyzed LL wave functions which are obtained through the Fermi-Bose transformation (2.15). This class of wave functions is quite general and corresponds to numerous situations of practical relevance. Let us discuss the case in which the initial bosonic wave function $\psi_{B0} = \psi_{B,c}(x_1, \ldots, x_N, 0)$ is a ground state of a repulsive LL gas in an experimentally realistic external potential $V(x)$, e.g., a harmonic oscillator potential. The eigenstates of the LL system in free space are of the form

$$\psi_{\{k\}} = \mathcal{N}(\{k\})\hat{O}_c \det[e^{ik_m x_j}]_{m,j=1}^N, \tag{3.10}$$

where the set of N real values $\{k\} = \{k_m \,|\, m = 1, \ldots, N\}$ uniquely determines the eigenstate; the normalization constant is given by

$$\frac{1}{\mathcal{N}(\{k\})} = \sqrt{(2\pi)^N N! \prod_{i<j} \left[1 + \left(\frac{k_j - k_i}{c}\right)^2\right]},$$

see Ref. [44]. In free space, there are no restrictions on the numbers k_m. If periodic boundary conditions are imposed as in Ref. [1] (i.e., the system is a ring of length L), the wave numbers k_j must obey a set of coupled transcendental equations [1, 38, 39, 71, 42] which depend on the strength of the interaction (see, e.g., Ref. [39]). The LL eigenstates $\psi_{\{k\}}$ possess the closure property [32] and they are complete [72]. Thus, our initial state ψ_{B0} can be expressed as a superposition of LL eigenstates,

$$\begin{aligned}
\psi_{B0} &= \sum_{\{k\}} b(\{k\})\psi_{\{k\}} \\
&= \hat{O}_c \sum_{\{k\}} \mathcal{N}(\{k\})b(\{k\}) \det[e^{ik_m x_j}]_{m,j=1}^N,
\end{aligned} \tag{3.11}$$

where the coefficients $b(\{k\})$ can be obtained by projecting the initial condition ψ_{B0} onto the LL eigenstates. By comparing Eqs. (3.1) and (3.11) we find that

22

the initial fermionic wave function is

$$\psi_{F0} = \mathcal{N}_c^{-1} \sum_{\{k\}} \mathcal{N}(\{k\}) b(\{k\}) \det[e^{ik_m x_j}]_{m,j=1}^N. \tag{3.12}$$

Since we have assumed that $V(x)$ is an experimentally realistic smooth function, also ψ_{F0} is smooth and differentiable such that the operator $\hat{O}_c$ can be applied.

The connection between the asymptotic state (3.9) and the initial state ψ_{B0} is made through the Fourier transform of the initial fermionic wave function $\tilde{\psi}_F(\{k\})$. More insight into the connection between the initial state and the asymptotic state can be made by expressing $\tilde{\psi}_F(\{k\})$ through the coefficients $b(\{k\})$ utilized in the expansion (3.11). First, let us note that the coefficients $b(\{k\}) = b(k_1, k_2, \ldots, k_N)$ are antisymmetric with respect to the interchange of any two arguments k_i and k_j $(i \neq j)$. This follows from the fact that the LL eigenstates $\psi_{\{k\}}$ possess the same property, see Ref. [44]. By using this property of $b(\{k\})$, Eq. (3.12) can be rewritten as

$$\begin{aligned}
\psi_{F0} &= \mathcal{N}_c^{-1} \sum_{\{k\}} \mathcal{N}(\{k\}) b(\{k\}) \sum_P (-)^P e^{i \sum_{j=1}^N k_{Pj} x_j} \\
&= \mathcal{N}_c^{-1} \sum_P \sum_{\{k\}} \mathcal{N}(k_{P1}, k_{P2}, \ldots, k_{PN}) \\
&\quad \times b(k_{P1}, k_{P2}, \ldots, k_{PN}) e^{i \sum_{j=1}^N k_{Pj} x_j} \\
&= \mathcal{N}_c^{-1} N! \sum_{\{k\}} \mathcal{N}(\{k\}) b(\{k\}) e^{i \sum_{j=1}^N k_j x_j}. \tag{3.13}
\end{aligned}$$

By comparing Eqs. (3.13) and (3.2) we obtain

$$\tilde{\psi}_F(\{k\}) = \mathcal{N}_c^{-1} N! \mathcal{N}(\{k\}) b(\{k\}). \tag{3.14}$$

Evidently, the Fourier transform of the initial fermionic wave function $\tilde{\psi}_F(\{k\})$ is directly proportional to the projections $b(\{k\})$ of the initial bosonic wave function onto the LL eigenstates. From this relation we can conclude that the asymptotic wave function (3.9) has TG structure as a consequence of the antisymmetry of the coefficients $b(\{k\})$, which originates from the antisymmetry of the LL eigenstates with respect to k_j arguments [44]. It is also worthy to note that Eq. (3.4), and therefore our main result, can be obtained without
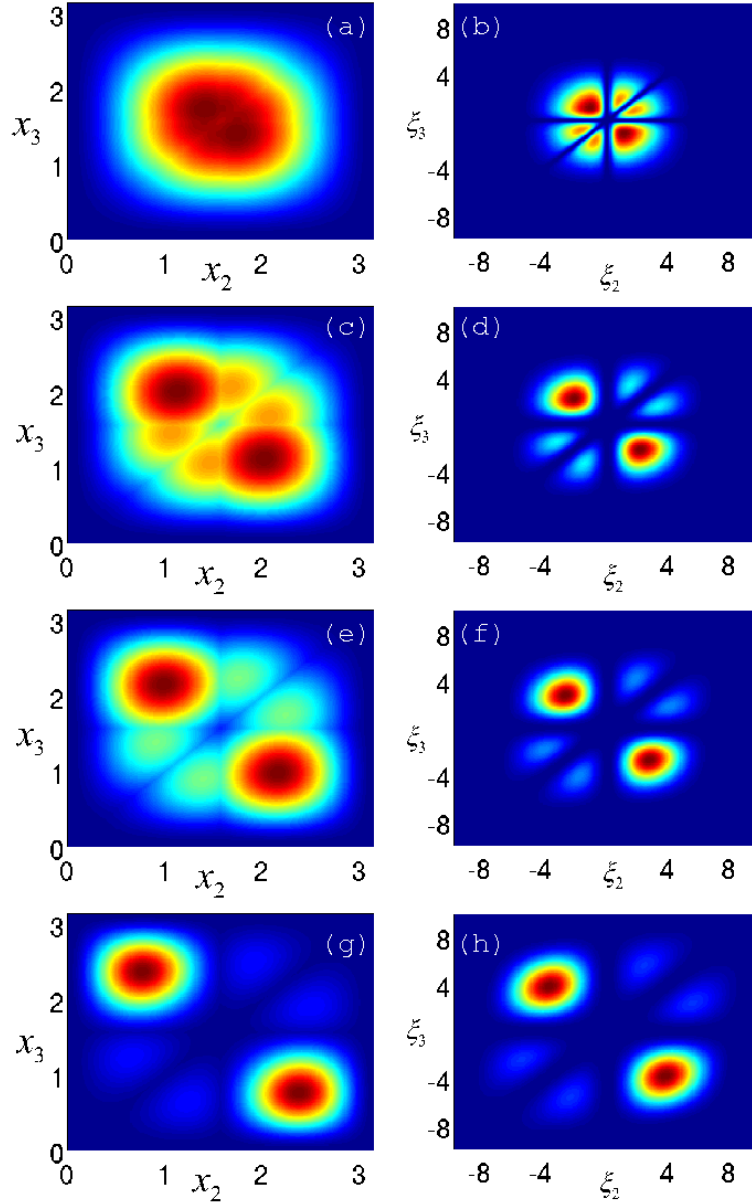
23

Figure 3.1: Contour plots illustrating free expansion of $N = 3$ bosons from the ground state of a LL gas in a box with infinitely high walls ($L = \pi$). The left column depicts the initial ground state $|\psi_{B0}(L/2, x_2, x_3)|^2$, and the right column depicts the asymptotic state $|\psi_\infty(0, \xi_2, \xi_3)|^2$, for $c = 0.2$ (a,b), $c = 1$ (c,d), $c = 2$ (e,f), and $c = 10$ (g,h). The density of the asymptotic state is zero when two coordinates ξ_i and ξ_j ($i \neq j$) coincide.

explicit use of the Fermi-Bose transformation; by writing the time dependent LL states as $\psi_{B,c} = \sum_{\{k\}} b(\{k\})\psi_{\{k\}}\exp(-i\sum_j k_j^2 t)$, and after employing the antisymmetry of $b(\{k\})$ [equivalently as in Eq. (3.13)] one obtains Eq. (3.4). Formulae (3.9) and (3.14) provide, under general conditions, the asymptotic form of the wave functions for the freely expanding LL gas, and the connection between these asymptotic states and the initial states.

For the sake of the clarity, let us illustrate the asymptotic state of the LL gas on a particular example. Suppose that initially the LL gas is in the ground state, enclosed in an infinitely deep box of length L. The ground state ψ_{B0} for this potential was found by employing the superposition of the Bethe ansatz wave functions in Ref. [36]. The coefficients $b(\{k\})$ can be relatively easily found for a few particles by employing a computer program for algebraic manipulation (Mathematica). In Fig. 3.1 we illustrate the initial state and the asymptotic state for the case of $N = 3$ particles, and for values of $c = 0.2, 1, 2$, and 10, by showing the contour plots of the probabilities $|\psi_{B0}(L/2, x_2, x_3)|^2$ (left column) and $|\psi_\infty(0, \xi_2, \xi_3)|^2$ (right column). Thus, one particle is fixed in the center of the system, while the plots illustrate the probability of finding the other two particles in space. The left column illustrating the initial states shows that the system becomes more correlated with increasing interaction strenght c and it enters the TG regime for sufficiently large c (e.g., for $c = 10$ depicted in Fig. 3.1 (g) the ground state of the system is in the TG regime). The right column illustrating the asymptotic state shows that the wave function is zero whenever two of the coordinates coincide. However, it is important to note that the properties of the asymptotic wave functions, even though they possess the TG structure, can significantly differ from the properties of the TG gas in the equilibrium ground state. This can be seen by comparing the asymptotic state in Fig. 3.1 (b), and the TG ground state shown in Fig. 3.1 (g). The asymptotics of Fig. 3.1 (b) is obtained after free expansion from a weakly interacting ground state ($c = 0.2$); from Fig. 3.1 (b) we observe that when one particle is fixed at zero, there is still a relatively large probability of finding the other two particles to the left and to the right of the fixed one. In contrast, for the TG ground state shown in Fig. 3.1 (g), if one particle is fixed in the center of the system, the other two are on the opposite sides of that one. Furthermore, by comparing the asymptotic states in Figs. 3.1 (b), (d), (f), and (h), we see that their properties depend on the

25

interaction strength c. It is worthy to mention again that free expansion can be utilized to deduce information on the initial state (see, e.g., Refs. [20] and references therein); free 1D expansion can distinguish between different initial regimes of the LL gas [52].

Let us now address the case of attractive interactions. For $c < 0$, the cusp condition assumes a form that is identical to that for $c > 0$ (see, e.g., Ref. [38]). Therefore, by acting on some fermionic time-dependent wave function obeying Eq. (2.14) with the Fermi-Bose transformation operator $\hat{O}_{c<0}$, one obtains an exact solution for the attractive time-dependent LL gas in the form $\hat{O}_{c<0}\psi_F$ (see Appendix A); our derivation holds for this family of wave functions. Experiments where the attractive quasi-1D Bose gas is suddenly released from a trapping potential were used to study solitons made of attractively interacting BEC [73]. Exact studies of such a system within the framework of the LL model are expected to provide deeper insight into nonequilibrium phenomena beyond the Gross-Pitaevskii mean-field regime, where interesting dynamical effects can occur [74, 75].

It should be noted that the time scale it takes for the LL system to reach the TG regime depends on the initial condition. The next-to-leading term of the asymptotic wave function is suppressed relative to the leading term by a factor $1/t$, as obtained by the stationary phase expansion in Eq. (3.7). From this we can deduce the scaling of the interaction energy, defined as

$$E_{\text{int}} = 2c \int dx_1 \cdots dx_N \, |\psi_{B,c}|^2 \sum_{1 \leq i < j \leq N} \delta(x_i - x_j), \qquad (3.15)$$

as $t \to \infty$. Since the interaction strength c is finite, and since the asymptotic density $|\psi_\infty(\xi_1, \ldots, \xi_N, t)|^2$ equals zero for any pair of arguments being equal, $\xi_i = \xi_j$, one concludes that asymptotically the leading term of the interaction energy vanishes. Since the first correction to the leading TG term of the wave function is of order t^{-1}, and since $\delta(x_i - x_j) = t^{-1}\delta(\xi_i - \xi_j)$, the interaction energy asymptotically decays to zero as $E_{\text{int}} \propto t^{-3}$. This power law decay of the interaction energy is illustrated in the following section.

3.2 Example: Fermionic wave function expanding from a harmonic trap

In Ref. [34], a particular family of time-dependent wave functions describing a freely expanding Lieb-Liniger gas has been constructed. The wave functions were obtained by acting with the Fermi-Bose mapping operator onto a specific time-dependent fermionic wave function,

$$
\begin{aligned}
\psi_F \;\propto\; & \exp\left\{ -i\frac{N^2\nu}{2}\tau(t) - \frac{\nu - i\nu^2 t}{4}\sum_{j=1}^{N}\left[\frac{x_j}{b(t)}\right]^2 \right\} \\
& \times\, b(t)^{-N^2/2} \prod_{1\le i<j\le N}(x_j - x_i),
\end{aligned}
\tag{3.16}
$$

which describes free expansion of noninteracting fermions in one spatial dimension. The initial fermionic wave function at $t = 0$ corresponds to a fermionic ground state in a harmonic trap $V(x) = \nu^2 x^2/4$ (see, e.g., Ref. [76]). Here, ν corresponds to the trapping frequency, $b(t) = \sqrt{1 + t^2\nu^2}$, and $\tau(t) = \arctan(\nu t)/\nu$. The limiting form of the Lieb-Liniger wave function for $t \to \infty$, $\psi_{B,c}(\eta_1 b(t), \ldots, \eta_N b(t), t)$, was shown to have the following form characteristic for a TG gas:

$$
\begin{aligned}
\psi_{B,c}(\eta_1 b(t), \ldots, \eta_N b(t), t) \propto\; & b(t)^{-N/2}\exp\left\{ -i\frac{N^2\nu}{2}\tau(t) - \frac{\nu - i\nu^2 t}{4}\sum_{j=1}^{N}\eta_j^2 \right\} \\
& \times \prod_{1\le i<j\le N} g(\eta_j - \eta_i) + \mathcal{O}(1/t),
\end{aligned}
\tag{3.17}
$$

where $g(\eta) = |\eta| + i\nu\eta^2/2c$. Equation (3.9) is a generalization of this result given first in Ref. [34]. Since Eq. (3.9) was obtained with the help of the stationary phase approximation, whereas (3.17) is obtained straightforwardly from the exact form of the specific LL wave function (see Ref. [34]), it is worthy to verify that Eq. (3.9) reproduces Eq. (3.17) as a special case. In order to do so, we calculate the Fourier transform of the initial fermionic wave function, i.e., $\psi_F(x_1, \ldots, x_N, 0)$ from Eq. (3.16). Interestingly, the Fourier transform has
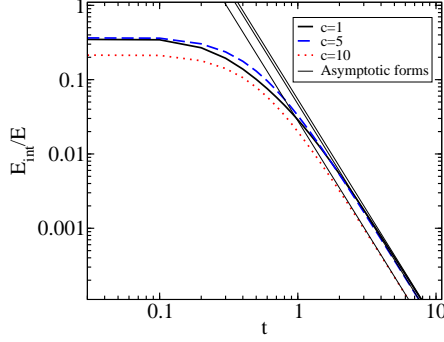
Figure 3.2: Time-evolution of the interaction energy $E_{\text{int}}(t)$, expressed in units of the total energy E. The three curves correspond to values of $c = 1$ (solid line), $c = 5$ (dashed line), and $c = 10$ (dotted line). The straight lines depict the asymptotic power law behavior of the interaction energy, $E_{\text{int}}(t) \propto t^{-3}$ (see text for details).

exactly the same functional form as the initial condition in x-space:

$$\tilde{\psi}_F \propto e^{-\sum_{j=1}^N k_j^2/\nu} \prod_{1 \leq i < j \leq N} (k_j - k_i). \tag{3.18}$$

By plugging this form into Eq. (3.9) we obtain:

$$
\begin{aligned}
\psi_\infty \quad \propto \quad & t^{-N/2} e^{-\sum_{j=1}^N \xi_j^2/(4\nu)} e^{(i/4)\sum_{j=1}^N \xi_j^2 t} \\
& \times \prod_{1 \leq i < j \leq N} [|\xi_j - \xi_i| + \frac{i}{2c}(\xi_j - \xi_i)^2].
\end{aligned} \tag{3.19}
$$

After replacing $\xi_j = x_j/t$ with $\nu\eta_j = \nu x_j/b(t)$ which asymptotically approaches $\nu\eta_j \sim x_j/t = \xi_j$, we obtain the functional form identical to Eq. (3.17). This verifies the validity of Eq. (3.9) in the special case studied in Ref. [34].

In order to verify the asymptotic power law decay of the interaction energy E_{int} obtained in the previous section, let us calculate the time-evolution of E_{int} for the specific family of LL wave functions discussed in this section. We calculate integral (3.15) for $N = 3$ particles, and $\nu = 2$. Given these parameters, E_{int} depends on the strength of the interaction c and time t. Figure 3.2 illustrates time-evolution of the interaction energy for three values of c; displayed curves depict the ratio $E_{\text{int}}(t)/E$, where E denotes the total energy, which is a constant of motion. Evidently, after some initial transient period
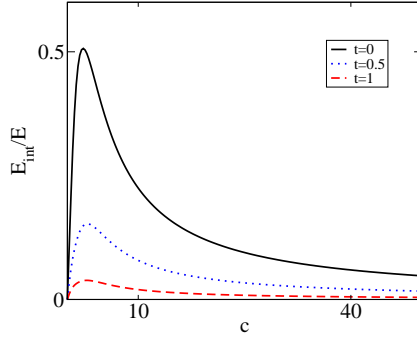
Figure 3.3: The ratio E_{int}/E as a function of the interaction strength c, at three values of time, $t = 0$ (solid line), $t = 0.5$ (dotted line), and $t = 1$ (dashed line) (see text for details).

the interaction energy starts its asymptotic power law decay $E_{\text{int}}(t) \propto t^{-3}$. It should be noted that the contribution of the interaction energy to the total energy depends on the interaction strength c. This is illustrated in Fig. 3.3 which shows $E_{\text{int}}(t)/E$ as a function of c at three points in time. At $t = 0$, the contribution of the interaction energy to the total energy is non-monotonous with the increase of c; it is zero at $c = 0$ and in the TG limit $c \to \infty$, with a specific maximal value in between. The form of the curve is preserved for finite values of t, with the evident decay of the interaction energy to zero as $t \to \infty$. Note that an equivalent non-monotonous behavior of the interaction energy as a function of c was found for the Lieb-Liniger gas in the ground state for $c > 0$ and with periodic boundary conditions [38].

3.3 One-body observables of interest

In principle, from the time-dependent LL wave function $\psi_{B,c}(x_1, \ldots, x_N, t)$ one can extract the physically relevant observables (in practice, this is a difficult task). In the following sections, we will consider one-body observables contained within the reduced single-particle density matrix (RSPDM),

$$
\rho_{B,c}(x, y, t) = N \int dx_2 \cdots dx_N \psi_{B,c}(x, x_2, \ldots, x_N, t)^*
$$
$$
\times \psi_{B,c}(y, x_2, \ldots, x_N, t). \tag{3.20}
$$

The single-particle (SP) density in real space is simply $\rho_{B,c}(x, x, t)$, whereas the momentum distribution is defined as

$$n_B(k, t) = \frac{1}{2\pi} \int dx\, dy\, e^{ik(x-y)} \rho_{B,c}(x, y, t). \qquad (3.21)$$

The eigenfunctions of the RSPDM, $\Phi_i(x, t)$ are called the natural orbitals (NOs),

$$\int dx\, \rho_{B,c}(x, y, t) \Phi_i(x, t) = \lambda_i(t) \Phi_i(y, t), \quad i = 1, 2, \ldots; \qquad (3.22)$$

the eigenvalues $\lambda_i(t)$ are the occupancies of these orbitals. Apparently, in a nonequilibrium situation, the effective single particle states $\Phi_i(x, t)$ and their occupancies $\lambda_i(t)$ may change in time.

3.4   Asymptotic single-particle density

Given the asymptotic form of the wave function, we now consider the asymptotic form of the single-particle density which is of considerable interest for experiment. The single-particle density is defined as $\rho_c(x, t) = N \int dx_2 \cdots dx_N$ $|\psi_{B,c}(x, x_2, \ldots, x_N, t)|^2$. For studying asymptotics, it is convenient to define the asymptotic form in terms of the rescaled coordinates $\xi = x/t$:

$$\rho_\infty(\xi) = \mathcal{N}_\infty t^N \int_{-\infty}^{\infty} d\xi_2 \ldots d\xi_N |\psi_\infty(\xi, \xi_2, \ldots, \xi_N, t)|^2; \qquad (3.23)$$

here the normalization constant $\mathcal{N}_\infty$ is chosen such that $\int d\xi\, \rho_\infty(\xi) = N$, the total number of particles, while the factor t^N cancels the trivial time-scaling of the asymptotic single-particle density.

For the specific asymptotic form of the wave function (3.19) we can analytically calculate the asymptotic form of the density for a few particles. As an example, for $N = 3$, the normalization constant is

$$\mathcal{N}_{\infty, N=3} = \frac{c^6}{\sqrt{2\pi^3 \nu^9}(8c^6 + 48c^4\nu + 90c^2\nu^2 + 45\nu^3)}, \qquad (3.24)$$

while the single-particle density has the following structure:

$$
\begin{aligned}
\rho_\infty(\xi) \;=\; & \mathcal{N}_{\infty,N=3} \frac{\pi\nu^2}{8c^6} e^{-\xi^2/(2\nu)} \\
& \times\, [32c^6(3\nu^2+\xi^4) \\
& +\, 16c^4(33\nu^3 - 3\nu^2\xi^2 + 9\nu\xi^4 + \xi^6) \\
& +\, 2c^2(465\nu^4 - 60\nu^3\xi^2 + 90\nu^2\xi^4 + 20\nu\xi^6 + \xi^8) \\
& +\, 3\nu(165\nu^4 - 60\nu^3\xi^2 + 30\nu^2\xi^4 + 4\nu\xi^6 + \xi^8)].
\end{aligned}
\tag{3.25}
$$

This expression shows that the Gaussian shape of the single-particle density is modulated with the N-hump structure characteristic for the single-particle density of a TG gas in the ground state of some external potential. The corresponding density (3.25), in terms of $\eta = \xi/\nu$ is shown in Fig. 2 of Ref. [34]. It should be noted that such an asymptotic form of the single-particle density corresponds to a particular family of time-dependent wave functions obtained in Ref. [34]. For different initial conditions one can obtain a different shape of the asymptotic single-particle density as follows from Eqs. (3.9) and (3.14); the asymptotic single-particle density depends on $\tilde{\psi}_F(\{k\})$, that is $b(\{k\})$.

3.5 Comparison with the hydrodynamic approximation

Besides providing insight into the physics of interacting time-dependent many-body systems, our motivation to study exact solutions of such systems is to utilize those solutions as a benchmark against various approximations. Free expansion of a Lieb-Liniger gas has been studied in Ref. [52] by employing the formalism introduced in Ref. [12], referred to as the hydrodynamic approximation. This formalism can be written in a form of a nonlinear evolution equation for a single-particle wave function $\psi_H(x,t)$ [see Eq. (9) in Ref. [52]],

$$
i\frac{\partial \psi_H(x,t)}{\partial t} = -\frac{\partial^2 \psi_H}{\partial x^2} + V(x)\psi_H + c^2 f\left(\frac{c}{|\psi_H|^2}\right)\psi_H,
\tag{3.26}
$$

where $|\psi_H(x,t)|^2$ is the single-particle density normalized to $\int |\psi_H(x,t)|^2 dx = N$, while the function f which appears in the nonlinear term is defined in Ref.
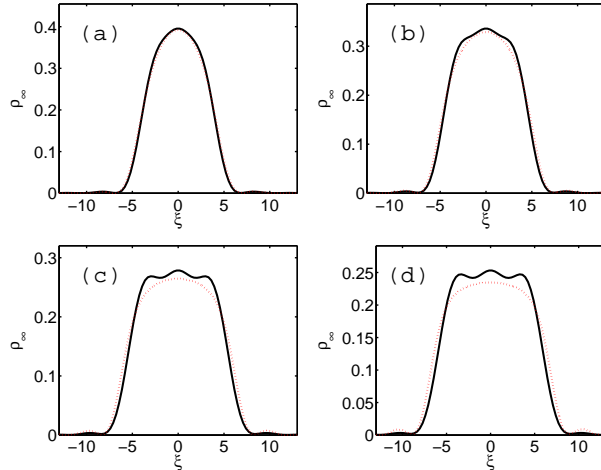
Figure 3.4: The asymptotic form of the SP density obtained exactly (black solid line), and with the hydrodynamic approach (red dotted line). The parameters used in the calculation are $N = 3$, $L = \pi$, $c = 1$ (a), $c = 2$ (b), $c = 5$ (c), and $c = 10$ (d). (see text for details).

[12], and also tabulated in Ref. [19] of Ref. [12]. The potential is $V(x) = 0$ during free expansion. The hydrodynamic approximation was used to obtain Eq. (3.26), which is written in units corresponding to the Lieb-Liniger model of Eq. (2.11). The nonlinear equation above reduces to the standard Gross-Pitaevskii equation for small interactions, and to the nonlinear equation from Ref. [77] for strong interactions [52]. The hydrodynamic approximation over-estimates the coherence in the system, and therefore it may not be accurate for analyzing observables strongly connected to coherence. However, it is reasonable to compare the exact asymptotic form of the single-particle density after free expansion with the asymptotic form obtained from the hydrodynamic approximation.

Let us follow upon our example from Section 3.1, that is, let us consider the asymptotic form of the single particle density $\rho_\infty(\xi)$ of a LL gas which is initially in the ground state of a box with infinitely high walls; the length of the box is $L = \pi$. The calculation of the exact SP density demands performing multi-dimensional integration over $N - 1$ variables which is not a simple task. For this reason, the number of particles in our calculation of the exact SP density is $N = 3$. For the initial condition of the hydrodynamic approach $\psi_H(x, t = 0)$ we could choose $\psi_H(x, t = 0) = \sqrt{N/L}$ within the box, and zero

otherwise. This would be a good initial condition in the thermodynamic limit (large N, $N/L = const.$). However, since for our exact calculation we used $N = 3$, we have chosen, in order to be able to compare between the two approaches, the hydrodynamic initial field $\psi_H(x, t = 0) = \sqrt{n_{\text{exact}}}$, where n_{exact} is the exact SP density of the initial ground state (this can be calculated by employing Ref. [36]). Figure 3.4 displays the exact asymptotic form of the SP density, and the hydrodynamic asymptotic SP density. The latter is obtained numerically by solving Eq. (3.26) with the standard split-step Fourier technique; the nonlinear term in Eq. (3.26), that is, the function $f(c/|\psi_H(x)|^2)$ is calculated by using values tabulated in Ref. [19] of Ref. [12]. The asymptotic dynamics in the hydrodynamic approach occurs after sufficiently long propagation, when the SP density starts exhibiting self-similar propagation (see also [52]).

The agreement is qualitatively excellent for all values of the interaction strength, and quantitatively excellent for $c < 1$. The width of the SP density as a function of $\xi = x/t$ indicates the velocity of the expansion of the cloud. The asymptotic FWHM (full-width at half maximum) expansion velocity is in good agreement for all values of c. The hydrodynamic approximation does not reproduce small humps in the SP density, characteristic in the TG regime after expansion from the ground state; this discrepancy is expected to be smaller if we had calculated expansion from the ground state with large N, where the hydrodynamic approximation is expected to work even better.

Another possible comparison that can be made with the hydrodynamic approximation is the following. The LL wave function which is utilized as the initial condition in Sec. 3.2 and Ref. [34] is obtained by acting with the operator $\hat{O}_c$ onto the fermionic ground state ψ_{F0} in the harmonic trapping potential $V(x) = \nu^2 x^2/4$. This wave function can approximate the ground state only when the commutator $[\hat{O}_c, V(x)]$ can be neglected [34]. The SP density of this state can be compared with the static hydrodynamic density obtained in Ref. [12] for the LL gas in a harmonic trap. Due to the properties of the operator $\hat{O}_c$ [34] and the fermionic ground state in the harmonic trap ψ_{F0}, it is straightforward to verify that the shape of the SP density corresponding to the state $\hat{O}_c\psi_{F0}$ scales as $\rho(x) \to \rho(x/s)/s$ under the transformation $\nu \to \nu/s^2$, $c \to c/s$, that is, the shape of the SP density does not change under this transformation. The same is true for the shape of the (ground-state) SP density obtained with the hydrodynamic approach, which has been shown [12] to depend on a single

parameter $\eta = (\frac{3N\nu}{4c^2})^{\frac{2}{3}}$ that is invariant under the transformation $\nu \to \nu/s^2$, $c \to c/s$. This is fully analogous to the case of a homogeneous LL gas where the only governing parameter $\gamma = c/n$ is invariant under a simultaneous rescaling of the interaction strength c and the linear particle density n [1]. The shape of the SP density of the state $\hat{O}_c\psi_{F0}$ (calculated for $N = 3$) agrees with the shape obtained in Ref. [12] only in the Tonks-Girardeau limit ($\eta \ll 1$) where $\hat{O}_c\psi_{F0}$ is a good approximation for the ground state. If we reduce the interaction strength c by keeping ν fixed, thereby increasing η, the two SP densities will no longer have a similar shape; this stems from a simple fact that $\hat{O}_c\psi_{F0}$ is an excited state for sufficiently small values of c, because the commutator $[\hat{O}_c, V(x)]$ cannot be neglected, whereas the hydrodynamic solution approximates the ground state.

3.6 Asymptotic form of the momentum distribution

In this section we derive the asymptotic form of the momentum distribution of a Lieb-Liniger gas after free expansion from an initially localized state defined by $G(k_1, \ldots, k_N)$ [we should keep in mind that $G(k_1, \ldots, k_N)$ also depends upon the coordinates x_j via the sgn functions, see Eq. (3.5)]. The momentum distribution defined in Eq. (3.21) can be rewritten by using Eqs. (3.4) and (3.20) as

$$
\begin{aligned}
n_B(k) = \frac{N}{2\pi} &\int dx\, dy\, e^{ik(x-y)} \int dx_2 \cdots dx_N \\
&\times \left(\int dk_1 \cdots dk_N G(k_1, \ldots, k_N) e^{i\sum_{j=1}^N (k_j x_j - k_j^2 t)} \right)^*_{x_1 = x} \\
&\times \left(\int dq_1 \cdots dq_N G(q_1, \ldots, q_N) e^{i\sum_{j=1}^N (q_j x_j - q_j^2 t)} \right)_{x_1 = y} \\
= \frac{N}{2\pi} &\int dx_2 \cdots dx_N \int dx\, dy\, dk_1 \cdots dk_N\, dq_1 \cdots dq_N \\
&\times G(k_1, \ldots, k_N)^*|_{x_1 = x}\, G(q_1, \ldots, q_N)|_{x_1 = y}\, e^{i\phi}, \qquad (3.27)
\end{aligned}
$$

where the phase ϕ is

$$\phi(k_1, \ldots, k_N, q_1, \ldots, q_N, x, y) = -\sum_{j=2}^{N}(k_j x_j - k_j^2 t) + \sum_{j=2}^{N}(q_j x_j - q_j^2 t)$$
$$- k_1 x + k_1^2 t + q_1 y - q_1^2 t + k(x - y).$$

The integrals over $k_1, \ldots, k_N, q_1, \ldots, q_N, x, y$ in Eq. (3.27) are evaluated with the stationary phase approximation. The point of stationary phase is defined by the following equations:

$$\left.\frac{\partial \phi}{\partial k_j}\right|_{k_j'} = \left.\frac{\partial \phi}{\partial q_j}\right|_{q_j'} = \left.\frac{\partial \phi}{\partial x}\right|_{x'} = \left.\frac{\partial \phi}{\partial y}\right|_{y'} = 0, \text{ for } 1 \le j \le N.$$

The stationary phase point is:

$$k_j' = q_j' = x_j/(2t), \text{ for } 2 \le j \le N,$$
$$k_1' = q_1' = k, \text{ and}$$
$$x' = y' = 2kt. \tag{3.28}$$

The phase ϕ can be rewritten as

$$\phi = t \sum_{j=2}^{N}\left[(k_j - \frac{x_j}{2t})^2 - (q_j - \frac{x_j}{2t})^2\right] + [(k - k_1)x + k_1^2 t] - [(k - q_1)y + q_1^2 t]. \tag{3.29}$$

We notice that $\phi(k_1', \ldots, k_N', q_1', \ldots, q_N', x', y') = 0$. In the stationary phase approximation, the function G in Eq. (3.27) is evaluated at the stationary phase point defined in Eq. (3.28), which yields

$$n_{B,\infty}(k) \approx \frac{N}{2\pi} \int dx_2 \cdots dx_N \left|G(k, \frac{x_2}{2t}, \ldots, \frac{x_N}{2t})\right|^2$$
$$\times \int dx dk_1 e^{i[(k-k_1)x + k_1^2 t]} \int dy dq_1 e^{-i[(k-q_1)y + q_1^2 t]}$$
$$\times \left(\int dk_2 e^{it(k_2 - \frac{x_2}{2t})^2}\right)^{N-1} \left(\int dq_2 e^{-it(q_2 - \frac{x_2}{2t})^2}\right)^{N-1}$$

$$= \frac{N}{(2\pi)^3} \int dx_2 \cdots dx_N \left| G(k, \frac{x_2}{2t}, \dots, \frac{x_N}{2t}) \right|^2$$

$$\times e^{ik^2 t} e^{-ik^2 t} \left(\sqrt{\frac{\pi}{t}} e^{i\pi/4} \right)^{N-1} \left(\sqrt{\frac{\pi}{t}} e^{-i\pi/4} \right)^{N-1}. \qquad (3.30)$$

It is convenient now to introduce variables $\xi_j = x_j/t$; from (3.30) we obtain the asymptotic form of the momentum distribution of a freely expanding LL gas

$$n_{B,\infty}(k) \propto \int d\xi_2 \cdots d\xi_N \, |G(k, \xi_2/2, \dots, \xi_N/2)|^2. \qquad (3.31)$$

We note that in the asymptotic regime, the momentum distribution acquires the same functional form as the asymptotic SP density. In the asymptotic regime, the SP density exhibits self-similar (ballistic) expansion (this is not true in the transient period preceding the asymptotic regime, see Ref. [52]). It is most convenient to express the asymptotic SP density in variable $\xi = x/t$ (see Chapter 2),

$$\rho_\infty(\xi) \propto \int d\xi_2 \cdots d\xi_N \, |G(\xi/2, \xi_2/2, \dots, \xi_N/2)|^2; \qquad (3.32)$$

we normalize $\rho_\infty(\xi)$ such that $\int \rho_\infty(\xi) d\xi = N$. The variable $\xi = x/t$ has units of velocity; the self-similar asymptotic SP density can be interpreted as the distribution of velocities of particles in a gas, which is in a simple manner related to the momentum distribution $n_{B,\infty}(k)$.

Equation (3.31) can be thought of as a generalization of the dynamical fermionization of the momentum distribution which has been demonstrated for a freely expanding TG gas ($c \to \infty$) [47, 49]. Free expansion in the TG regime is solved by the Fermi-Bose mapping [2, 46]. In this regime, the SP density is identical on both sides of the map. Since fermions are noninteracting, the asymptotic form of the SP density (for both TG bosons and free fermions) is identical to the fermionic momentum distribution, which does not change in time. Equations (3.31) and (3.32) immediately yield that the asymptotic momentum distribution for TG bosons has the same shape as the asymptotic SP density, which has the shape of the fermionic momentum distribution, i.e., we obtain the result of Refs. [47, 49]. We also note that equivalent relation between the asymptotic SP density and momentum distribution was found in

Ref. [79] for a different model with emphasis that the time of flight measurements do not give the initial momentum distribution. The derived formula (3.31) is verified numerically on a particular example in the next section.

3.7 Free expansion from a box: Dynamics of the momentum distribution and the occupancies $\lambda_i(t)$

In this section we calculate free expansion of three LL bosons, which are initially (at $t = 0$) in the ground state in an infinitely deep box of length $L = \pi$. The analytical expression for the LL box ground state has been found in Ref. [36]. By using this result it is straightforward to calculate $G(k_1, k_2, k_3)$ (which depends on the interaction strength c) for this particular initial condition; we have outlined this calculation in Appendix B for N particles. The next step is calculation of the Fourier integral in Eq. (3.4), which is performed numerically by employing the Fast Fourier Transform algorithm. From the numerically obtained LL wave function $\psi_{B,c}(x_1, x_2, x_3, t)$ we calculate the momentum distribution $n_B(k, t)$, the SP density $\rho_c(x, t)$, natural orbitals and their occupancies, and study their evolution during free expansion from the box ground state.

First let us explore the dynamics of the wave function $\psi_{B,c}(x_1, x_2, x_3, t)$. Figure 3.5 displays contour plots of the probability density $|\psi_{B,c}(0, x_2, x_3, t)|^2$ for $c = 1$, at two different times, $t = 0$ and $t = 3$. We see that as the LL gas expands, the probability density decreases at the hyperplanes $x_i = x_j$ ($i \neq j$) where the particles are in contact. This is in agreement with the result of Section 3.1, where it was shown (by using the stationary phase approximation) that the leading term of $\psi_{B,c}(\xi_1 t, \xi_2 t, \xi_3 t, t)$ has Tonks-Girardeau form for sufficiently large t; that is, the leading term is zero for $\xi_i = \xi_j$ ($i \neq j$). However, this does not necessarily mean that the properties of such an asymptotic state correspond to the properties of a TG gas, which was usually studied in the ground state of some external potential. For example, suppose that the initial state is a weakly correlated ground state in the box; despite the fact that, during expansion, the particles get strongly correlated in the close vicinity of the hyperplanes of contact, the absence of correlations in the initial state sur-
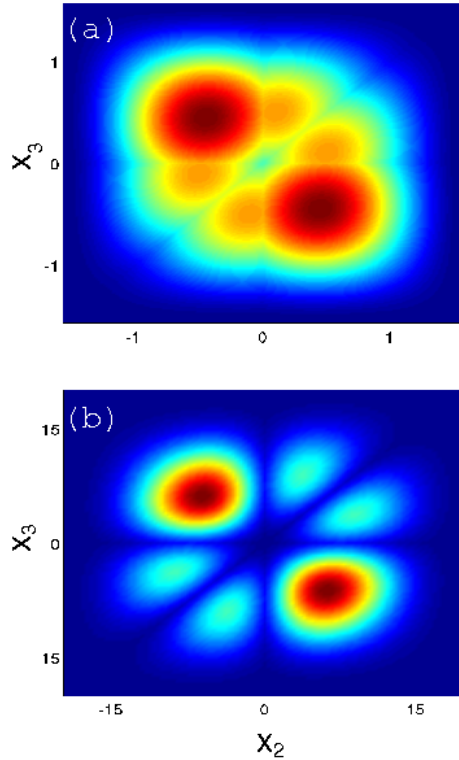
Figure 3.5: Contour plots of $|\psi_{B,c}(0, x_2, x_3, t)|^2$ for $c = 1$ at (a) t=0, and (b) t=3. As the time t increases, the probability density at the hyperplanes where particles are in contact decreases.

vives as an overall feature through to the asymptotic state (see the discussion in Section 3.1 and the second item of Ref. [34]). Thus, even though that the asymptotic state is described by a wave function with the TG structure, the physical properties of the expanded gas can considerably differ from the properties of a TG gas.

In order to further study the properties of the state in expansion, Fig. 3.6 illustrates the occupation of the lowest natural orbital in time, $\lambda_1(t)$, for several values of c. The asymptotic values of the occupancies, which are obtained by using the asymptotic forms of the wave functions (see Section 3.1), are indicated with horizontal lines. We observe that the occupancy of the leading NO, $\lambda_1(t)$, decreases during time evolution. However, for the plotted interaction strengths, the decrease of $\lambda_1(t)$ is not too large. This means that the coherence of the system (described by the occupations of the natural orbitals) for

38
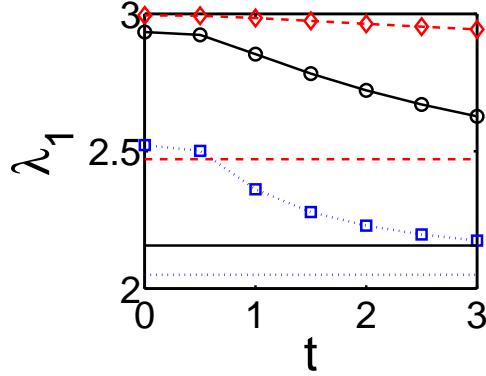
Figure 3.6: The lowest natural orbital $\lambda_1(t)$ as a function of time for three values of c. Red diamonds (dashed line) is for $c = 0.25$, black circles (solid line) for $c = 1$, and blue squares (dotted line) for $c = 5$; the lines connecting the markers are guides for the eye. The corresponding horizontal lines without markers denote the asymptotic occupancies, calculated from the asymptotic wave functions (see Chapter 2).

the plotted parameters only partially decreases during free expansion due to the interactions. It should be noted that in the TG limit $c \to \infty$, for hard-core bosons on the lattice [47], it has been shown that the leading natural orbitals slightly increase during free expansion [47], which differs from the finite c results obtained here. It is reasonable to associate the decrease of $\lambda_1(t)$ to the change of the LL wave functions at the hyperplanes of contact; this change does not occur in the TG regime, where the wave functions are zero at the contact hyperplanes at any time of the expansion.

Let us explore the dynamics of the momentum distribution $n_B(k,t)$, and its connection to the SP density $\rho_c(x,t)$ at large times t. The time-evolution of $\rho_c(x,t)$ and $n_B(k,t)$ is illustrated in Figs. 3.7 and 3.8; we display x- and k-space densities for various values of the parameter c, at several times t. Initially, all momentum distributions have a typical bosonic property: they peak at $k = 0$. We observe that the qualitative changes in the shape of $n_B(k,t)$ are more pronounced for larger values of c. Circles in Figs. 3.7 and 3.8 show the asymptotic values calculated by using Eqs. (3.31) and (3.32). We see that at the maximal value of time t in the plots, the momentum distribution agrees well with that obtained with the stationary phase approximation in Eq. (3.31). Our numerical calculation is in agreement with the findings presented

in Eqs. (3.31) and (3.32). We would like to point out that, even though the observables $n_B(k,t)$ and $\rho_c(x,t)$ are well approximated by the stationary phase approximation at the maximal expansion time reached in our numerical simulations (see Figs. 3.7 and 3.8), the system is strictly speaking not yet fully in the asymptotic regime (e.g., note that the occupancies of the natural orbitals have not reached their asymptotic values) and even better agreement should be expected at larger times. Unfortunately, the maximal time allowed in our numerical calculations is limited by the computer memory and time.

In order to further study the asymptotic forms of the momentum distribution and the SP density, let us calculate the asymptotic expansion velocity as a function of the interaction parameter c. Since different parts of the cloud expand at different velocities, a definition of this quantity has a certain degree of freedom. Here we define this quantity as a root mean square of the asymptotic SP density [82] in variable $\xi = x/t$ (i.e., velocity):

$$\xi_\infty = \sqrt{\frac{1}{N} \int \xi^2 \rho_\infty(\xi) d\xi};$$

(3.33)

the factor $1/N$ simply reflects the fact that $\rho_\infty(\xi)$ is normalized to the number of particles N. The asymptotic velocity ξ_∞ is connected to the total energy E stored in the system. During free expansion, the interaction energy is transferred to the kinetic energy; in the asymptotic regime all of the energy is kinetic, and it can be expressed via the momentum distribution:

$$E = \int k^2 n_{B,\infty}(k) dk.$$

(3.34)

By using Eqs. (3.31) and (3.32), we obtain

$$\xi_\infty = \sqrt{\frac{4}{N}} \sqrt{E},$$

(3.35)

that is, $E = N\xi_\infty^2/4$ which is the classical expression for the kinetic energy of N particles with velocity ξ_∞ and mass $1/2$ (recall that we use units where the kinetic energy operator in Eq. (2.11) is $-\sum_{i=1}^{N} \partial^2/\partial x_i^2$). The quantities $\sqrt{E}$ and ξ_∞ are displayed in Fig. 3.9 for various values of the interaction strength c; the plots underpin Eq. (3.35). The total energy was calculated simply as
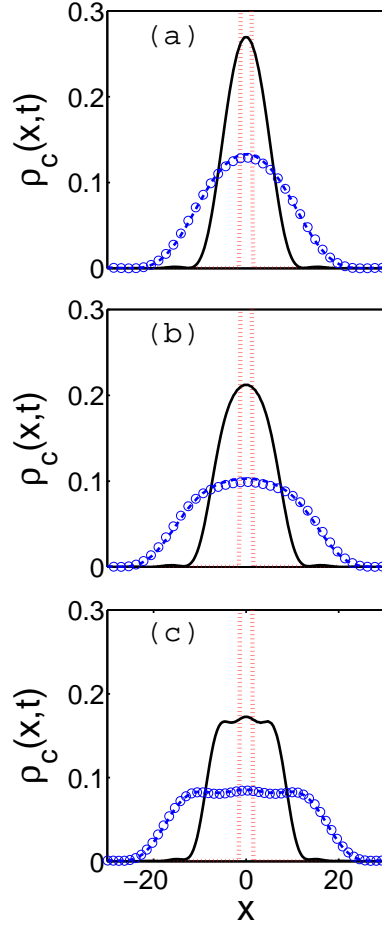
Figure 3.7: Evolution of the x-space density in time for various interaction strengths c: (a) $c = 0.25$, at $t = 0$ (red dotted line), $t = 2$ (solid black line), $t = 4$ (blue dashed line); (b) $c = 1$, at $t = 0$ (red dotted line), $t = 2$ (solid black line), $t = 4$ (blue dashed line); (c) $c = 10$, at $t = 0$ (red dotted line), $t = 1$ (solid black line), $t = 3$ (blue dashed line). The asymptotic x-space density $\rho_\infty(\xi)$ (circles), is plotted as a function of $x = \xi t$ corresponding to the largest time in each subplot.
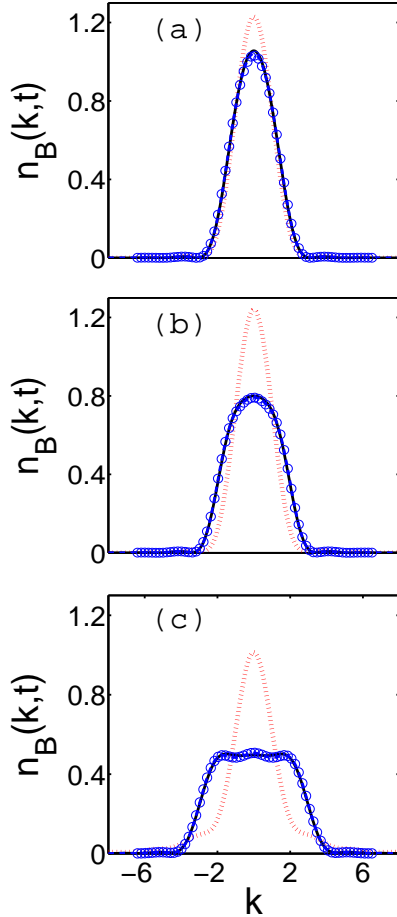
Figure 3.8: Evolution of the momentum distribution in time for various interaction strengths c. The lines and colors for different values of c and t are identical as in Fig 3.7. Solid black and blue dashed line are almost indistinguishable.

$E = q_1^2 + q_2^2 + q_3^2$ where quasimomenta q_i are obtained by solving transcendental Bethe equations for the initial state [36] (see Appendix B). The asymptotic velocity was obtained via Eq. (3.34) by numerical integration. Our numerical calculations are in good agreement (better than 99%) with Eq. (3.35); we attribute the discrepancy to inaccuracy of the numerical integration.
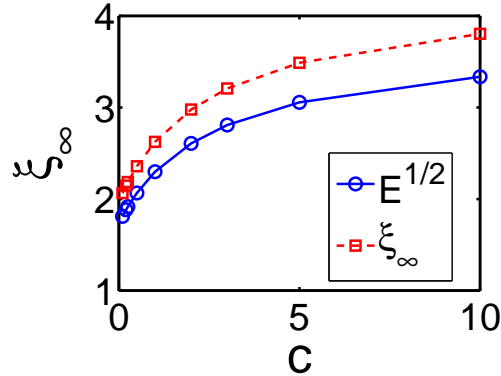
Figure 3.9: Asymptotic expansion velocity, ξ_∞ (squares, dashed line), and the square root of the total energy, $\sqrt{E}$ (circles, solid line) for various interaction strengths c; lines serve to guide the eye (see text for details).

3.8 Conclusion

We have derived the asymptotic form of the wave function describing a freely expanding Lieb-Liniger gas. It is shown to have the Tonks-Girardeau structure [see Eq. (3.9)], that is, the wave functions vanish when any two of the particle coordinates coincide. We have pointed out that the properties of these asymptotic states can significantly differ from the properties of a TG gas in a ground state of an external potential (see Fig. 3.1). The dependence of the asymptotic state on the initial state was discussed [see Eq. (3.14)]. The analysis was performed for time-dependent Lieb-Liniger wave functions which can be obtained through the Fermi-Bose transformation (2.15). This encompasses initial conditions which correspond to the ground state of a repulsive Lieb-Liniger gas in physically realistic external potentials. Thus, our analysis characterizes the free expansion from such a ground state, after the potential is suddenly switched off. In deriving our main result, Eq. (3.9), we have used the stationary phase approximation. This generalizes and adds upon the result from Ref. [34] which was derived for a particular family of time-dependent Lieb-Liniger wave functions. We have demonstrated that the interaction energy of the freely expanding LL gas asymptotically decays according to a power law, $E_{int} \propto t^{-3}$. Furthermore, we have calculated the asymptotic single-particle density for free expansion of a LL gas from an infinitely deep box potential. We have compared our exact calculation with the hydrodynamic approxima-

43

tion introduced in Ref. [12], and employed in Ref. [52] in the context of free expansion, obtaining good agreement for all values of the interaction strength.

For sufficiently large times the momentum distribution coincides (up to a scaling transformation) with the shape of the real-space single-particle density (the expansion is asymptotically ballistic). This result can be considered as a generalization of the dynamical fermionization of the momentum distribution in the Tonks-Girardeau regime, which has been pointed to occur in the course of free expansion [47, 49]. We have shown that the occupancy of the lowest natural orbital of the system decreases with time while approaching its asymptotic value. This was related to the build-up of correlations of the hyperplanes of contact of the particles. Finally, we have calculated the expansion velocity in asymptotic regime and pointed out its relation to the overall energy of the system.

We have numerically studied free expansion of a few Lieb-Liniger bosons, which are initially in the ground state of an infinitely deep hard-wall trap. This numerical calculation has been carried out by employing a standard Fourier transform, as follows from the Fermi-Bose transformation for a time-dependent Lieb-Liniger gas. We have studied the evolution of the momentum distribution, the real-space single-particle density, and the occupancies of natural orbitals, both in the non-trivial transient regime of the expansion and asymptotically. We have derived analytically (by using the stationary phase approximation) the formula which connects the asymptotic shape of the momentum distribution and the initial state. In order to gain further understanding of a freely expanding LL gas, it would be desirable to investigate transient dynamics of the observables for larger number of particles, and also for different initial conditions (e.g., the ground state of a LL gas in different initial trapping potentials).

Chapter 4

Reflection of a Lieb-Liniger wave packet from the hard-wall potential

We have already outlined in Chapter 2, and used in Chapter 3 an interesting exact method which has been discovered by Gaudin way back in 1983 [32]: A time-dependent Lieb-Liniger wave function on an infinite line, in the absence of an external potential, can be constructed by acting with a differential operator (which contains the interaction strength parameter c) onto a time-dependent wave function describing noninteracting (spin polarized) 1D fermions [32, 34] (see also Chapter 2). For dynamics of a Lieb-Liniger wave packet comprised of N particles, this method reduces to finding an N-dimensional Fourier transform, which can be used to extract the asymptotic behavior of the wave function and some observables during the course of 1D free expansion (see Chapters 2 and 3). In this chapter we investigate the possibility of extending this approach to study dynamics of a Lieb-Liniger wave packet in the presence of the hard-wall potential,

$$V(x) = \begin{cases} 0, & \text{if } x > 0 \\ \infty, & \text{if } x \leq 0. \end{cases} \tag{4.1}$$

Our interest in quantum dynamics in the presence of the hard-wall potential is in part motivated by experiments. More specifically, the interaction of Bose-

Einstein condensates (BEC) with surfaces is of interest for implementations of atom interferometry on chips [83]. A BEC falling under gravity, and then reflecting from a light-sheet, has been experimentally and theoretically studied in Ref. [84]. Moreover, one of the prominent experimental activities nowadays is deceleration of atomic beams by reflection from a moving mirror. This work first started with neutrons being cooled by reflecting from a moving Ni surface [85]. In cold atoms physics, there have been several experiments for manipulation and slowing down atomic beams with the use of reflection mirrors [86, 87, 88].

In this chapter we explore, by using exact methods, dynamics of Lieb-Liniger wave packets in the presence of the hard-wall potential, more specifically, reflection of a Lieb-Liniger wave packet from such a wall. The outline of the chapter is as follows. In Sec. 4.1 we outline the construction of eigenstates in the given external potential. In Sec. 4.2 we analytically discuss time-dependent quantum dynamics of the system which starts from a general initial condition. By employing the symmetries of the Lieb-Liniger eigenstates, we demonstrate that a time-dependent Lieb-Liniger wave packet reflecting from the wall can be calculated by solving an N-dimensional Fourier transform, where N is the number of particles. This opens the way to calculate the asymptotic properties of the wave packet by employing the stationary phase approximation as in Chapter 3 for free expansion. In Sec. 4.3 we utilize the formalism to numerically study dynamics of single-particle density and momentum distribution of a few-body wave packet reflecting from the wall. We find that the wave packets for smaller interaction strength c get reflected at a slower rate, because they get compressed more strongly as the wave packet hits the wall. The interference fringes which occur during the dynamics have larger visibility for smaller values of c.

4.1 Eigenstates in the presence of the hard-wall potential

In the present chapter, we focus ourselves on the dynamics (in time) of a Lieb-Liniger wave packet in the presence of the hard-wall potential (4.1). We will show that the solution of this problem can be constructed by solving an

N-dimensional Fourier transform. To this end, we need eigenstates of a Lieb-Liniger gas in the hard-wall potential. First, let us write down the Lieb-Liniger eigenstates in free space (i.e., $x \in (-\infty, \infty)$ without external potentials and any boundary conditions):

$$
\begin{aligned}
\psi_{\{k\}} &= \mathcal{N}(\{k\}) \sum_P (-1)^P \prod_{i<j} \left[\text{sgn}(x_j - x_i) + \frac{i}{c}(k_{Pj} - k_{Pi}) \right] e^{i \sum_j k_{Pj} x_j} \\
&= \mathcal{N}(\{k\}) \sum_P (-1)^P a(P, \{k\}) e^{i \sum_j k_{Pj} x_j}
\end{aligned}
\tag{4.2}
$$

where $\{k\} = \{k_m \,|\, m = 1, \ldots, N\}$ is a set of (real) distinct quasimomenta which uniquely determine the eigenstate, P denotes a permutation of N numbers, $P \in S_N$, and we have implicitly defined $a(P, \{k\})$. The normalization of these eigenstates is given by [44, 45]

$$
\frac{1}{\mathcal{N}(\{k\})} = \sqrt{N!(2\pi)^N \prod_{i<j} \left[1 + \left(\frac{k_j - k_i}{c} \right)^2 \right]},
$$

that is, within the fundamental sector in k-space, $k_1 < \cdots < k_N$ and $k_1' < \cdots < k_N'$, we have

$$
\int_{-\infty}^{\infty} \psi_{\{k\}}^* \psi_{\{k'\}} dx_1 \cdots dx_N = \prod_{j=1}^N \delta(k_j - k_j').
\tag{4.3}
$$

The Lieb-Liniger eigenstates in the presence of the hard-wall (denoted by $\phi_{\{k\}}$) were first constructed by Gaudin [36] as a superposition of 2^N free-space eigenstates. This superposition obeys the hard-wall boundary condition: $\phi_{\{k\}}(x_1 = 0, x_2, \ldots, x_N) = 0$ in the fundamental sector $R_1 : x_1 < x_2 < \ldots < x_N$ of x-space. These eigenstates are expressed as follows:

$$
\phi_{\{k\}} = \sum_{\{\epsilon\}} A(\{\epsilon\}, \{k\}) \psi_{\{\epsilon k\}},
\tag{4.4}
$$

where $\{\epsilon\} = \{\epsilon_m \,|\, \epsilon_m \in \{-1, 1\}, m = 1, \ldots, N\}$ and $\{\epsilon k\} = \{\epsilon_m k_m \,|\, \epsilon_m \in \{-1, 1\}, m = 1, \ldots, N\}$; evidently, there are 2^N such sets and therefore 2^N

terms in the sum (4.4). The quantity $A(\{\epsilon\}, \{k\})$ is defined by

$$A(\{\epsilon\}, \{k\}) = \epsilon_1 \cdots \epsilon_N \ A'(\epsilon_1 k_1, \epsilon_2 k_2, \ldots, \epsilon_N k_N), \qquad (4.5)$$

where

$$A'(k_1, k_2, \ldots, k_N) \equiv \frac{\prod_{i<j} \left[1 + \frac{i}{c}(k_j + k_i)\right]}{\sqrt{\prod_{i<j} \left[1 + \left(\frac{k_j+k_i}{c}\right)^2\right]}}, \qquad (4.6)$$

are the coefficients utilized in the superposition. It is straightforward to verify that indeed $\phi_{\{k\}}(x_1 = 0, x_2, \ldots, x_N) = 0$ in the fundamental sector R_1 [36].

However, it is not simple to prove that these eigenstates are orthogonal and normalized. This is of key importance if one wishes to project some initial state onto these eigenstates and calculate time-evolution in the standard fashion via superposition over eigenstates. In Section 4.3 we discuss the normalization of eigenstates (4.4), and based on our numerical investigations conjecture that these eigenstates are orthogonal and normalized.

4.2   Many-body dynamics in time via a Fourier transform

In this section we demonstrate that a solution of the time-dependent equation (2.11) with the hard-wall potential (4.1) can be expressed in terms of an N-dimensional Fourier transform. We assume that at time $t = 0$ the wave packet is localized in the vicinity of the wall. For example, the initial state ψ_0 can be the ground state wave function in some external trapping potential; if at $t = 0$ this potential is suddenly turned off, the wave packet will start expanding and some of its components will be reflected from the wall which will give rise to interference effects. Such a scenario is possible to create with today's experimental capabilities [7]. One possible (similar) scenario is as follows: suppose that at $t = 0$ the aforementioned trapping potential is turned off, and that in the next instance the many body wave packet is given some momentum kick, say towards the wall; the reflection and interference phenomena will depend on the interactions and imparted momentum. During the reflection, particles will collide and one may ask to which extent will the initial conditions

be forgotten (or blurred) after the reflection?

To describe quantum dynamics from the initial conditions described above, we write the initial state ψ_0 as a superposition over complete set of eigenstates $\phi_{\{k\}}$:

$$\psi_0 = \int_{0<k_1<\cdots<k_N} b(k_1,\ldots,k_N)\phi_{\{k\}}dk_1\ldots dk_N. \tag{4.7}$$

The subsequent derivation is based on the following two relations obeyed by the eigenstates $\phi_{\{k\}}$:

$$\phi_{\{k\}} = (-1)^P \phi_{\{Pk\}}, \tag{4.8}$$

and

$$\phi_{\{k\}} = -\phi_{\{k_1,\ldots,k_{j-1},-k_j,k_{j+1}\ldots,k_N\}}. \tag{4.9}$$

Equation (4.8) follows from the definition of $\phi_{\{k\}}$ in Eq. (4.4), and the fact that the Lieb-Liniger eigenstates in free space $\psi_{\{k\}}$ obey identical relation: $\psi_{\{k\}} = (-1)^P \psi_{\{Pk\}}$; this identity can be traced to the fact that $\psi_{\{k\}}$ are antisymmetric with respect to the interchange of any two variables k_i and k_j [44]. The derivation of Eq. (4.9) is straightforward. Let us define a set $\{\epsilon'\}$, which corresponds to the set $\{\epsilon\}$ as follows: $\{\epsilon'_1,\ldots,\epsilon'_N\} = \{\epsilon_1,\ldots,\epsilon_{j-1},-\epsilon_j,\epsilon_{j+1},\ldots,\epsilon_N\}$; it is evident from the definition (4.4) that $\phi_{\{k\}} = \sum_{\{\epsilon'\}} A(\{\epsilon'\},\{k\})\psi_{\{\epsilon'k\}}$. Furthermore, let us denote $\{k'\} = \{k_1,\ldots,k_{j-1},-k_j,k_{j+1}\ldots,k_N\}$, i.e., the set of k-values $\{k'\}$ is identical to the set $\{k\}$ except that k_j is reversed in sign. By using $A(\{\epsilon\},\{k\}) = -A(\{\epsilon'\},\{k'\})$ and $\{\epsilon'k'\} = \{\epsilon k\}$ we have

$$\phi_{\{k'\}} = \sum_{\{\epsilon'\}} A(\{\epsilon'\},\{k'\})\psi_{\{\epsilon'k'\}} = -\sum_{\{\epsilon\}} A(\{\epsilon\},\{k\})\psi_{\{\epsilon k\}} = -\phi_{\{k\}}, \tag{4.10}$$

that is, we obtain Eq. (4.9). We note in passing that if any $k_j = 0$, then $\phi_{\{k\}} = 0$, which follows from Eq. (4.9); furthermore, $\phi_{\{k\}}$ is also zero whenever any two of the quasimomenta k_i and k_j are equal.

Due to the symmetry of the hard-wall eigenstates $\phi_{\{k\}}$ presented in Eqs. (4.8) and (4.9), a complete set of eigenstates is spanned in the region of the k-space defined by $0 < k_1 < \ldots < k_N$, which we will refer to as the fundamental region in k-space, and denote it with Q_1^+. Hence, the integral in Eq. (4.7) spans over Q_1^+. Furthermore, by employing relations (4.8) and (4.9), ψ_0 can

be written as an integral over the whole k-space:

$$\psi_0 = \int_{-\infty}^{\infty} dk_1 \cdots dk_N G_{hw}(k_1, \ldots, k_N) e^{i \sum_j k_j x_j}, \qquad (4.11)$$

where the function G_{hw} is defined as

$$G_{hw}(k_1, \ldots, k_N) = b(k_1, \ldots, k_N) A'(k_1, \ldots, k_N) \mathcal{N}(\{k\})$$
$$\times \prod_{i<j} \left[\operatorname{sgn}(x_j - x_i) + \frac{i}{c}(k_j - k_i) \right]. \qquad (4.12)$$

From Eq. (4.12) it immediately follows that the time-evolution of a Lieb-Liniger wave packet in the presence of the hard-wall can be calculated from an N-dimensional Fourier transform.

In order to derive Eqs. (4.11) and (4.12), first note that due to (4.8) and (4.9), the projection coefficients satisfy

$$b(k_1, \ldots, k_N) = (-1)^P b(k_{P1}, \ldots, k_{PN}), \qquad (4.13)$$

and

$$b(k_1, \ldots, k_N) = -b(k_1, \ldots, k_{j-1}, -k_j, k_{j+1}, \ldots, k_N); \qquad (4.14)$$

the latter identity can conveniently be rewritten as

$$b(k_1, \ldots, k_N) = \epsilon_1 \cdots \epsilon_N b(\epsilon_1 k_1, \ldots, \epsilon_N k_N). \qquad (4.15)$$

By employing the symmetries of the Lieb-Liniger hard-wall eigenstates, which are inherited by the expansion coefficients $b(k_1, \ldots, k_N)$, Eq. (4.7) can be rewritten as follows:

$$\psi_0 = \frac{1}{N!} \int_{k_1>0,\ldots,k_N>0} dk_1 \cdots dk_N b(k_1, \ldots, k_N) \sum_{\{\epsilon\}} A(\{\epsilon\}, \{k\})$$
$$\times \mathcal{N}(\epsilon_1 k_1, \ldots, \epsilon_N k_N) \sum_P (-1)^P a(P, \{\epsilon k\}) e^{i \sum_j \epsilon_{Pj} k_{Pj} x_j} \qquad (4.16)$$
$$= \frac{1}{N!} \int_{k_1>0,\ldots,k_N>0} dk_1 \cdots dk_N \sum_{\{\epsilon\}} b(\epsilon_1 k_1, \ldots, \epsilon_N k_N) A'(\epsilon_1 k_1, \ldots, \epsilon_N k_N)$$
$$\times \mathcal{N}(\epsilon_1 k_1, \ldots, \epsilon_N k_N) \sum_P (-1)^P a(P, \{\epsilon k\}) e^{i \sum_j \epsilon_{Pj} k_{Pj} x_j} \qquad (4.17)$$

50

$$
= \frac{1}{N!} \int_{-\infty}^{\infty} dk_1 \cdots dk_N \; b(k_1, \ldots, k_N) A'(k_1, \ldots, k_N)
$$

$$
\times \mathcal{N}(k_1, \ldots, k_N) \sum_P (-1)^P a(P, \{k\}) e^{i \sum_j k_{Pj} x_j} \tag{4.18}
$$

$$
= \frac{1}{N!} \sum_P \int_{-\infty}^{\infty} dk_1 \cdots dk_N \; b(k_{P1}, \ldots, k_{PN}) A'(k_{P1}, \ldots, k_{PN})
$$

$$
\times \mathcal{N}(k_{P1}, \ldots, k_{PN}) a(P, \{k\}) e^{i \sum_j k_{Pj} x_j} \tag{4.19}
$$

$$
= \frac{1}{N!} \sum_P \int_{-\infty}^{\infty} dk_{P1} \cdots dk_{PN} \; b(k_{P1}, \ldots, k_{PN}) A'(k_{P1}, \ldots, k_{PN})
$$

$$
\times \mathcal{N}(k_{P1}, \ldots, k_{PN}) a(P, \{k\}) e^{i \sum_j k_{Pj} x_j}, \tag{4.20}
$$

from which we immediately obtain Eqs. (4.11) and (4.12) because the sum over all permutations P is a sum over $N!$ identical integrals. In the derivation above, the first identity, Eq. (4.16), follows from the properties (4.8) and (4.13). The second identity (4.17) is due to (4.15) and the definition of $A(\{\epsilon\}, \{k\})$ in Eq. (4.5). By employing Eqs. (4.9) and (4.15), the sum over $\{\epsilon\}$ in Eq. (4.17) can be replaced by integrating over the whole k-space to obtain the third equality, Eq. (4.18). By using identities $A'(k_{P1}, \ldots, k_{PN}) = A'(k_1, \ldots, k_N)$ and $\mathcal{N}(k_{P1}, \ldots, k_{PN}) = \mathcal{N}(k_1, \ldots, k_N)$, together with Eq. (4.13), we obtain (4.19).

The time-dependent solution of the many-body Schrödinger Eq. (2.11) with $V(x)$ given by (4.1) is simply

$$
\psi = \int_{-\infty}^{\infty} dk_1 \ldots dk_N G_{hw}(k_1, \ldots, k_N) e^{i \sum_j (k_j x_j - k_j^2 t)}. \tag{4.21}
$$

Thus, by knowing the function G_{hw} which contains all information about the initial condition, and which is simply related to the projection coefficients $b(k_1, \ldots, k_N)$ of the initial state onto hard-wall Lieb-Liniger eigenstates $\phi_{\{k\}}$, we can compute the time-dependent Lieb-Liniger wave function in the hard-wall potential by employing the Fourier transform. With this identification, an exact analysis of this many-body problem is at least conceptually considerably simplified.

We note that the asymptotic behavior of the many-body state and the observables such as single-particle density or momentum distribution can be straightforwardly extracted from expression (4.21) by using the stationary

phase approximation, as it was done in Chapter 3 for the case of free expansion of a Lieb-Liniger gas [e.g., see (3.9), (3.31), and (3.32)]. From these methods, and Eqs. (4.21) and (4.12), it follows that the initial conditions are imprinted into asymptotic states. It is straightforward to infer that the asymptotic wave functions, $\psi_\infty(\eta_1, \ldots, \eta_N, t) = \psi(\eta_1 t, \ldots, \eta_N t, t)$ for sufficiently large t, vanish at the hyperplanes of contact between particles $\eta_i = \eta_j$ $(i \neq j)$, which is characteristic for Tonks-Girardeau wave functions [2]. However, it should be emphasized that the properties of such asymptotic states can considerably differ from the physical properties of a Tonks-Girardeau gas in the ground state of some trapping potential (see Chapter 3 and also the second item of Ref. [34]). Moreover, the asymptotic momentum distribution coincides, up to a simple scaling transformation, with the shape of the asymptotic single-particle density in x-space, reflecting the fact that the dynamics is asymptotically ballistic (see Chapter 3); this means that at asymptotic times, despite of the fact that the wave functions have attained the Tonks-Girardeau structure, interactions do not affect the dynamics any more. From the connection between the asymptotic momentum distribution and single-particle density one finds that the asymptotic momentum distribution is zero at $k = 0$, and it is located on the positive k-axis, which simply means that for sufficiently large times the particles move away from the wall.

4.3 Example: A Lieb-Liniger wave packet incident on the hard wall

In this section we study a specific example of a localized Lieb-Liniger wave packet comprised of a $N = 3$ particles reflecting from the hard-wall potential. More specifically, we assume that for $t < 0$ the Lieb-Liniger system is in the ground state of an infinitely deep box denoted by $\psi_{g.s.}(x_1, x_2, x_3)$. The analytic expression for this ground state was found in Ref. [36]; for reasons of completeness, in Appendix B we present its construction. In our simulations, the box is in the interval $[1.5\pi, 2.5\pi]$, i.e., $\psi_{g.s.}(x_1, x_2, x_3)$ is zero whenever any x_i is outside of this interval. At $t = 0$ the box potential is suddenly turned off, and the wave packet is simultaneously (and suddenly) imparted some momentum of magnitude $K \geq 0$ towards the wall: $\psi(x_1, x_2, x_3, t = 0) =$
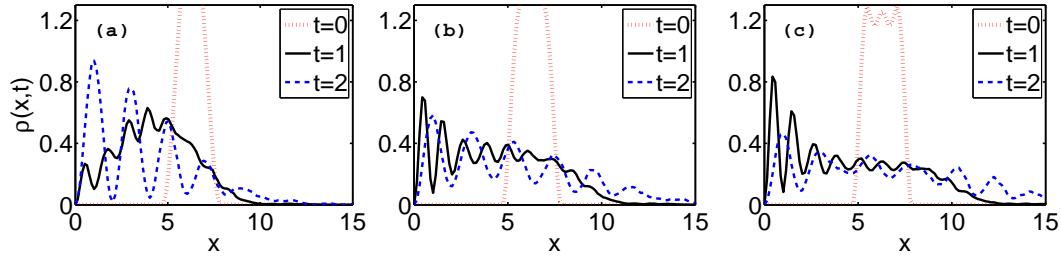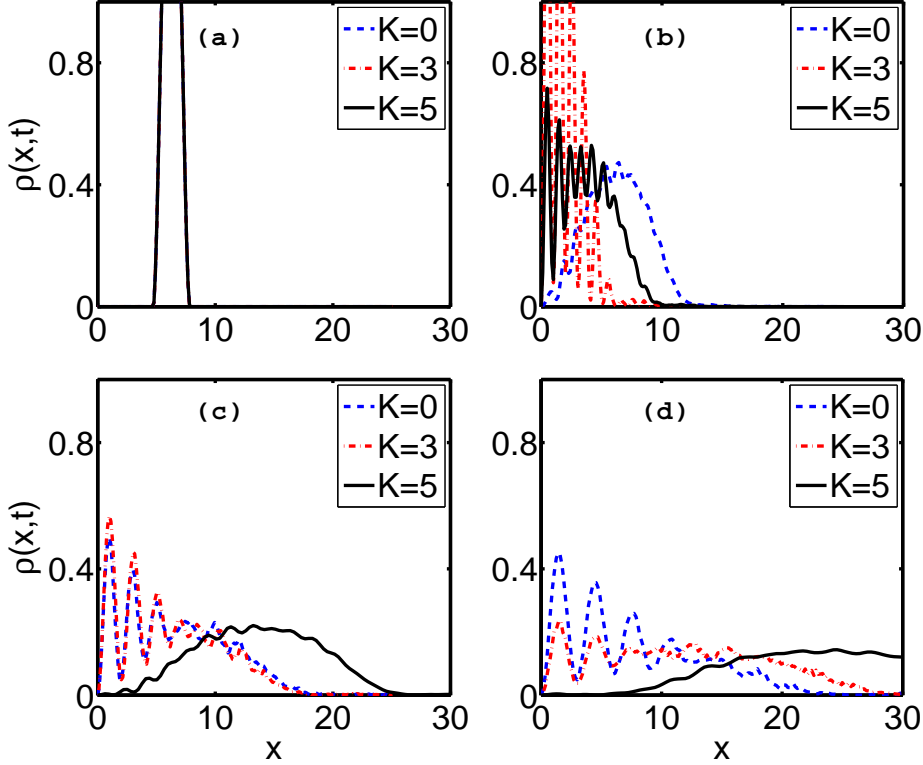
Figure 4.1: Density evolution of a Lieb-Liniger wave packet comprised of $N = 3$ bosons, which is given some momentum kick K (per particle) towards the wall. Insets correspond to the interaction strengths (a) $c = 0.25$, (b) $c = 3$, and (c) $c = 10$. The imparted momentum is $K = 1$. Red dotted lines are for $t = 0$, black solid lines are for $t = 1$, and blue dashed-lines are for $t = 2$.
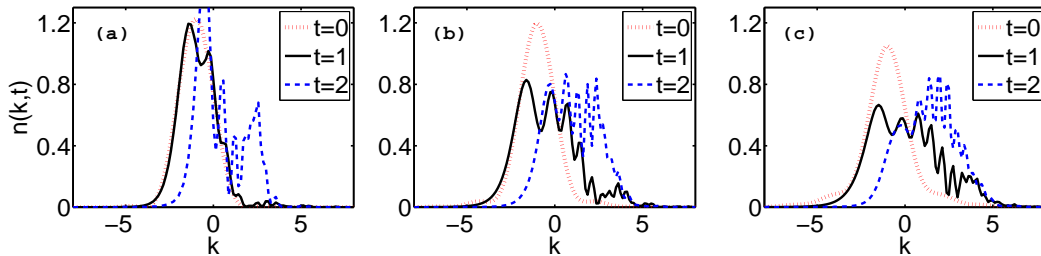
Figure 4.2: The same as in Fig. 4.1 but for the momentum distribution

$\psi_{g.s.}(x_1, x_2, x_3) \exp[-iK(x_1 + x_2 + x_3)]$; apparently, K denotes the imparted momentum per particle. From such an initial state, we are able to find projection coefficients $b(k_1, k_2, k_3)$ defined in Eq. (4.7), that is, we can find the corresponding function $G_{hw}(k_1, k_2, k_3)$ which is needed to calculate the Fourier transform (4.21). The Fourier integral in (4.21) is in this particular example 3-dimensional, and it is calculated numerically by using the fast Fourier transform algorithm in MATLAB. This provides us with the time-dependent wave function $\psi(x_1, x_2, x_3, t)$, which we use to study dynamics of observables such as the single-particle (SP) density $\rho(x, t)$ or the momentum distribution $n(k, t)$.

First, let us explore the effect of the interactions on the reflections of a few-body Lieb-Liniger wave packet. In Figures 4.1 and 4.2 we plot the time-evolution of single-particle densities and distributions of the momenta, respectively. The plots are made at three different times, $t = 0$, 1, and 2, and for three values of the coupling parameter, $c = 0.25$, 3, and 10. The magnitude of

the imparted momentum per particle is $K = 1$. Note that the wave packets broaden in time due to the repulsive interactions between the particles, and also due to the wave dispersion effects; the wave packets for larger values of c spread at a faster rate than the wave packets for smaller c. From Figs. 4.1 and 4.2 we observe that wave packets with a larger interaction parameter c get reflected faster than the wave packets for smaller c; for wave packets with smaller repulsion between the particles (smaller c), the compression of the wave packet is stronger, and therefore reflection of the momenta occurs at a slower rate. We also observe that all wave packets exhibit interference fringes during the reflection process. However, we find the interference fringes to be deeper for smaller values of c, which follows from the fact that the wave packets for smaller c are more spatially coherent. This can be seen also from Fig. 4.2 which displays momentum distributions. The distribution $n(k,t)$ for $c = 0.25$, at the largest time shown $t = 2$, has one strong well-defined peak (the one closest to zero), and several smaller peaks of the wave components with larger magnitude of the momentum [see Fig. 4.2(a)]. In contrast, for $c = 10$ this most dominant peak close to $k = 0$ is much smaller [see Fig. 4.2(c)].

Next we explore dependence of the time-evolution on the imparted momentum. To this end we fix the interaction strength at $c = 1$, and observe the time-evolution for three different initial conditions (see Figs. 4.3 and 4.4): (i) expansion in the presence of the wall occurs when $K = 0$, (ii) reflection at an intermediate value $K = 3$, and (iii) for large value of the imparted momentum $K = 5$. The wave packets for $K = 3$ and 5 have the property that basically all of the initial momentum distribution is directed towards the wall, i.e., the distributions at $t = 0$ is on the negative k-axis. In contrast, exactly half of the initial momentum distribution of the wave packet for $K = 0$ is positive (negative). The basic distinction between these cases is that the wave packets with sufficiently large imparted momentum K get simply reflected from the wall and at larger times the interference fringes are almost negligible. For example, the wave packet with $K = 5$ is practically completely reflected from the wall at $t = 2$, see solid black lines in Figs. 4.3(c) and 4.4(c); the momentum distribution is on the positive k-axis and the interference fringes are essentially absent. In contrast, for $K = 0$ half of the momentum distribution is already positive (corresponding to motion away from the wall), and this part interferes with the reflected component at all times of the evolution. Note that the wave

54

Figure 4.3: Density evolution of a Lieb-Liniger wave packet comprised of $N = 3$ bosons, which is given some momentum kick K (per particle) towards the wall. Insets correspond to the times (a) $t = 0$, (b) $t = 1$, (c) $t = 2$, and (d) $t = 3$. The interaction strength is $c = 1$. Blue dashed-lines are for $K = 0$, red dot-dashed lines are for $K = 3$, and black solid lines are for $K = 5$.

packet with $K = 0$ is still in the process of reflection from the wall at $t = 2$ because a large fraction of its momentum distribution is still on the negative k-axis, see dashed blue line in Fig. 4.4(c); the interference fringes are the largest in this case, see dashed blue line in Fig. 4.3(c).

Exact solutions can serve as a benchmark to check the range of validity of other methods which may be used to analyze nonequilibrium dynamics of interacting systems. We have compared the solutions obtained with the Fourier transform method presented here with the so-called hydrodynamic formalism [12], which describes the Lieb-Liniger system via the nonlinear Schrödinger equation with variable nonlinearity [52]. In Figs. 4.5 (a)-(d), we show density profiles for two different couplings ($c = 0.25$ and $c = 3$) at two different times
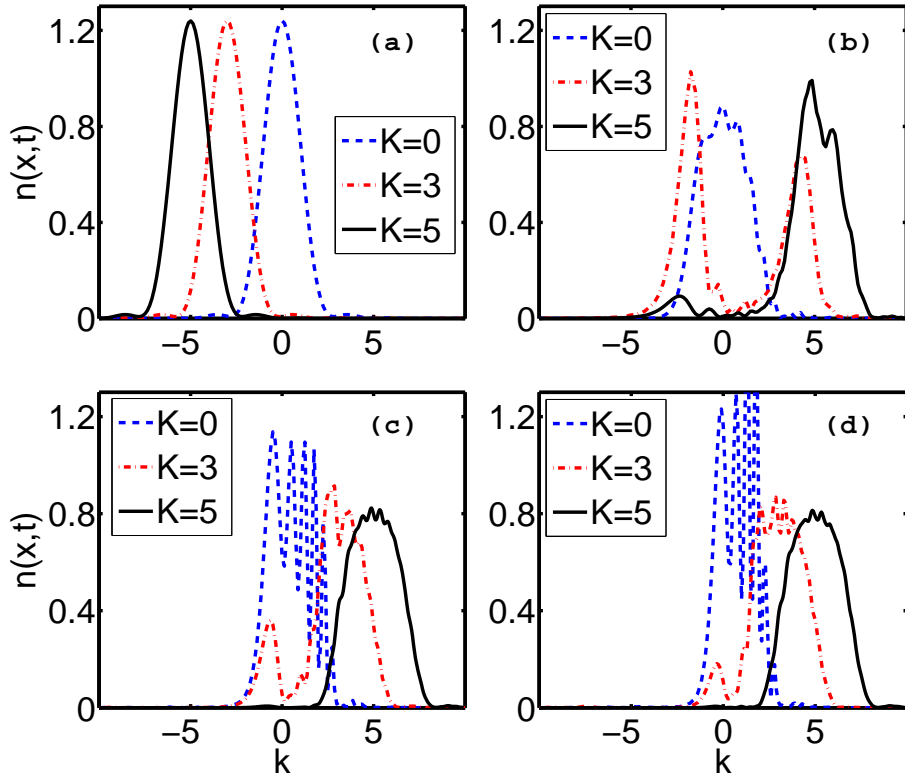
Figure 4.4: The same as in Fig. 4.3 but for the momentum distribution

($t = 1$ and $t = 2$). We find that the single-particle density (and momentum distribution), calculated within this method, are in good agreement with our simulations for small values of the coupling parameter c (up to $c = 1$); this upper limit for c also depends on the initial density of the 1D Bose gas, as it is well known that the effective interaction strength parameter is c divided by the linear density [1]. However, for larger values of c, the hydrodynamic formalism goes beyond its range of validity for the simulations presented here. For example, for the simulations at intermediate interaction strength $c = 3$ [see Figs. 4.5 (c) and (d)], the hydrodynamic formalism predicts deeper interference fringes than those obtained via the Fourier transform method; this is attributed to the fact that the hydrodynamic formalism overestimates the spatial coherence of the wave packet [12, 52]. For sufficiently large c, the system is in the Tonks-Girardeau regime, and one can employ the Fermi-Bose mapping [2, 46] to study the dynamics. In Fig. 4.5 (e) and (f) we compare
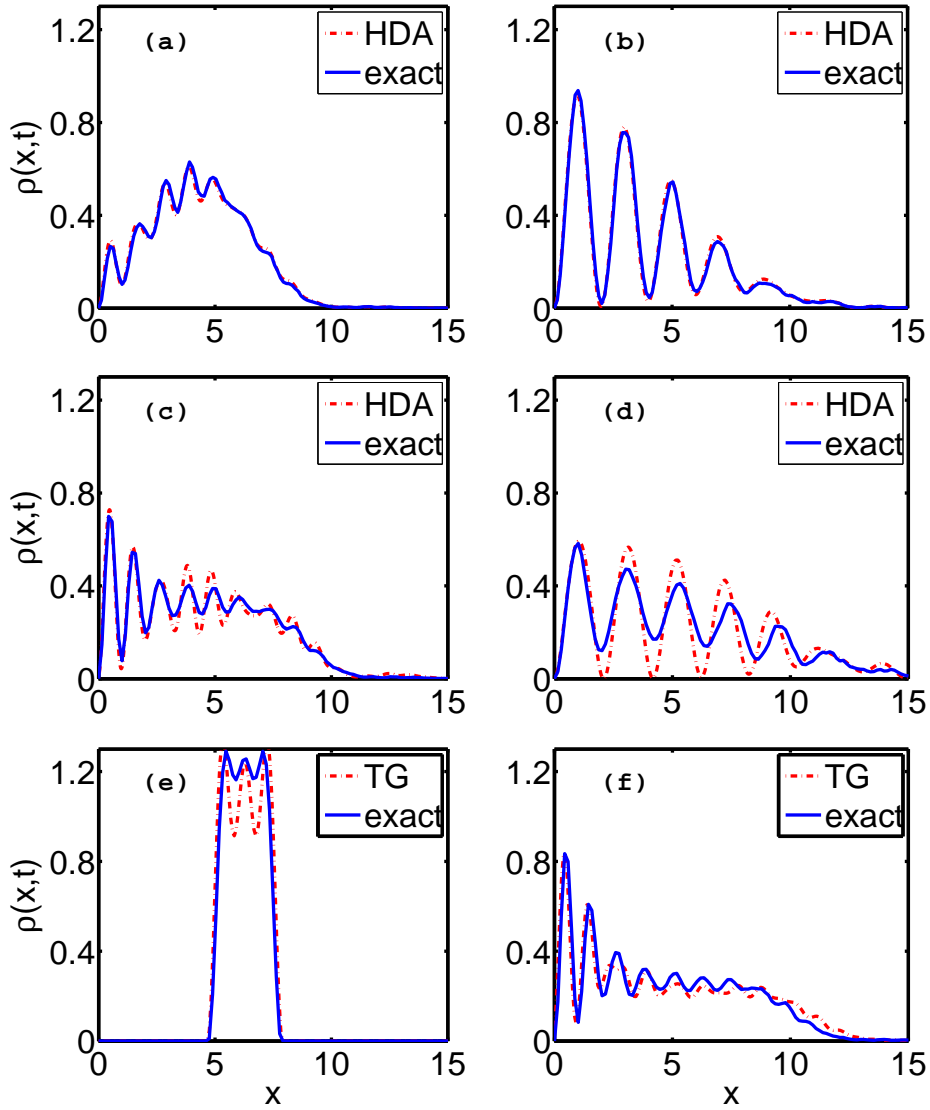
Figure 4.5: Comparison of the density evolution in the exact calculation, with the hydrodynamic approximation (HDA) [(a)-(d)], and the Fermi-Bose mapping [(e) and (f)] valid in the Tonks-Girardeau (TG) regime. The interaction strengths c and times t in the insets are: (a) $c = 0.25$, $t = 1$; (b) $c = 0.25$, $t = 2$; (c) $c = 3$, $t = 1$; (d) $c = 3$, $t = 2$; (c) $c = 10$, $t = 0$; (d) $c = 10$, $t = 1$. The initially imparted momentum is $K = 1$ for all figures.

our calculation with that obtained via Fermi-Bose mapping ($c = \infty$, [2, 46]) for a large value of the interaction strength $c = 10$; we observe that qualitative features of the Tonks-Girardeau regime such as the N peaks in the initial single-particle density coincide in the two calculations, however, even larger c is needed to obtain better quantitative agreement.

4.3.1 Normalization of eigenstates

In order to numerically check our conjecture that the Lieb-Liniger hard-wall eigenstates defined in (4.4) are properly normalized, we have compared the initial state obtained via $\psi_{g.s.}(x_1, x_2, x_3) \exp[-iK(x_1 + x_2 + x_3)]$, and the wave function obtained via Eq. (4.11) by employing the function $G_{hw}(k_1, k_2, k_3)$, which is calculated from the projection coefficients $b(k_1, k_2, k_3)$ as in Eq. (4.12). We found that the relative agreement between the two wave functions is on the order of 1% or better, which is on the order of the numerical accuracy for the size of our numerical grid, which is limited by computer memory. We have performed this comparison for various initial conditions (different K and c values). Unfortunately, a rigorous proof of normalization of Lieb-Liniger hard-wall eigenstates is to the best of our knowledge still lacking.

4.4 Conclusion

We have studied reflections of a Lieb-Liniger wave packet from the hard-wall potential. By employing the symmetry of the many-body eigenstates with respect to the change of the sign and permutation of their quantum numbers (i.e., quasimomenta), that is, Equations (4.8) and (4.9), we have demonstrated that time-evolution of this interacting many-body wave packet can be represented in terms of an N-dimensional Fourier transform, where N is the number of particles in the wave packet. This result simplifies our understanding of the time-evolution in this many-body problem and enables straightforward calculation of the time-asymptotic properties of the system.

We have utilized the formalism to numerically study dynamics of single-particle density and momentum distribution of a few-body wave packet reflecting from the wall (the wave packet is initially close to the wall). Reflection dynamics and interference phenomena depend on the strength of the interac-

tion between the particles c and the imparted momentum K towards the wall. The wave packets for smaller c get reflected at a slower rate, because they get compressed more strongly as the wave packet hits the wall. Moreover, the interference fringes are deeper (larger visibility) for smaller values of c. If K is sufficiently large such that the initial momentum distribution is on the negative k-axis, the wave packet gets reflected and the interference fringes become small as soon as most of the momenta become positive. On the other hand, for $K = 0$, the interference effects are fairly large.

Chapter 5

Lieb-Liniger gas in a constant-force potential

For the finite coupling Lieb-Liniger gas (c finite), the method of Gaudin has been shown to be valid in the absence of any external potential (i.e., on an infinite line [34]), and has been used to study free expansion from localized initial conditions in Chapters 2 and 3; in this case the time-dependent wave function can be calculated via an N-dimensional Fourier transform. Interestingly, such a transform can be also utilized for a Lieb-Liniger gas reflecting from the wall (Chapter 4). However, Gaudin's method (at least in its current form) is not applicable to find eigenstates of a Lieb-Liniger gas in generic trapping potentials $V(x)$ (such as the harmonic oscillator); technically, this arises because the differential operator $\hat{O}_c$ does not generally commute with such potentials.

Here, we study the Lieb-Liniger model in the constant-force (linear) potential. Exact stationary solutions for this system are constructed (we call these wave functions the Lieb-Liniger-Airy states) by employing Gaudin's operator $\hat{O}_c$. The construction is enabled by the fact that this operator commutes with the linear (constant-force) potential. We calculate the ground-state properties of the Lieb-Liniger gas in the wedgelike potential [$V(x) = \alpha x$ for $x > 0$ ($\alpha > 0$), and ∞ otherwise] in the strongly interacting regime. This is achieved in the Tonks-Girardeau regime and below that regime in $1/c$ approximation by employing the pseudopotential approach [89]. Finally, we point out that the time-dependent Lieb-Liniger wave packets in the linear potential can be calculated via an N-dimensional Fourier transform.

5.1 Lieb-Liniger-Airy states

In this section we consider this system placed in a linear external potential. The stationary Schrödinger equation for the many-body wave function $\psi_B(x_1, \ldots, x_N)$ in such a system is

$$E\psi_B = -\sum_{i=1}^{N} \frac{\partial^2 \psi_B}{\partial x_i^2} + \sum_{1 \leq i < j \leq N} 2c\,\delta(x_i - x_j)\psi_B + \alpha \sum_{i=1}^{N} x_i \psi_B, \qquad (5.1)$$

where $c > 0$ denotes the strength of the interaction, and $\alpha > 0$ is the constant external force. Solutions of Eq. (5.1) for a single particle ($N = 1$) are the Airy functions. For this reason, in what follows, we will call the solutions of Eq. (5.1) for $N > 1$ the Lieb-Liniger-Airy (LLA) states (we are interested only in those solutions which decay to zero when $x \to \infty$). The constant force in ultracold atomic experiments can arise from the gravity force (e.g., if the one-dimensional atomic wave guides are tilted with respect to gravity).

In what follows, we will demonstrate that LLA states can be constructed via Gaudin's Fermi-Bose transformation [32]. Because of the bosonic symmetry of the wave functions, one can consider only the fundamental permutation sector of the coordinate space $R_1 : x_1 < x_2 < \ldots < x_N$. Within this sector, the Schrödinger equation (5.1) reads

$$E\psi_B = -\sum_{i=1}^{N} \frac{\partial^2 \psi_B}{\partial x_i^2} + \alpha \sum_{i=1}^{N} x_i \psi_B. \qquad (5.2)$$

The interaction term is taken into account as a boundary condition (the so called cusp condition), which is imposed upon ψ_B at the borders of R_1 (i.e., when two particles touch [1]; see Chapter 2 for details):

$$\left[1 - \frac{1}{c}\left(\frac{\partial}{\partial x_{j+1}} - \frac{\partial}{\partial x_j}\right)\right]_{x_{j+1}=x_j} \psi_B = 0. \qquad (2.12)$$

Equation (5.2) holds in all other permutation sectors, whereas the interaction cusp (2.12) can be re-expressed on the borders of other sectors as well. To construct the LLA states we utilize Gaudin's Fermi-Bose mapping operator

[32],

$$\hat{O}_c = \prod_{1 \leq i < j \leq N} \left[\mathrm{sgn}(x_j - x_i) + \frac{1}{c} \left(\frac{\partial}{\partial x_j} - \frac{\partial}{\partial x_i} \right) \right], \qquad (2.16)$$

which acts upon an antisymmetric (fermionic) wave function ψ_F. The wave function ψ_F must obey the Schrödinger equation for noninteracting spinless fermions in the linear potential:

$$E\psi_F = -\sum_{i=1}^{N} \frac{\partial^2 \psi_F}{\partial x_i^2} + \alpha \sum_{i=1}^{N} x_i \psi_F. \qquad (5.3)$$

The wave function ψ_F can be written in the form of Slater determinant with Airy functions as entries:

$$\psi_F = \alpha^{-\frac{N}{6}} \frac{1}{\sqrt{N!}} \det_{i,j=1}^{N} \mathrm{Ai}(\alpha^{\frac{1}{3}} x_j - \alpha^{-\frac{2}{3}} E_i), \qquad (5.4)$$

where $E = \sum_{i=1}^{N} E_i$.

The LLA states [i.e., solutions of the Schrödinger Eq. (5.2), together with the cusp condition (2.12)], are given by

$$\psi_{B,c} = \mathcal{N}_c \hat{O}_c \psi_F, \qquad (5.5)$$

where $\mathcal{N}_c$ is the normalization constant. It is known that all wave functions of the form (5.5) obey the cusp conditions throughout the configuration space [32, 34]. To show that $\psi_{B,c}$ is also a solution of Eq. (5.2), it is sufficient to prove that the following commutators are zero: $\left[\sum_i \partial^2/\partial x_i^2, \hat{O}_c \right] = 0$ and $\left[\sum_i x_i, \hat{O}_c \right] = 0$; this is sufficient because ψ_F obeys Eq. (5.3). The first commutator is trivially satisfied, and therefore we are left to verify that

$$\left[\sum_i x_i, \hat{O}_c \right] = 0. \qquad (5.6)$$

As a first step, we restrict ourselves to the case of two particles, $N = 2$. By

63

using $[x_j, \partial/\partial x_i] = -\delta_{j,i}$, we have

$$\left[x_1 + x_2, \text{sgn}(x_2 - x_1) + \frac{1}{c}\left(\frac{\partial}{\partial x_2} - \frac{\partial}{\partial x_1}\right)\right] = \frac{1}{c}\left[x_2, \frac{\partial}{\partial x_2}\right] - \frac{1}{c}\left[x_1, \frac{\partial}{\partial x_1}\right] = 0.$$
(5.7)

Now we generalize this for any number of particles N. Let us write the differential operator as $\hat{O}_c = \prod_{1 \leq i < j \leq N} \hat{B}_{i,j}$, where

$$\hat{B}_{i,j} = \left[\text{sgn}(x_j - x_i) + \frac{1}{c}\left(\frac{\partial}{\partial x_j} - \frac{\partial}{\partial x_i}\right)\right].$$
(5.8)

A general expression, $\left[\hat{V}, \prod_{l=1}^{M} \hat{W}_l\right] = \sum_{l=1}^{M} \hat{W}_1 \cdots \hat{W}_{l-1}\left[\hat{V}, \hat{W}_l\right] \hat{W}_{l+1} \cdots \hat{W}_M$, valid for operators $\hat{V}$ and $\hat{W}_l$, $l = 1, \ldots, M$, enables us to write the required commutator for the case of N particles:

$$\left[\sum_k x_k, \hat{O}_c\right] = \sum_{i<j} \hat{B}_{N-1,N} \cdots \left[\sum_k x_k, \hat{B}_{i,j}\right] \cdots \hat{B}_{1,2}.$$
(5.9)

Now Eq. (5.6) follows immediately because for any $\hat{B}_{i,j}$ we have $\left[\sum_k x_k, \hat{B}_{i,j}\right] = \left[x_i + x_j, \hat{B}_{i,j}\right] = 0$, as is verified for the $N = 2$ case. This completes the proof that the wave function $\psi_{B,c}$ defined in (5.5) is a solution of Eq. (5.1).

In this section we have found exact closed form solutions of Eq. (5.1). We point out that the eigenstates (5.5) with total energy E are degenerate, because the choice of single particle energies E_i for which $E = \sum_{i=1}^{N} E_i$ is not unique. By superposition of degenerate eigenstates (5.5), one can construct eigenstates which are of different mathematical form. In [90] the authors study Eq. (5.1) for $N = 2$ and $N = 3$ particles. They constructed solutions by introducing a new set of coordinates and separating Eq. (5.1). For $N = 2$ they separate the center of mass and relative motion. Their solution for a given energy can be written as a superposition of eigenstates (5.5). For $N = 3$ the procedure in [90] becomes more cumbersome, which clearly points out the advantage of using Fermi-Bose transformation for solving Eq. (5.1).

5.2 The Lieb-Liniger gas in a wedgelike potential: Strongly interacting limit

In this section, we consider the Lieb-Liniger gas in the wedgelike potential defined as

$$V(x) = \begin{cases} x & \text{if } x \geq 0; \\ \infty & \text{if } x < 0. \end{cases} \tag{5.10}$$

For simplicity, we have fixed the value of the constant force to $\alpha = 1$. Solutions for any other value can be obtained by simple rescaling: $x \to \alpha^{1/3} x$ and $E \to \alpha^{-2/3} E$.

In order to find the ground state in such a potential, one should find solutions of Eqs. (5.2) and (2.12) (assuming we work in the fundamental sector R_1), together with the following boundary condition: $\psi_{B,c}(x_1 = 0, x_2, \ldots, x_N) = 0$. The first idea that may come to mind in attempting to find such a ground state is to utilize Eq. (5.5) as an ansatz, since it apparently obeys (5.2) and (2.12), and try to adjust the N free parameters E_i such that $\psi_{B,c}(x_1 = 0, x_2, \ldots, x_N) = 0$. Namely, such a procedure leads to the solutions for the ground states of a Lieb-Liniger gas on the ring [1], where instead of the ansatz (5.5) with Airy functions, one utilizes an ansatz with plane waves, $\psi_{B,c} = \mathcal{N}_c \hat{O}_c \det_{m,j=1}^{N} e^{ik_j x_m}$ (e.g., see [44]), and instead of E_j, one adjusts the quasimomenta k_j (which have to obey Bethe's equations) to acquire the proper boundary conditions. However, for this wedge like potential such a line of reasoning fails. Mathematically, this occurs because the first derivative of the Airy function is not simply related to the Airy function itself (whereas a derivative of a plane wave is proportional to the plane wave itself).

Nevertheless, we can find solutions in the form (5.5) in the Tonks-Girardeau limit ($c \to \infty$), and we can utilize some form of $1/c$ approximation to find deviations from the Tonks-Girardeau ground state for large but finite c. The Tonks-Girardeau ground state is constructed by symmetrizing the Slater determinant of N lowest single-particle eigenstates [2]:

$$\psi_{TG} = \Pi_{k<m} \text{sgn}(x_m - x_k) \frac{1}{\sqrt{N!}} \det_{i,j=1}^{N} \phi_i(x_j), \tag{5.11}$$
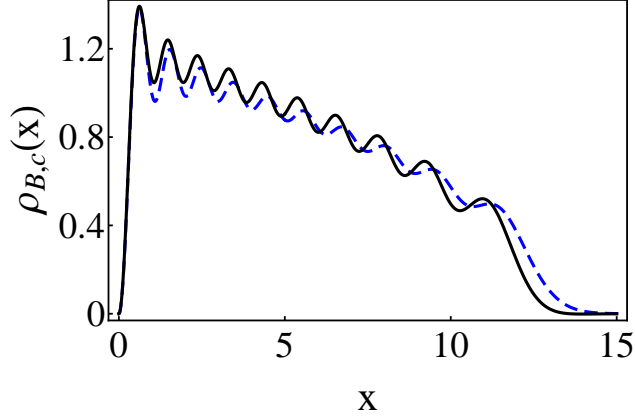
Figure 5.1: The single particle density $\rho_{B,c}(x)$ (solid black line) of $N = 10$ Lieb-Liniger bosons in a wedgelike potential ($c = 40$, $\alpha = 1$). Dashed blue line shows the density in the Tonks-Girardeau limit.

where

$$\phi_i(x) = \frac{\text{Ai}(x - E_i)}{\text{Ai}'(-E_i)}. \tag{5.12}$$

The single-particle energies E_i are such that $\text{Ai}(-E_i) = 0$ [i.e., $\phi_i(0) = 0$], and the eigenstates form an orthonormal set: $\int_0^\infty \phi_i^*(x)\phi_j(x)dx = \delta_{i,j}$. The ground-state energy is simply $E_{TG} = \sum_{i=1}^N E_i$. As an illustration, in Fig. 5.1 we display the single-particle density for the Tonks-Girardeau ground state (dashed blue line) comprising $N = 10$ particles.

An approximative perturbative approach for calculating the properties of a Lieb-Liniger gas in the strongly interacting regime has been suggested by Sen [89]. It can be shown that the perturbation around $c = \infty$ (the Tonks-Girardeau limit) is correctly described by a pseudopotential [89]

$$\hat{V}_{pp} = -\frac{4}{c} \sum_{i<j} \delta''(x_i - x_j), \tag{5.13}$$

that is, the pseudopotential (5.13) is utilized as a small perturbation around the Tonks-Girardeau ground state (unperturbed state) for large c. It gives the correct first-order correction to the ground-state energy and wave function when plugged into the standard perturbation expressions with $1/c$ as a small parameter.

In the $1/c$ approximation, the ground-state energy of the Lieb-Liniger system

66

is

$$E_{B,c} = E_{TG} + \left\langle \psi_{TG} \left| \hat{V}_{pp} \right| \psi_{TG} \right\rangle$$

$$= E_{TG} - \frac{1}{c}N(N-1). \tag{5.14}$$

Result (5.14) is obtained by a direct calculation of the expectation value of the pseudopotential $\hat{V}_{pp}$ for the Tonks-Girardeau ground state. Such matrix elements are readily evaluated by using Slater-Condon rules:

$$\left\langle \psi_{TG} \left| \hat{V}_{pp} \right| \psi_{TG} \right\rangle = -\frac{4}{c} \sum_{i<j} \int_0^\infty dx \left(\phi_i^*(x)\phi_i(x)\frac{d^2}{dy^2}[\phi_j^*(y)\phi_j(y)]_{y=x} \right.$$

$$\left. - \phi_i^*(x)\phi_j(x)\frac{d^2}{dy^2}[\phi_j^*(y)\phi_i(y)]_{y=x} \right). \tag{5.15}$$

We have verified (5.14) numerically (by employing Mathematica) up to $N = 20$ particles, and we conjecture that the expression is valid for any number of particles trapped by the potential (5.10).

To first order in $1/c$, the Lieb-Liniger wave function is given by [89]

$$\psi_{B,c} \approx \psi_{TG} + \sum_{n\leq N, m>N} \frac{\left\langle \psi_{TG}^{(m;n)} \left| \hat{V}_{pp} \right| \psi_{TG} \right\rangle}{E_n - E_m} \psi_{TG}^{(m;n)}$$

$$+ \sum_{\substack{n<n'\leq N \\ m'>m>N}} \frac{\left\langle \psi_{TG}^{(m,m';n,n')} \left| \hat{V}_{pp} \right| \psi_{TG} \right\rangle}{E_n + E_{n'} - E_m - E_{m'}} \psi_{TG}^{(m,m';n,n')}, \tag{5.16}$$

where $\psi_{TG}^{(m;n)}$ labels an excited Tonks-Girardeau state; this state is obtained from the ground state ψ_{TG} by replacing the single-particle state ϕ_n, where $n \leq N$, with the single-particle state ϕ_m of higher energy, $m > N \geq n$. Analogously, $\psi_{TG}^{(m,m';n,n')}$ labels two particle excitation of the TG gas state. The expression for the single-particle density $\rho_{B,c}(x) = N \int dx_2 \cdots dx_N |\psi_{B,c}|^2$ can be calculated straightforwardly by employing the wave function from Eq.

(5.16), by keeping the terms up to $1/c$:

$$\rho_{B,c}(x) \approx \rho_{TG}(x)$$

$$+ N \sum_{n \leq N, m > N} \left(\frac{\left\langle \psi_{TG}^{(m;n)} \left| \hat{V}_{pp} \right| \psi_{TG} \right\rangle}{E_n - E_m} \int dx_2 \cdots dx_N \psi_{TG}^* \psi_{TG}^{(m;n)} + c.c. \right)$$

$$\approx \rho_{TG}(x) + \frac{1}{c} \sum_{n \leq N, m > N} \frac{V_{pp}^{(m;n)}}{E_n - E_m} \phi_n(x) \phi_m(x). \qquad (5.17)$$

Here, the matrix element $V_{pp}^{(m;n)} \equiv -8 \left\langle \psi_{TG}^{(m;n)} \left| \sum_{i<j} \delta''(x_i - x_j) \right| \psi_{TG} \right\rangle$ of the single-particle excitation from the level $n \leq N$ with energy E_n, to the level $m > N$ with energy E_m is given by

$$V_{pp}^{(m;n)} = -8 \sum_{i=1, i \neq n}^{N} \int_0^\infty dx$$

$$\times \left(\phi_m^*(x) \phi_n(x) \frac{d^2}{dy^2} [\phi_i^*(y) \phi_i(y)]_{y=x} - \phi_m^*(x) \phi_i(x) \frac{d^2}{dy^2} [\phi_i^*(y) \phi_n(y)]_{y=x} \right).$$

$$(5.18)$$

In Fig. 5.1 we illustrate the single-particle density $\rho_{B,c}(x)$ in $1/c$ approximation (solid black line), which is obtained by using Eq. (5.17) for $N = 10$ and $c = 40$. It should be mentioned that the two-particle excitations [second sum in Eq. (5.16)] do not yield any contribution to the first-order single particle density $\rho_{B,c}(x)$, due to the vanishing of the overlap of the wave functions in calculation of the density (in the same way as demonstrated for the case of bosons confined in an infinitely deep box [89]). In our calculation of the density $\rho_{B,c}$ via (5.17), we have included only a finite number of terms, where the cutoff is chosen to be sufficiently large, such that the contribution of the remaining terms is negligible [for the calculation illustrated in Fig. 5.1, we kept 150 terms in Eq. (5.17) with the highest contribution].

5.3 Exact quantum dynamics via a Fourier transform

In this section we discuss the time-dependent solutions of the Lieb-Liniger system in a linear potential. Before proceeding, we note that dynamics in the strongly interacting regime (i.e., dynamics of a Tonks-Girardeau gas in a linear potential) was studied in Ref. [91]. Here, we assume that the bosons are initially localized by some external trapping potential. At time $t = 0$, this potential is suddenly turned off, and bosons are released to evolve in the linear potential. This problem can be related to free expansion of the Lieb-Liniger wave packet by simple rescaling of the coordinates. If the wave function $\psi_{free}(x_1, \ldots, x_N, t)$ obeys the equation,

$$i\frac{\partial \psi_{free}}{\partial t} = -\sum_{i=1}^{N} \frac{\partial^2 \psi_{free}}{\partial x_i^2} + \sum_{1 \leq i < j \leq N} 2c\,\delta(x_i - x_j)\psi_{free}, \qquad (5.19)$$

(i.e., ψ_{free} describes free expansion (see Chapter 3)), then the wave function

$$\psi_{B,c}(x_1, \ldots, x_N, t) = e^{-i\alpha t \sum_{i=1}^{N}(x_i + \alpha t^2/3)}\, \psi_{free}(x_1 + \alpha t^2, \ldots, x_N + \alpha t^2, t) \tag{5.20}$$

is the solution of the time-dependent problem in the constant-force potential,

$$i\frac{\partial \psi_{B,c}}{\partial t} = -\sum_{i=1}^{N} \frac{\partial^2 \psi_{B,c}}{\partial x_i^2} + \sum_{1 \leq i < j \leq N} 2c\,\delta(x_i - x_j)\psi_{B,c} + \alpha\sum_{i=1}^{N} x_i \psi_{B,c}. \qquad (5.21)$$

The initial conditions coincide (i.e., at $t = 0$ we have $\psi_{B,c} = \psi_{free}$). Note that the phase factor in Eq. (5.20) accounts for the momentum per particle αt, which is acquired in time in the field of constant force α (in units used here, $m = 1/2$, and therefore the classical acceleration is 2α). Transformation (5.20) can be verified by direct substitution in Eq. (5.21), from which it becomes evident that it is valid for any two-particle interaction $V(x_i - x_j)$. Namely, transformation $x_i \to x_i + \alpha t^2$ does not affect the two-particle interaction term $V(x_i - x_j)$ [in fact, because of this, Eq. (5.20) can be deduced from the well-known solution for a single-particle wave packet in a linear potential].

It is known that freely expanding Lieb-Liniger wave packets can be calculated

by solving an N-dimensional Fourier transform (see Chapter 2):

$$\psi_{free}(x_1, \ldots, x_N, t) = \int dk_1 \cdots dk_N G(k_1, \ldots, k_N) e^{i \sum_{i=1}^{N} \left(k_i x_i - k_i^2 t \right)}. \quad (5.22)$$

We note that the function G is *not* the Fourier transform of the wave function ψ_{free} because it depends on the coordinates x_j through the $\text{sgn}(x_j - x_i)$ terms (see Chapter 3 for details), that is, it differs from one permutation sector in x space to the next. Nevertheless, by calculating the integral in Eq. (5.22) in one sector (say R_1), we obtain ψ_{free} in that sector, which is sufficient due to bosonic symmetry. The function G contains all information on initial conditions and it can be expressed in terms of the projections of the initial wave function on the Lieb-Liniger free space eigenstates (e.g., see Chapter 3). By using Eqs. (5.22) and (5.20) we can express $\psi_{B,c}$ in terms of an N-dimensional Fourier transform:

$$\psi_{B,c}(x_1, \ldots, x_N, t) = \int dk_1 \cdots dk_N \ G(k_1, \ldots, k_N)$$

$$\times \exp \left\{ i \sum_{i=1}^{N} \left[(k_i - \alpha t) x_i + \frac{(k_i - \alpha t)^3 - k_i^3}{3\alpha} \right] \right\}. \quad (5.23)$$

We would like to note that result (5.23) can be obtained by straightforward use of Fermi-Bose transformation. The time-dependent wave function ψ_F which describes the system of N noninteracting fermions in a linear potential $V(x) = \alpha x$ can be written via its Airy transform:

$$\psi_F(x_1, \ldots, x_N, t) = \int dE_1 \cdots dE_N$$

$$\times \bar{\psi}_F(E_1, \ldots, E_N) e^{-it \sum_{i=1}^{N} E_i} \prod_{i=1}^{N} \text{Ai}(\alpha^{-2/3}(\alpha x_i - E_i)).$$

$$(5.24)$$

Here, $\bar\psi_F(E_1, \dots, E_N)$ contains information on initial conditions,

$$\bar\psi_F(E_1, \dots, E_N) = \left(\frac{1}{\alpha^{1/3}}\right)^N \int dx_1 \cdots dx_N$$

$$\times \, \psi_F(x_1, \dots, x_N, 0) \prod_{i=1}^{N} \mathrm{Ai}(\alpha^{-2/3}(\alpha x_i - E_i)). \qquad (5.25)$$

By using the well-known relation between the Airy and Fourier transform $\tilde\psi_F$ [92],

$$\bar\psi_F(E_1, \dots, E_N) = \left(\frac{1}{\alpha^{2/3}}\right)^N \int dk_1 \cdots dk_N \; \tilde\psi_F e^{i\sum_{i=1}^{N}\left(k_i E_i - k_i^3/3\right)/\alpha}, \qquad (5.26)$$

we find

$$\psi_F(x_1, \dots, x_N, t) = \int dk_1 \cdots dk_N$$

$$\times \, \tilde\psi_F \exp\left\{ i \sum_{i=1}^{N} \left[(k_i - \alpha t)x_i + \frac{(k_i - \alpha t)^3 - k_i^3}{3\alpha} \right] \right\}. \qquad (5.27)$$

The time-dependent solution of the Lieb-Liniger model [i.e. Eq. (5.23)], can now be found directly from the expression above by applying the Fermi-Bose transformation operator $\hat O_c$ onto Eq. (5.27).

Our discussion in this section adds upon the previous studies of Lieb-Liniger wave-packet dynamics on an infinite line (see Refs.[32, 34] and Chapter 3), and in the presence of the hard-wall potential (Chapter 4); in all these cases the motion of an interacting Lieb-Liniger wave packet can be calculated by using an N-dimensional Fourier transform.

In order to illustrate the connection between (5.19) and (5.20), we present the following numerical example. The system of three Lieb-Liniger bosons are trapped in the ground state of an infinitely deep box of length $L = \pi$; at $t = 0$, the trap is turned off and the bosons start to experience the constant force $\alpha = 3$. The exact initial wave function is constructed as a superposition of free space eigenstates [36]. From this state we can find the function $G(k_1, \dots, k_N)$ which keeps all information on initial conditions (see Chapters 2 and 3). By numerically calculating the integral in (5.23), we obtain the time-dependent wave function $\psi_{B,c}(x_1, \dots, x_N, t)$ describing the sys-

tem. Here, we plot two relevant physical quantities, the single-particle density, $\rho_{B,c}(x,t) = N \int dx_2 \cdots dx_N \left| \psi_{B,c}(x,\ldots,x_N,t) \right|^2$, and the momentum distribution $n(k,t)$ (density in k space).

From Eq. (5.20) it follows that the density in coordinate space will be the same as in the case of free expansion ($\alpha = 0$), with mere translation of the coordinates $[\rho_{B,c}(x,t) = \rho_{free}(x + \alpha t^2, t)]$. The momentum distribution will be equivalent also up to the simple transformation $k \to k - \alpha t$. The density profile and momentum distribution of the wave packet are plotted in Figs. 5.2 and 5.3, respectively, for three various interactions strengths c: (a) $c = 0.25$, (b) $c = 3$, and (c) $c = 10$. Starting from $t = 0$, the wave packet evolves to the left in x space with the center of mass motion αt^2, while at the same time it spreads in width independently. For large c, the spread is more pronounced, as can also be conjectured from the initial momentum distribution. For very large c, the wave packet will asymptotically experience fermionization of the momentum distribution [47, 49].

5.4   Conclusion

We have studied the Lieb-Liniger model in the constant-force (linear) potential. Exact stationary solutions for this system, referred to as the Lieb-Liniger-Airy states, were constructed by employing Gaudin's Fermi-Bose mapping operator $\hat{O}_c$. This was enabled by the fact that the operator commutes with the linear potential: $[\hat{O}_c, \sum_j \alpha x_j] = 0$. We have calculated the ground-state properties of the Lieb-Liniger gas, in the strongly interacting regime, in the wedgelike potential: $V(x) = \alpha x$ for $x > 0$ ($\alpha > 0$), and $V(x) = \infty$ for $x < 0$. This was achieved in the Tonks-Girardeau regime and in $1/c$ approximation by employing the pseudopotential approach [89]. Finally, we have pointed out that the time-dependent Lieb-Liniger wave packets in the linear potential can be found by employing an N-dimensional Fourier transform.
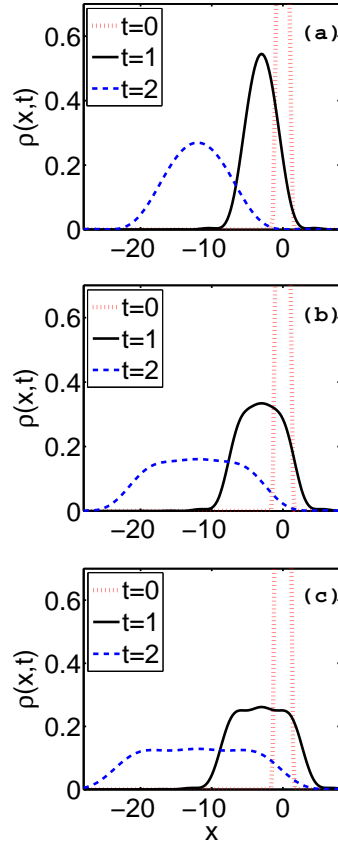
Figure 5.2: Evolution of $N = 3$ Lieb-Liniger bosons in the linear potential αx ($\alpha = 3$) from the ground state of a box with infinitely high walls. Single-particle density in time for various interaction strengths c: (a) $c = 0.25$, (b) $c = 3$, and (c) $c = 10$. Red dotted lines are for $t = 0$, solid black lines are for $t = 1$, and blue dashed lines are for $t = 2$.
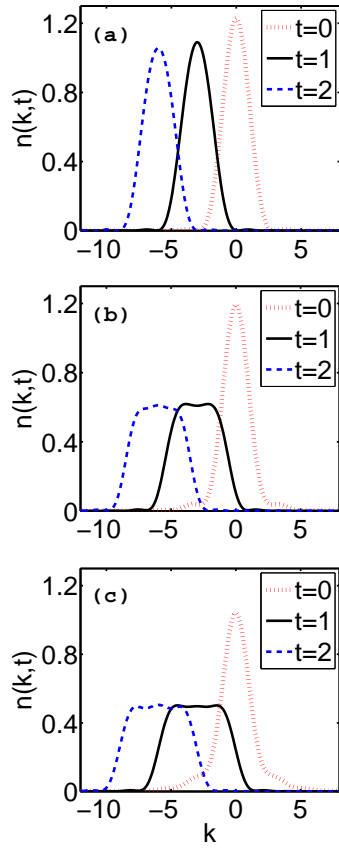
Figure 5.3: Evolution of the momentum distribution. The colors and lines for different c and t are identical as in Fig. 5.2.

Chapter 6

Anderson localization of a Tonks-Girardeau gas in potentials with controlled disorder

The phenomenon of Anderson localization [62], which was originally theoretically predicted in the context of condensed matter physics, has been experimentally demonstrated in other wave systems including optical waves [93, 94, 95, 96, 97] and ultracold atomic gases (matter waves) [63, 64]. In the context of Bose-Einstein condensates (BECs), Anderson localization was obtained by placing ultracold atomic BECs in elongated, essentially one-dimensional disordered [63] and quasiperiodic incommensurate potentials [64], which were created optically (see Ref. [98] for a recent review of the topic). The matter waves utilized in those experiments were condensates, i.e., they were spatially coherent in the sense that their one-body density matrix factorizes $\rho(x_1, x_2) \approx \Phi^*(x_1)\Phi(x_2)$, where $\Phi(x)$ is the condensate wave function. However, in reality interactions and/or the presence of the thermal cloud affects the spatial coherence in the system. Naturally, the spatial coherence in the system is expected to have important implications on localization phenomena, since the phenomenon of Anderson localization is deeply connected to interference of multiple reflected waves. This motivates us to study Anderson localization in a Tonks-Girardeau gas, which is a relatively simple example of partially-

spatially-coherent Bose gas (i.e., it is not condensed).

The Tonks-Girardeau model describes a system of strongly repulsive ("impenetrable") bosons, confined in one-dimensional (1D) geometry [2]. Exact solutions of the model are found by employing the Fermi-Bose mapping [2, 46], wherein the Tonks-Girardeau wave function (for both the stationary and the time-dependent problems) is constructed from a wave function describing non-interacting spinless fermions. In Ref. [10] it was suggested that the Tonks-Girardeau model can be experimentally realized with ultracold atoms in effectively 1D atomic waveguides. This regime is reached at low temperatures, for sufficiently tight transverse confinement, and with strong effective interactions [10, 11, 12]. Indeed, in 2004 two groups have experimentally realized the Tonks-Girardeau gas [5, 6]. Furthermore, nonequilibrium dynamics of a 1D Bose gas (including the Tonks-Girardeau regime) has been experimentally addressed in the context of relaxation to equilibrium [7]. It is known that ground states of the Tonks-Girardeau gas on the ring [99], or in a harmonic potential [100] are not condensates, because the population of the leading natural orbital scales as $\sqrt{N}$, where N is the number of particles. Thus, the Tonks-Girardeau gas is only partially spatially coherent. The free expansion of the Tonks-Girardeau gas from some initial state has been of great interest over the past few years [47, 49, 50, 51]; this type of scenario, i.e., expansion from an initial state which is localized (say by a trapping potential) can be used to address Anderson localization [63].

The experimental demonstrations of Anderson localization in ultracold atomic gases were preceded by theoretical investigations of this topic (e.g., see Refs. [101, 102, 103], see also Ref. [98] and references therein). The interplay of disorder (or quasiperiodicity) and interactions in a Bose gas (from weakly up to strongly correlated regimes), has been often studied in the context of the Bose-Hubbard model [101, 102, 104, 105, 106, 107, 108, 109, 110, 111, 112, 113, 114]. Within the model, a transition from a superfluid to a Bose glass phase has been predicted to occur [104, 105]. The aforementioned interplay has been studied by using versatile methods including calculating the energy absorption rate [114], momentum distribution and correlations [107, 112], and expansion dynamics [110, 111]. In the limit of strong repulsion, the system can be described by using hard-core bosons on the lattice [107, 110, 114]. For these systems, by employing the Jordan-Wigner transformation the bosonic system is mapped

76

to that of noninteracting spinless fermions, and all one-body observables can be furnished from the one body density matrix both in the stationary (e.g., see [68]) and out-of-equilibrium systems [47]. The ground state properties of the hard-core Bose gas in a random lattice have been studied in [107], whereas expansion dynamics was considered in [110]; both approaches predict the loss of quasi long-range order.

In this chapter we study Anderson localization within the framework of the Tonks-Girardeau model [2] in one-dimensional disordered potentials. We study the expansion of a Tonks-Girardeau wave packet in a potential with controlled disorder. The potential is characterized by its correlation distance parameter σ. At $t = 0$, the initial wave packet is in the ground state of a harmonic trap with frequency ω (with small disorder superimposed upon it), and then the trap is suddenly turned off. After some time, we find that the system reaches a steady state characterized by exponentially decaying tails of the density. We show that the exponents decrease with the increase of ω and the decrease of σ in the investigated parameter span ($\sigma = 0.13 - 0.40$ μm and $\omega = 5 - 10$ Hz). The one-body density matrix $\rho_B(x, y, t)$ of the steady state, that is its amplitude $|\rho_B(0, x, t)|$, decays exponentially on the tails of the localized wave packet. However, in the region of these tails the degree of first order coherence $|\mu_B(0, x, t)| = |\rho_B(0, x, t)|/\sqrt{\rho_B(0, 0, t)\rho_B(x, x, t)}$ reaches a plateau. These plateaus are connected to the behavior of the single-particle states used to construct the Tonks-Girardeau wave function, from which we find that the spatial coherence increases in the tails. This increase of coherence in the tails has its counterpart in incoherent optical solitons [115], a phenomenon well understood in terms of the modal theory for incoherent light [115].

6.1 Numerical results on Anderson localization in a Tonks-Girardeau gas

In order to investigate Anderson localization of the Tonks-Girardeau gas, we perform numerical simulations designed in the fashion of optical [96] and matter wave [63] experiments which were conducted recently to demonstrate Anderson localization. We investigate dynamics of a Tonks-Girardeau wave packet in a disordered potential $V_D(x)$, where the initial wave packet (at $t = 0$)

is localized in space by some trapping potential. After long time of propagation the wave packet reaches some steady state. Anderson localization is indicated by the exponential decay of the density of the wave packet in this steady state.

More specifically, we assume that initially, at $t = 0$, the gas is in the ground state of the harmonic oscillator potential, with the small controlled disordered potential superimposed upon it, that is,

$$V(x) = V_D(x) + \nu^2 x^2 \text{ for } t < 0. \tag{6.1}$$

At $t = 0$ the trapping potential is suddenly turned off, i.e.,

$$V(x) = V_D(x) \text{ for } t > 0, \tag{6.2}$$

after which the density and correlations of the gas begin to evolve. This means that at $t = 0$ the wave function ψ_B is given by Eqs. (2.4) and (2.5) where $\psi_m(x, t = 0)$ is the mth single-particle eigenstate of the potential $V_D(x) + \nu^2 x^2$. The subsequent evolution of ψ_m is given by Eq. (2.6) where the potential is given solely by the disordered term $V(x) = V_D(x)$.

The disordered potential can be characterized in terms of its correlation functions; the autocorrelation function is defined by

$$A_C(x) = \langle \overline{V}_D(x' - x) \overline{V}_D(x') \rangle_{x'}, \tag{6.3}$$

where $\overline{V}_D(x) = V_D(x) - \langle V_D(x') \rangle_{x'}$, and $\langle \cdots \rangle_{x'}$ denotes a spatial average over x'. For the disordered potentials in our simulations we have approximately

$$A_C(x) = V_0^2 \frac{\sin^2(x/\sigma)}{(x/\sigma)^2}, \tag{6.4}$$

where σ denotes the spatial correlation length of the disordered potential, whereas $V_0^2 = \langle \overline{V}_D^2(x) \rangle_x$ denotes its amplitude. The spatial power spectrum of the potential has support in the interval $[-K_{cut}, K_{cut}]$, where the cut-off value is $K_{cut} = 2/\sigma$. Thus, the potential $V_D(x)$ has the autocorrelation function identical to that of the optical speckle potentials used in the experiments, e.g., see [63].

The asymptotic steady state of the system depends on the parameters of the disordered potential σ and V_0, and on the initial state, that is, the harmonic

78
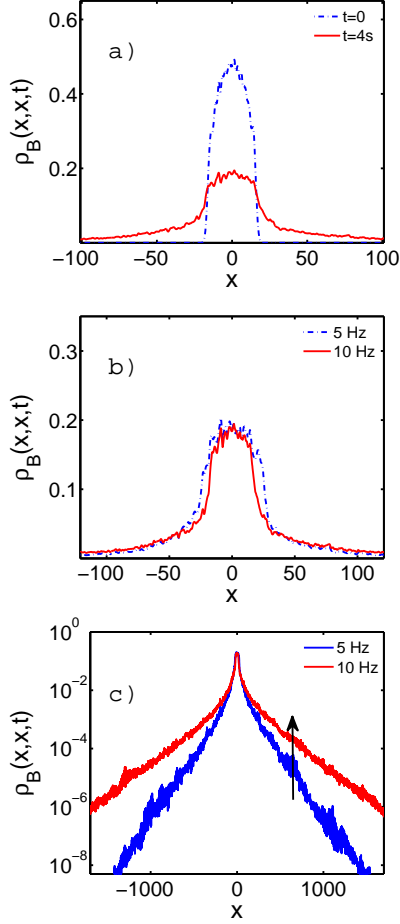
Figure 6.1: Anderson localization in a Tonks-Girardeau gas in dependence of the initial trap parameter ν (i.e., ω). The parameters of the disordered potential are ($\sigma = 0.13$ and $V_0 = 0.465$). (a) The averaged density of the Tonks-Girardeau wavepacket at $t = 0$ and after $t = 1450$ (=4 s) of propagation. The initial state corresponds to $\nu = 8.67 \times 10^{-2}$ ($\omega = 10$ Hz). (b) Shown is the density of a Tonks-Girardeau gas (in the localized steady state) after $t = 1450$ (=4 s) of propagation in a disordered potential. Blue dot-dashed line corresponds to $\nu = 4.34 \times 10^{-2}$ ($\omega = 5$ Hz), whereas red solid line corresponds to $\nu = 8.67 \times 10^{-2}$ ($\omega = 10$ Hz). (c) Same as figure (b) on a logarithmic scale. Blue line corresponds to ($\omega = 5$ Hz), and red line corresponds to $\omega = 10$ Hz; arrow indicates the increase of ω. For $|x|$ larger than some value (call it L_t), the density decays exponentially, which characterizes Anderson localization. The density-tails decay slower for larger initial trap parameter ω (see text for details).

trap parameter ν. In fact, since the dynamics of the Tonks-Girardeau gas is governed by a set of uncoupled Schrödinger equations, it follows from the
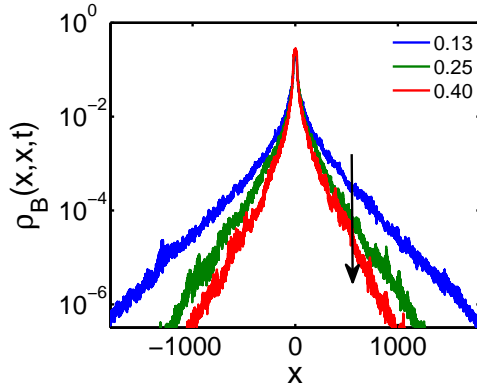
Figure 6.2: Anderson localization in a Tonks-Girardeau gas in dependence of the disorder parameter σ. The averaged density of a Tonks-Girardeau gas after $t = 1450$ (=4 s) of propagation in the disordered potential. The plots correspond to $\sigma = 0.13$ (blue line), $\sigma = 0.25$ (green line), and $\sigma = 0.40$ (red line); arrow indicates the increase of σ. The initial state corresponds to $\omega = 10$ Hz, while the amplitude of the disordered potential is $V_0 \approx 0.47$ (see text for details).

simple scaling of units outlined below Eq. (2.2), that there are in fact only two independent parameters; thus we investigate the dynamics in dependence of ν and σ, and keep V_0 at an approximately constant value. We have performed our numerical simulations in a region of the parameter space which was accessible with our numerical capabilities, but which is relevant to experiments [63, 64]. We have varied the correlation length σ of the potential from 0.13 up to 0.40 (corresponding to 0.13 μm and 0.40 μm since the spatial scale is chosen to be $X_0 = 1$ μm), and the harmonic trap parameters in the interval $\nu = 4.34 - 8.67 \times 10^{-2}$ (corresponding to $\omega = 5 - 10$ Hz). The number of particles used in our simulations is relatively small, $N = 13$, due to the computer limitations, however, despite of this, one can use our simulations to infer general conclusions that would be valid in an experiment with larger N. It should be emphasized that all plots of densities and correlations are ensemble averages made over 40 realizations of the disordered potentials.

First we investigate the behavior of the single-particle density. In Figure 6.1 we show $\rho_B(x, x, t = 1450)$ versus x for $(\sigma, V_0) = (0.13, 0.465)$, and two values of ν: $\nu = 4.34 \times 10^{-2}$ ($\omega = 5$ Hz) and $\nu = 8.67 \times 10^{-2}$ ($\omega = 10$ Hz). In Fig. 6.1(a) we compare the initial density (at $t = 0$), with the density at time $t = 1450$ (= 4 s), at which the steady state regime is already achieved

(all graphs below which describe the steady state are also calculated at this time). We observe that the steady-state density has a broad central part with a fairly flat top, and decaying tails on its sides. The central part is composed of many single-particle states ψ_j. In Fig. 6.1(b) we plot the steady state density for two values of ω. For $\omega = 5$ Hz, the central part is broader than for $\omega = 10$ Hz, but the tails are decaying faster with the increase of $|x|$, as shown in Fig. 6.1(c), where the densities are plotted in the logarithmic scale. We clearly see that for $|x|$ larger than some value (call it L_t), the density decays exponentially, which indicates Anderson localization. We have fitted the tails to the exponential curve $\rho_B(x, x, t) \propto \exp(-\Lambda|x|)$ and obtained $\Lambda = 0.0097$ for $\omega = 5$ Hz, and $\Lambda = 0.0053$ for $\omega = 10$ Hz, that is, we find that the density-tails decay slower for larger initial trap parameter ω. For larger values of ω, the trap is tighter and the initial state has larger energy and broader momentum distribution, therefore, it is harder to achieve localization of the wave packet (e.g., see [103, 116]). Another way to interpret these simulations is in terms of the spatial correlation distance of the wave packet. An incoherent wave packet can be characterized by using the spatial correlation distance, which determines a spatial degree of coherence; this quantity is inversely proportional to the width of the spatial power spectrum. If the spatial correlation distance decreases, it is harder to achieve localization.

In Fig. 6.2 we display dependence of the density $\rho_B(x, x, t)$ versus x for $\nu = 8.67 \times 10^{-2}$ ($\omega = 10$ Hz), and three values of (σ, V_0): $(0.13, 0.465)$, $(0.25, 0.478)$, and $(0.40, 0.485)$. Note that V_0 can be regarded as a constant close to 0.47 and we will omit to explicitly write the values of V_0 besides σ in further text; the variations of V_0 are a consequence of the method utilized to construct the random potential. We observe that the exponential tails decay faster for larger values of σ.

Next we focus on correlations contained within the reduced single-particle density matrix $\rho_B(x, y, t)$. Suppose that we are interested in the phase correlations between the center (at zero) and the rest of the cloud (at some x-value); the quantity $\rho_B(0, x, t)$ will decay to zero with the increase of $|x|$ even if the field is perfectly coherent simply because the density decays to zero on the tails. In order to extract solely correlations from the RSPDM, we observe the
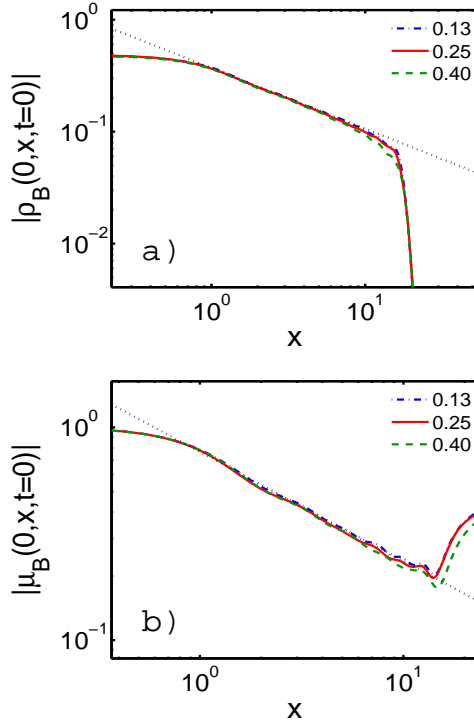
Figure 6.3: First-order correlations in the initial state decay algebraically. Shown are the single-particle density matrix $|\rho_B(0, x, 0)|$ (a), and the degree of first-order coherence $|\mu_B(0, x, 0)|$ (b), at $t = 0$ for the initial state corresponding to $\omega = 10$ Hz. The graphs are plotted for three values of σ as indicated in the legend. Black dotted lines depict the fitted curves $|\rho_B(0, x, 0)| \sim |x|^{-0.54}$ and $|\mu_B(0, x, 0)| \sim |x|^{-0.51}$.

behavior of the quantity [118]

$$\mu_B(x, y, t) = \frac{\rho_B(x, y, t)}{\sqrt{\rho_B(x, x, t)\rho_B(y, y, t)}}, \qquad (6.5)$$

which is the degree of first-order coherence [118] (in optics it is sometimes referred to as the complex coherence factor [119]). In the context of ultracold gases $\mu_B(x, y, t)$ can be interpreted as follows: If two narrow slits were made at points x and y of the 1D Tonks-Girardeau gas, and if the gas was allowed to drop from these slits, expand and interfere, $\mu_B(x, y, t)$ expresses the modulation depth of the interference fringes. In this work we investigate correlations between the central point of the wave packet and the tails: $\mu_B(0, x, t)$.

In Fig. 6.3 we show the averages of the magnitudes of the one-body density

82
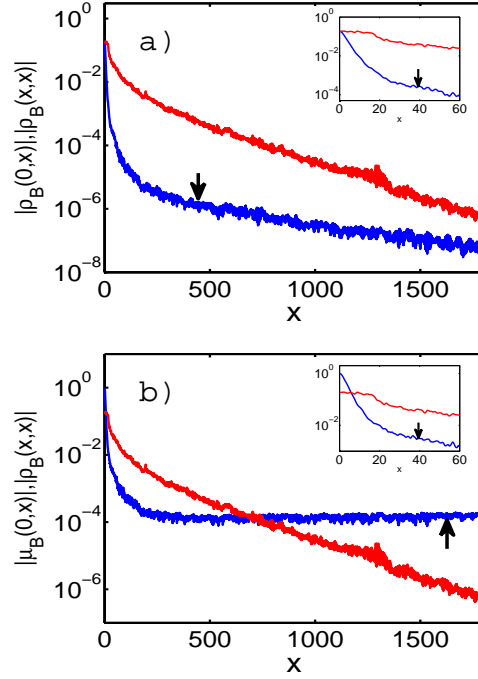
Figure 6.4: Correlations in the steady (Anderson localized) state. The single-particle density matrix $|\rho_B(0, x, t)|$ [blue line in (a), indicated with the arrow], and the degree of first order coherence $|\mu_B(0, x, t)|$ [blue line in (b), indicated with the arrow], at the time 4 s. The parameters used are $\sigma = 0.13$ and $\omega = 10$ Hz. Red lines (in both panels) depict the single particle density $\rho_B(x, x, t)$. Insets enlarge the region where $|x|$ is small and where correlations decay approximately exponentially. For $|x|$ in the region of the density tails ($|x| > L_t$), $|\mu_B(0, x, t)|$ reaches a plateau. See text for details.

matrix $|\rho_B(0, x, t)|$, and the degree of first order coherence $|\mu_B(0, x, t)|$, at time $t = 0$ for the initial state corresponding to $\omega = 10$ Hz and for three values of σ. From previous studies of the harmonic potential ground-state (e.g., see Ref. [100] for the continuous Tonks-Girardeau gas and [47] for hard-core bosons on the lattice) it follows that in a fairly broad interval of x-values, both $|\rho_B(0, x, t = 0)|$ and $|\mu_B(0, x, t = 0)|$ decay approximately as a power law $|x|^{-\gamma_0}$ with the exponent $\gamma_0 = 0.5$ [100, 47], despite of the fact that the density is not homogeneous; the density dependent factors multiplying the power law are also known [100, 47]. We have observed that the initial correlation functions are well fitted to the power law: $|\rho_B(0, x, 0)| \sim |x|^{-0.54}$ and $|\mu_B(0, x, 0)| \sim |x|^{-0.51}$ for $\omega = 10$ Hz (for $\omega = 5$ Hz, we obtain $|\rho_B(0, x, 0)| \sim |x|^{-0.60}$ and $|\mu_B(0, x, 0)| \sim |x|^{-0.55}$). The power-law decay of correlations indicates presence of quasi long-
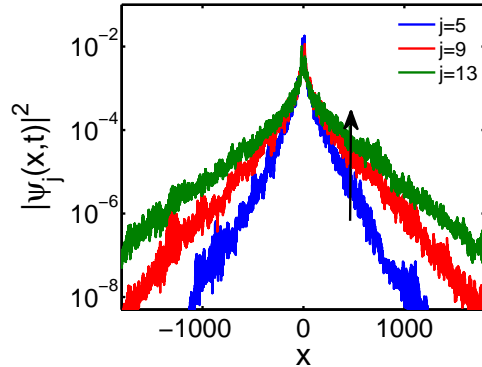
Figure 6.5: The single-particle states $|\psi_j(x,t)|^2$ for $j = 5, 9$, and 13 in the (Anderson localized) steady state. The arrow indicates increase of j. The parameters used are $\sigma = 0.13$ and $\omega = 10$ Hz. The single-particle states for larger j (larger in energy) decay slower with the increase of $|x|$. See text for details.

range order. Apparently, the properties of the small random potential do not significantly affect the correlations of the initial state for the trap strengths ω, and disorder parameters used in our simulations. This happens because the initial single particle states are localized by the trapping potential, rather than by disorder (their decay is Gaussian). The effect of disorder on these states becomes more significant for weaker traps, because the disordered potential becomes nonegligible in comparison to the harmonic term $\nu^2 x^2$ in a broader region of space. In fact, we expect that if one keeps the number of particles constant, for sufficiently shallow traps, disorder would qualitatively change the behavior of the correlations in the initial state, in a similar fashion as when the trap is absent. However, probing Anderson localization by using transport (i.e., expansion of an initially localized wave packet), is perhaps more meaningful for tighter initial traps, where the initial wave packets are localized by the trap rather than by disorder.

For very small values of $|x|$, and for very large values (at the very tails of the wave packet) there are deviations from the power law behavior [100, 47]. The behavior of $|\mu_B(0, x, 0)|$ at the tails, where $|\mu_B(0, x, 0)|$ starts to grow up to some constant value is attributed to the fact that higher single-particle states $\psi_m(x, 0)$ decay at a slower rate with the increase of $|x|$, and therefore spatial coherence increases in the tails (see also the discussion below).

After the Tonks-Girardeau gas expands in the disordered potential and

84
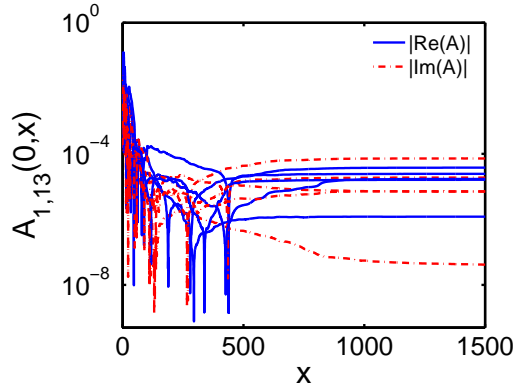
Figure 6.6: The absolute value of the real and imaginary part of $A_{ij}(0,x,t)$ for $i = 1$ and $j = 13$, and five different realizations of the disordered potential. The parameters used in the simulation are $\sigma = 0.13$ and $\omega = 10$ Hz. For sufficiently large $|x|$, $A_{ij}(0,x,t)$ reaches a constant value. See text for details.

reaches a steady-state, the behavior of $\rho_B(0,x,t)$ and $\mu_B(0,x,t)$ significantly differs from that at $t = 0$. This is shown in Fig. 6.4, where we display the magnitude of the two functions for $\sigma = 0.13$ and $\omega = 10$ Hz. We observe that $|\rho_B(0,x,t)|$ exhibits a fairly fast exponential decay for small values of $|x|$, that is, in the region where the density is relatively large [see the inset in Fig. 6.4(a)]. This fast decay slows down up to sufficiently large values of x, i.e., $|x| > L_t$, where we observe slower exponential decay of $|\rho_B(0,x,t)|$, which corresponds to the exponentially decaying tails in the single-particle density of the localized steady state. Regarding the degree of first-order coherence $|\mu_B(0,x,t)|$, we find that for sufficiently small $|x|$, it decays exponentially [see the inset in Fig. 6.4(b)]; however, as x approaches the region of exponentially decaying tails $|x| > L_t$, the exponential decay of $|\mu_B(0,x,t)|$ slows down until it reaches roughly a constant value in the region $|x| > L_t$. This plateau occurs because single-particle states ψ_j decay slower for larger j values (they are higher in energy and momentum), and due to the fact that for sufficiently large $|x|$, the matrix elements $A_{ij}(0,x,t)$, which are important ingredients in expression (2.9) for $|\rho_B(0,x,t)|$, also reach a constant value. This is depicted in Figs. 6.5 and 6.6, which display $|\psi_j(x,t)|^2$ for $j = 5, 9$, and 13, and $A_{1,13}(0,x,t)$ (real and imaginary part) for five different realizations of the disordered potential. We clearly see that $A_{ij}(0,x,t)$ reaches a constant value (generally complex off the diagonal), which differs from one realization of the disorder to the next; this

is connected to the fact that the integral $\int_0^x dx' \psi_i^*(x', t)\psi_j(x', t)$ converges to a constant value for sufficiently large x, which is a consequence of the exponential localization. The fluctuations in $A_{ij}(0, x, t)$ are reflected onto the fluctuations of the plateau value of $|\mu_B(0, x, t)|$. We have compared the averages of the matrix elements $A_{ij}(0, x, t)$ for large x (at the plateau) for all values of i and j. They are all within one order of magnitude with $A_{13,13}(0, x, t)$ ($N = 13$) being the largest, more specifically, the averages of some of the absolute value in our simulations are $|A_{13,13}(0, x, t)| = 0.25 \times 10^{-3}$, $|A_{7,7}(0, x, t)| = 0.16 \times 10^{-3}$, $|A_{1,1}(0, x, t)| = 0.06 \times 10^{-3}$, and $|A_{1,13}(0, x, t)| = 0.03 \times 10^{-3}$. Thus, the values of the matrix elements to some extent enhance the contribution of the highest single-particle states in the correlations $|\mu(0, x, t)|$. It is worthy to mention that identical effect is observed in incoherent light solitons (e.g., see [115]), where the coherence also increases in the tails, which is observed in the complex coherence factor in optics (in the case of solitons, it is nonlinearity, rather than disorder which keeps the wave packet localized).

Let us now extrapolate our numerical calculations and results to larger particle numbers. Suppose that we keep all parameters fixed, and increase only N. The energy of the initial state as well as the high momentum cut-off k_{hcm} increase with the increase of N. Our simulations up to a finite time up of 4 s would not be able to see exponentially decaying tails of the asymptotic steady state. By employing the results of Ref. [116], one concludes that the steady state will always be localized, however, at larger values of N, the Born-approximation mobility edge [116] will be crossed and the exponents describing the exponentially decaying tails will be smaller. The plateaus in the correlations will still exist in the regions of these tails, however, the value $|\mu_B(0, x, t)|$ will decrease with the increase of N (simply because more single particle states ψ_j are needed to describe the Tonks-Girardeau state), and both the exponentially decaying tails together with the plateaus will be harder to observe. The effect where the coherence of the localized steady state increases in the tails should however be observable also with partially condensed BECs, below the Tonks-Girardeau regime.

6.2 Conclusion

We have investigated Anderson localization of a Tonks-Girardeau gas in continuous potentials [$V_D(x)$] with controlled disorder, by investigating expansion of the gas in such potentials; for the initial state we have chosen the Tonks-Girardeau ground state in a harmonic trap (with $V_D(x)$ superimposed upon it), and we have analyzed the properties of the (asymptotic) steady state obtained dynamically. We have studied the dependence of the Lyapunov exponents and correlations on the initial trap parameter ω [$5 - 10$ Hz], and the correlation length of the disorder σ [$0.13 - 0.40$ μm]. We found that the Lyapunov exponents of the steady state, decrease with the increase of ν. In the parameter regime considered the Lyapunov exponents increased with the increase of σ, which was underpinned by the perturbation theory. The behavior of the correlations contained in the one-body density matrix $\rho_B(x, y, t)$ and the degree of first order coherence indicate that the off diagonal correlations $|\rho_B(0, x, t)|$ decrease exponentially with the increase of $|x|$, due to the exponential decay of the density, however, in the region of the exponentially decaying tails, the degree of first-order coherence $|\mu_B(0, x, t)|$ reaches a plateau. This is connected to the behavior of the single-particle states used to construct the Tonks-Girardeau wave function and to the increase of coherence in the exponentially decaying tails. This effect is analogous to the one found in incoherent optical solitons, for which coherence also increases in the tails.

As a possible direction for further research we envision a study of Anderson localization for incoherent light in disordered potentials, Anderson localization within the framework of the Lieb-Liniger model describing a 1D Bose gas with finite strength interactions (which becomes identical to the Tonks-Girardeau model when the interaction strength becomes infinite). These studies should provide further insight into the influence of wave coherence (within the context of optics), and the influence of interactions on Anderson localization (within the context of effectively 1D ultracold atomic gases).

Chapter 7

Summary

Exactly solvable models describing interacting bosons in one-dimension (1D) have been studied over decades since the pioneering work of Girardeau [2], and Lieb and Liniger [1]. The interest in these models is greatly stimulated with recent experiments [3, 4, 5, 6, 7], in which ultracold atomic gases are tightly confined in 1D atomic waveguides, such that transverse excitations are suppressed. The Lieb-Liniger model describes 1D bosons with pointlike contact interactions of a given strength c [1]. In the limit of sufficiently strong interactions, the Lieb-Liniger gas enters the Tonks-Girardeau (TG) regime of impenetrable bosons [2]; the TG regime can be obtained at very low temperatures, with strong effective interactions, and low linear particle densities [10, 11, 12]. An interesting aspect of 1D Bose gases, which can be probed experimentally from weakly to the strongly interacting regime, is their behavior out of equilibrium (e.g., see Ref. [7]). An exact (analytical or numerical) theoretical calculation of nonequilibrium dynamics of a Lieb-Liniger gas is a complex many-body problem, which was previously studied in a few cases [32, 33, 34]. In the present thesis we contribute to the study of nonequilibrium dynamics of a Lieb-Liniger system. We have explored the free expansion, dynamics in the hard-wall and linear potential by an exact method. Specifically, we have shown that the wave function for N Lieb-Liniger bosons in these situations can be obtained by calculating an N-dimensional Fourier transform.

In Chapter 2 we have reviewed the Fermi-Bose mapping techniques used for solving Lieb-Liniger and Tonks-Girardeau model. In the TG regime, exact solutions in any external potential [2] and for time-dependent problems [2]

were constructed by mapping a wave function describing "impenetrable-core" bosons onto the wave function describing spinless fermions. For the finite strength of the delta interaction, i.e. the Lieb-Liniger system, the Fermi-Bose transformation was introduced [32, 34] to explore nonequilibrium dynamics in absence of external potentials. In this method, a wave function describing spinless fermions is transformed into a wave function of the Lieb-Liniger model.

In Chapter 3, the asymptotic form of the wave functions describing a freely expanding Lieb-Liniger gas was derived by using the Fermi-Bose transformation for time-dependent states, and the stationary phase approximation. We find that asymptotically the wave functions approach the Tonks-Girardeau (TG) structure as they vanish when any two of the particle coordinates coincide. We point out that the properties of these asymptotic states can significantly differ from the properties of a TG gas in a ground state of an external potential. The dependence of the asymptotic wave function on the initial state is discussed. The analysis encompasses a large class of initial conditions, including the ground states of a Lieb-Liniger gas in physically realistic external potentials. It is also demonstrated that the interaction energy asymptotically decays as a universal power law with time, $E_{\text{int}} \propto t^{-3}$. Moreover, we have derived analytically (by using the stationary phase approximation) the formula which connects the asymptotic shape of the momentum distribution and the initial state. For sufficiently large times the momentum distribution coincides (up to a simple scaling transformation) with the shape of the real-space single-particle density (the expansion is asymptotically ballistic).

We have also numerically studied of free expansion of a few Lieb-Liniger bosons, which are initially in the ground state of an infinitely deep hard-wall trap. Numerical calculation is carried out by employing a standard Fourier transform, as follows from the Fermi-Bose transformation for a time-dependent Lieb-Liniger gas. We have studied the evolution of the momentum distribution, the real-space single-particle density, and the occupancies of natural orbitals. Our numerical calculation allows us to explore the behavior of these observables in the transient regime of the expansion, where they are non-trivially affected by the particle interactions. Our analytical and numerical results are in good agreement.

Nonequilibrium dynamics of a Lieb-Liniger system in the presence of the hard-wall potential has been studied in Chapter 4. We have demonstrated

that a time-dependent wave function, which describes quantum dynamics of a Lieb-Liniger wave packet comprised of N particles, can be found by solving an N-dimensional Fourier transform; this follows from the symmetry properties of the many-body eigenstates in the presence of the hard-wall potential. The presented formalism is employed to numerically calculate reflection of a few-body wave packet from the hard wall for various interaction strengths and incident momenta.

We have used Gaudin's Fermi-Bose mapping operator to calculate exact solutions for the Lieb-Liniger model in a linear (constant-force) potential in Chapter 5 (the constructed exact stationary solutions are referred to as the Lieb-Liniger-Airy wave functions). The ground-state properties of the gas in the wedgelike trapping potential were calculated in the strongly interacting regime by using Girardeau's Fermi-Bose mapping and the pseudopotential approach in the $1/c$ approximation (c denotes the strength of the interaction). We point out that quantum dynamics of Lieb-Liniger wave packets in the linear potential can be calculated by employing an N-dimensional Fourier transform as in the case of free expansion.

Finally, in Chapter 6, we have theoretically demonstrated features of Anderson localization in the Tonks-Girardeau gas confined in one-dimensional (1D) potentials with controlled disorder. That is, we have investigated the evolution of the single particle density and correlations of a Tonks-Girardeau wave packet in such disordered potentials. The wave packet is initially trapped, the trap is suddenly turned off, and after some time the system evolves into a localized steady state due to Anderson localization. The density tails of the steady state decay exponentially, while the coherence in these tails increases. The latter phenomenon corresponds to the same effect found in incoherent optical solitons.

Appendix A

Fermi-Bose transformation

In this appendix we outline the proof that the wave function (2.15) obeys both the cusp condition imposed by the interactions and Eq. (2.13), i.e., that it obeys Eq. (2.11) with $V(x) = 0$. Without loss of generality we restrict our discussion to the fundamental permutation sector R_1. Let us write the differential operator as $\hat{O}_c = \prod_{1 \leq i < j \leq N} \hat{B}_{ij}$, where

$$\hat{B}_{ij} = \left[1 + \frac{1}{c} \left(\frac{\partial}{\partial x_j} - \frac{\partial}{\partial x_i} \right) \right]. \tag{A.1}$$

We first show that the wave function (2.15) obeys the cusp condition (2.12) (see Ref. [44]). Consider an auxiliary wave function

$$
\begin{aligned}
\psi_{\text{AUX}}(x_1, \ldots, x_N, t) &= \hat{B}_{j+1,j} \hat{O}_c \psi_F \\
&= \hat{B}_{j+1,j} \hat{B}_{j,j+1} \hat{O}'_{j,j+1} \psi_F,
\end{aligned}
\tag{A.2}
$$

where the primed operator $\hat{O}'_{j,j+1} = \hat{O}_c / \hat{B}_{j,j+1}$ omits the factor $\hat{B}_{j,j+1}$ as compared to $\hat{O}_c$. The auxiliary function can be written as

$$\psi_{\text{AUX}} = \left[1 - \frac{1}{c^2} \left(\frac{\partial}{\partial x_{j+1}} - \frac{\partial}{\partial x_j} \right)^2 \right] \hat{O}'_{j,j+1} \psi_F. \tag{A.3}$$

It is straightforward to verify that the operator $\hat{B}_{j+1,j} \hat{B}_{j,j+1} \hat{O}'_{j,j+1}$ in front of ψ_F is invariant under the exchange of x_j and x_{j+1}. On the other hand, the fermionic wave function ψ_F is fully antisymmetric with respect to the interchange of x_j and x_{j+1}. Thus, $\psi_{\text{AUX}}(x_1, \ldots, x_j, x_{j+1}, \ldots, x_N, t)$ is antisymmetric

with respect to the interchange of x_j and x_{j+1}, which leads to

$$\psi_{\mathrm{AUX}}(x_1, \ldots, x_j, x_{j+1}, \ldots, x_N, t)|_{x_{j+1}=x_j} = 0. \qquad (\mathrm{A}.4)$$

This is fully equivalent to the cusp condition (2.12), $\hat{B}_{j+1,j}\psi_{B,c}|_{x_{j+1}=x_j} = 0$. Thus, the wave function (2.15) obeys constraint (2.12) by construction.

Second, from the commutators $[\partial^2/\partial x_i^2, \hat{O}_c] = 0$ and $[i\partial/\partial t, \hat{O}_c] = 0$ follows that if ψ_F obeys Eq. (2.14), then $\psi_{B,c}$ obeys Eq. (2.13), which completes the proof.

If we use the expression

$$\hat{B}_{ij} = \left[\mathrm{sgn}(x_j - x_i) + \frac{1}{c}\left(\frac{\partial}{\partial x_j} - \frac{\partial}{\partial x_i} \right) \right], \qquad (\mathrm{A}.5)$$

we obtain $\hat{O}_c = \prod_{1 \le i < j \le N} \hat{B}_{ij}$ as in Eq. (2.16), which is valid inside any sector of the configuration space (see [32]). Note that for $c \to \infty$, one recovers Girardeau's Fermi-Bose mapping [2], where the operator $\hat{O}_{c=\infty} = \prod_{1 \le i < j \le N} \mathrm{sgn}(x_j - x_i)$ maps a noninteracting fermionic to a bosonic Tonks-Girardeau wave function.

Appendix B

The function $G(k_1, \ldots, k_N)$ for the box ground state

In Sec. 3.7 we have studied free expansion of three LL bosons, which are initially (at $t = 0$) in the ground state in an infinitely deep box of length $L = \pi$. Here we present exact analytical expression for function $G(\{k\}) \equiv G(k_1, \ldots, k_N)$ for this particular case. First, we use the connection between $\tilde{\psi}_F(k_1, \ldots, k_N)$ and the projection coefficients $b(k_1, \ldots, k_N)$ of the initial bosonic wave functions onto the LL eigenstates in free space (see Chapter 3) to rewrite the expression for G:

$$G(\{k\}) = N! \mathcal{N}(\{k\}) b(\{k\}) \prod_{1 \le i < j \le N} [\operatorname{sgn}(x_j - x_i) + \frac{i}{c}(k_j - k_i)]. \qquad \text{(B.1)}$$

Here, $\mathcal{N}(\{k\})$ is the normalization constant for LL eigenstates in free space [44],

$$\frac{1}{\mathcal{N}(\{k\})} = \sqrt{(2\pi)^N N! \prod_{i < j} \left[1 + \left(\frac{k_j - k_i}{c} \right)^2 \right]}, \qquad \text{(B.2)}$$

and coefficients $b(\{k\})$ are found by using the solution for the LL box ground state [36],

$$b(\{k\}) \propto \mathcal{N}(\{k\}) \sum_{P'} (-1)^{P'} \prod_{1 \le i < j \le N} \left[1 - \frac{i}{c} (k_{P'j} - k_{P'i}) \right]$$

$$\times \sum_{\{\epsilon\}} \sum_{P} \epsilon_1 \cdots \epsilon_N \prod_{1 \le i < j \le N} (1 - \frac{ic}{q_i + q_j})(1 + \frac{ic}{q_{Pi} - q_{Pj}})$$

$$\times \int_{-L/2}^{L/2} dx_1 \int_{x_1}^{L/2} dx_2 \cdots \int_{x_{N-1}}^{L/2} dx_N$$

$$\times \exp\left\{ i \sum_{j=1}^{N} \left[(q_{Pj} - k_{P'j}) x_j - q_{Pj} \frac{L}{2} \right] \right\}. \tag{B.3}$$

In the expression above, summations are taken over all permutations P and P' which are of order N, whereas the set $\{\epsilon\}$ is defined such that each ϵ_i is either $+1$ or -1 (here $i = 1, \ldots, N$, i.e., there are 2^N combinations in the set $\{\epsilon\}$). The ground state quasimomenta are defined as $q_i = \epsilon_i |q_i|$, for $i = 1, \ldots, N$, and their magnitudes $|q_i|$ are found by solving (numerically) the system of coupled transcendental equations [36]

$$|q_i| L = \pi + \sum_{j \ne i} \left(\tan^{-1} \frac{c}{|q_i| - |q_j|} + \tan^{-1} \frac{c}{|q_i| + |q_j|} \right). \tag{B.4}$$

Finally, let us mention that the constant of proportionality in Eq. (B.3) is fixed such that the wave function $\psi_{B,c}$ is properly normalized.

Appendix C

The ground state of a Lieb-Liniger gas in an infinitely deep box

In Sec. 4.3 we study Lieb-Liniger dynamics in the presence of the hard wall potential, with an example of three Lieb-Liniger bosons which are at $t < 0$ confined in the ground state of an infinitely deep box of length $L = \pi$. The ground state in fundamental permutation sector R_1 has been constructed by Gaudin in Ref. [36] via a superposition of 2^N free space eigenstates. For the box in the interval $[1.5\pi, 2.5\pi]$, the ground state (up to a normalization constant) reads

$$
\psi_{g.s.}(x_1, \ldots, x_N) \propto
$$
$$
\sum_{\{\epsilon\}} \epsilon_1 \cdots \epsilon_N \prod_{i<j} \left(1 - \frac{ic}{q_i + q_j}\right) \sum_P \prod_{i<j} \left(1 + \frac{ic}{q_{Pi} - q_{Pj}}\right) e^{i \sum_j q_{Pj}(x_j - 1.5\pi)}.
$$
$$
\text{(C.1)}
$$

Here, summations are taken over 2^N elements of set $\{\epsilon\}$, and $N!$ permutations P. The quasimomenta $q_j = \epsilon_j |q_j|$, for $j = 1, \ldots, N$, are determined by set of transcendental equations

$$
|q_i| L = \pi + \sum_{j \neq i} \left(\tan^{-1} \frac{c}{|q_i| - |q_j|} + \tan^{-1} \frac{c}{|q_i| + |q_j|} \right). \qquad \text{(C.2)}
$$

Eqs. (C.2) are solved numerically. For the initial state corresponding to three particles ($N = 3$), where $\psi(x_1, x_2, x_3, t = 0) = \psi_{g.s.}(x_1, x_2, x_3) \exp[-iK(x_1 + x_2 + x_3)]$, it is straightforward to obtain the projection coefficients $b(\{k\})$ by employing Eq. (4.7) and the orthonormality of eigenstates $\phi_{\{k\}}$.

Bibliography

[1] E. Lieb and W. Liniger, Phys. Rev. **130**, 1605 (1963);
    E. Lieb, Phys. Rev. **130**, 1616 (1963).

[2] M. Girardeau, J. Math. Phys. **1**, 516 (1960).

[3] F. Schreck, L. Khaykovich, K.L. Corwin, G. Ferrari, T. Bourdel, J. Cubi-
    zolles, and C. Salomon, Phys. Rev. Lett. **87**, 080403 (2001); A. Görlitz,
    J.M. Vogels, A.E. Leanhardt, C. Raman, T.L. Gustavson, J.R. Abo-
    Shaeer, A.P. Chikkatur, S. Gupta, S. Inouye, T. Rosenband, and W.
    Ketterle, *ibid.* **87**, 130402 (2001); H. Moritz, T. Stöferle, M. Kohl, and T.
    Esslinger, *ibid.* **91**, 250402 (2003); B. Laburthe-Tolra, K.M. O'Hara, J.H.
    Huckans, W.D. Phillips, S.L. Rolston, and J.V. Porto, *ibid.* **92**, 190401
    (2004); T. Stöferle, H. Moritz, C. Schori, M. Kohl, and T. Esslinger, *ibid.*
    92, 130403 (2004).

[4] M. Greiner, I. Bloch, O. Mandel, T.W. Hänsch, and T. Esslinger, Phys.
    Rev. Lett. **87**, 160405 (2001).

[5] T. Kinoshita, T. Wenger, and D.S. Weiss, Science **305**, 1125 (2004).

[6] B. Paredes, A. Widera, V. Murg, O. Mandel, S. Fölling, I. Cirac, G. V.
    Shlyapnikov, T. W. Hänsch, and I. Bloch, Nature (London) **429**, 277
    (2004).

[7] T. Kinoshita, T. Wenger, and D.S. Weiss, Nature (London) **440**, 900
    (2006).

[8] S. Hofferberth, I. Lesanovsky, B. Fischer, T. Schumm and J. Schmied-
    mayer, Nature **449**, 324 (2007).

[9] A. H. van Amerongen, J. J. P. van Es, P. Wicke, K. V. Kheruntsyan, and N. J. van Druten, Phys. Rev. Lett. **100**, 090402 (2008).

[10] M. Olshanii, Phys. Rev. Lett. **81**, 938 (1998).

[11] D.S. Petrov, G.V. Shlyapnikov, and J.T.M. Walraven, Phys. Rev. Lett. **85** 3745 (2000).

[12] V. Dunjko, V. Lorent, and M. Olshanii, Phys. Rev. Lett. **86** 5413 (2001).

[13] C. Pethick and H. Smith, *Bose-Einstein Condensation in Dilute Gases* (University Press, Cambridge, 2004).

[14] M.H. Anderson, J.R. Enscher, M.R. Matthews, C.E. Wieman, and E.A. Cornell, Science **269**, 198 (1995).

[15] C.C. Bradley, C.A. Sackett, J.J. Tollet, and R.G. Hulet, Phys. Rev. Lett. **75** 1687 (1995).

[16] K.B. Davis, M.-O. Mewes, M.R. Andrews, N.J. van Druten, D.S. Durfee, D.M. Kurn, and W. Ketterle, Phys. Rev. Lett. **75** 3969 (1995).

[17] M. Greiner, O. Mandel, T. Esslinger, T.W. Hänsch, and I. Bloch, Nature **415**, 39 (2002).

[18] M. Greiner, O. Mandel, T.W. Hänsch, and I. Bloch, Nature **419**, 51 (2002).

[19] I. Bloch, Nature Phys. **1**, 23 (2005).

[20] I. Bloch, J. Dalibard, and W. Zwerger, Rev. Mod. Phys. **80**, 885 (2008).

[21] R. Folman, P. Krüger, J. Schmiedmayer, J. Denschlag, and C. Henkel, Adv. At. Mol. Opt. Phys. **48**, 263 (2002).

[22] J. Fortagh, S. Kraft, A. Günther, P. Trück, P. Wicke, and C. Zimmermann, Opt. Commun. **243**, 45 (2004).

[23] H. Feshbach, Ann. Phys. (N.Y.) **5**, 357 (1958).

[24] M. Rigol, V. Dunjko, and M. Olshanii, Nature **452**, 854 (2008).

[25] F. Iglói and H. Rieger, Phys. Rev. Lett. **85**, 3233 (2000).

[26] K. Sengupta, S. Powell, and S. Sachdev, Phys. Rev. A **69**, 053616 (2004).

[27] M. Rigol, V. Dunjko, V, Yurovsky, and M. Olshanii, Phys. Rev. Lett. **98**, 050405 (2007).

[28] M. Cazalilla, Phys. Rev. Lett. **97**, 156403 (2006).

[29] P. Calabrese and J. Cardy, Phys. Rev. Lett. **96**, 136801 (2006).

[30] R.W. Cherng and L.S. Levitov, Phys. Rev. A **73**, 043614 (2006).

[31] C. Kollath, A.M. Läuchli, and E. Altman, Phys. Rev. Lett. **98**, 180601 (2007).

[32] M. Gaudin, *La fonction d'Onde de Bethe* (Paris, Masson, 1983).

[33] M.D. Girardeau, Phys. Rev. Lett. **91**, 040401 (2003).

[34] H. Buljan, R. Pezer, and T. Gasenzer, Phys. Rev. Lett. **100**, 080406 (2008); see also *ibid.* Phys. Rev. Lett. **102**, 049903(E) (2009).

[35] V. Gritsev, T. Rostunov, and E. Demler J. Stat. Mech. P05012 (2010).

[36] M. Gaudin, Phys. Rev. A **4**, 386 (1971).

[37] T. Busch, B.-G. Englert, K. Rzazewski, and M. Wilkens, Found. of Phys. **28**, 4 (1998).

[38] J.G. Muga and R.F. Snider, Phys. Rev. A **57**, 3317 (1998).

[39] K. Sakmann, A.I. Streltsov, O.E. Alon, and L.S. Cederbaum, Phys. Rev. A **72**, 033613 (2005).

[40] M.T. Batchelor, X.-W. Guan, N. Oelkers, and C. Lee, J. Phys. A **38**, 7787 (2005).

[41] Y. Hao, Y. Zhang, J.Q. Liang, and S. Chen, Phys. Rev. A **73**, 063617 (2006).

[42] A.G. Sykes, P.D. Drummond, and M.J. Davis, Phys. Rev. A **76**, 063620 (2007).

[43] R. Kanamoto, L.D. Carr, and M. Ueda, Phys. Rev. A **81**, 023625 (2010).

[44] V.E. Korepin, N.M. Bogoliubov, and A.G. Izergin, *Quantum Inverse Scattering Method and Correlation Functions* (Cambridge, Cambridge University Press, 1993).

[45] M. Gaudin, J. Math. Phys. **12**, 1677 (1971); *ibid.* **12**, 1674 (1971).

[46] M.D. Girardeau and E.M. Wright, Phys. Rev. Lett. **84**, 5691 (2000).

[47] M. Rigol and A. Muramatsu, Phys. Rev. Lett. **94**, 240403 (2005); *ibid.* Mod. Phys. Lett. B **19**, 861 (2005).

[48] R. Pezer and H. Buljan, Phys. Rev. Lett. **98**, 240403 (2007).

[49] A. Minguzzi and D.M. Gangardt, Phys. Rev. Lett. **94**, 240404 (2005).

[50] A. del Campo and J.G. Muga, Europhys. Lett. **74**, 965 (2006).

[51] D.M. Gangardt and M. Pustilnik, Phys. Rev. A **77**, 041604(R) (2008).

[52] P. Öhberg and L. Santos, Phys. Rev. Lett. **89**, 240402 (2002); P. Pedri, L. Santos, P. Ohberg, and S. Stringari, Phys. Rev. A **68**, 043601 (2003).

[53] G. Vidal, Phys. Rev. Lett., **93**, 040502 (2004).

[54] D. Muth, B. Schmidt, and M. Fleischhauer, New J. Phys. **12**, 083065 (2010).

[55] A.M. Rey, B.L. Hu, E. Calzetta, A. Roura, and C.W. Clark, Phys. Rev. A **69**, 033610 (2004).

[56] T. Gasenzer, J. Berges, M.G. Schmidt, and M. Seco, Phys. Rev. A **72**, 063604 (2005); J. Berges and T. Gasenzer, Phys. Rev. A **76**, 033604 (2007).

[57] O.E. Alon, A.I. Streltsov, and L.S. Cederbaum, Phys. Rev. A **77**, 033613 (2008).

[58] S. Zöllner, H.-D. Meyer, and P. Schmelcher, Phys. Rev. A, **78**, 013621 (2008).

[59] J.-S. Caux, P. Calabrese, and N. A. Slavnov, J. Stat. Mech. P01008 (2007).

[60] M.A. Cazalilla, R. Citro, T. Giamarchi, E. Orignac, and M. Rigol, Rev. Mod. Phys. **83**, 1405 (2011).

[61] A. del Campo, G. Garcia-Calderon, and J.G. Muga, Physics Reports **476**, 1 (2009).

[62] P.W. Anderson, Phys. Rev. **109**, 1492 (1958).

[63] J. Billy, V. Josse, Z. Zuo, A. Bernard, B. Hambrecht, P. Lugan, D. Clement, L. Sanchez-Palencia, P. Bouyer, A. Aspect, Nature **453**, 891 (2008).

[64] G. Roati, C. D'Errico, L. Fallani, M. Fattori, C. Fort, M. Zaccanti, G. Modugno, M. Modugno, M. Inguscio, Nature **453**, 895 (2008).

[65] K.K. Das, M.D. Girardeau, and E.M. Wright, Phys. Rev. Lett. **89**, 170404 (2002).

[66] T. Cheon and T. Shigehara, Phys. Rev. Lett. **82**, 2536 (1999).

[67] V.I. Yukalov and M.D. Girardeau, Laser Phys. Lett **2**, 375 (2005).

[68] M. Rigol and A. Muramatsu, Phys. Rev. A **70**, 031603(R) (2004); *ibid.* **72**, 013604 (2005).

[69] M.A. Cazalilla, Phys. Rev. A **70**, 041694(R) (2004).

[70] R. Pezer, T. Gasenzer, and H. Buljan, Phys. Rev. A **80**, 053616 (2009).

[71] P.J. Forrester, N.E. Frankel, and M.I. Makin, Phys. Rev. A **74**, 043614 (2006).

[72] T.C. Dorlas, Commun. Math. Phys. **154** 347 (1993).

[73] L. Khaykovich, F. Schreck, G. Ferrari, T. Bourdel, J. Cubizolles, L. D. Carr, Y. Castin, C. Salomon, Science **296** 1290 (2002).

[74] H. Buljan, M. Segev, and A. Vardi, Phys. Rev. Lett. **95** 180401 (2005).

[75] A.I. Streltsov, O.E. Alon, and L.S. Cederbaum, Phys. Rev. Lett. **100** 130401 (2008).

[76] M.D. Girardeau, E.M. Wright, and J.M. Triscari, Phys. Rev. A **63**, 033601 (2001).

[77] E.B. Kolomeisky, T.J. Newman, J.P. Straley, and X. Qi, Phys. Rev. Lett. **85**, 1146 (2000).

[78] E. Toth, A.M. Rey, R.P. Blakie, Phys. Rev. A **78**, 013627 (2008).

[79] B. Sutherland, Phys. Rev. Lett. **80**, 3678 (1998).

[80] F. Heidrich-Meisner, M. Rigol, A. Muramatsu, A. E. Feiguin, and E. Dagotto, Phys. Rev. A **78**, 013620 (2008).

[81] B-Y. Fang, P. Vignolo, C. Miniatura, and A. Minguzzi, Phys. Rev. A **79**, 023623 (2008).

[82] An alternate definition could be to define the asymptotic velocity as the half width at half maximum of the distribution $N^{-1}\rho_\infty(\xi)$.

[83] Y-J. Wang, D.Z. Anderson, V.M. Bright, E.A. Cornell, Q.Diot, T. Kishimoto, M. Prentiss, R.A. Saravanan, S.R. Segal, and S. Wu, Phys. Rev. Lett. **94**, 090405 (2005).

[84] K. Bongs, S. Burger, G. Birkl, K. Sengstock, W. Ertmer, K. Rzazewski, A. Sanpera, and M. Lewenstein, Phys. Rev. Lett. **83**, 3577 (1999).

[85] A. Steyerl, H. Nagel, F. X. Schreiber, K. A. Steinhauser, R. Gähler, W. Gläser, P. Ageron, J. M. Astruc, W. Drexel, G. Gervais, W. Mampe, Phys. Lett. A **116**, 347 (1986).

[86] A. Libson, M. Riedel, G. Bronshtein, E. Narevicius, U. Even, and M. G. Raizen, New. J. Phys. **8**, 77 (2006).

[87] E. Narevicius, A. Libson, M. F. Riedel, C. G. Parthey, I. Chavez, U. Even and M. G. Raizen, Phys. Rev. Lett. **98**, 103201 (2007).

[88] G. Reinaudi, Z. Wang, A. Couvert, T. Lahaye, and D. Guéry-Odelin, Eur. Phys. J. D. **40**, 405 (2006).

[89] D. Sen, Int. J. Mod. Phys. A **14** 1789 (1999); D Sen, J. Phys. A: Math. Gen. **36** 7517 (2003).

[90] S. Sen and A.R. Chowdhurry, J. Phys. Soc. Jpn. **57**, 1511 (1988).

[91] A. del Campo and J.G.Muga, J. Phys. A: Math. Gen. **39**, 5897 (2006).

[92] O. Vallée and M. Soares, *Airy Functions and Applications to Physics* (Imperial College Press, London, 2004).

[93] D.S. Wiersma, P. Bartolini, A. Lagendijk, R. Righini, Nature **390**, 671 (1997).

[94] A.A. Chabanov, M. Stoytchev, A.Z. Genack, Nature **404**, 850 (2000).

[95] M. Störzer, P. Gross, C.M. Aegerter, G. Maret, Phys. Rev. Lett. **96**, 063904 (2006).

[96] T. Schwartz, G. Bartal, S. Fishman, and M. Segev, Nature **446**, 52 (2007).

[97] Y. Lahini, A. Avidan, F. Pozzi, M. Sorel, R. Morandotti, D.N. Christodoulides, and Y. Silberberg, Phys. Rev. Lett. **100**, 013906 (2008).

[98] L. Sanchez-Palencia and M. Lewenstein, Nature Phys. **6**, 87 (2010).

[99] A. Lenard, J. Math. Phys. **5**, 930 (1964).

[100] P.J. Forrester, N.E. Frankel, T.M. Garoni, and N.S. Witte, Phys. Rev. A **67**, 043607 (2003); T. Papenbrock, Phys. Rev. A **67**, 041601 (2003).

[101] B. Damski, J. Zakrzewski, L. Santos, P. Zoller, and M. Lewenstein, Phys. Rev. Lett. **91**, 080403 (2003).

[102] R. Roth and K. Burnett, Phys. Rev. A **68**, 023604 (2003).

[103] L. Sanchez-Palencia, D. Clement, P. Lugan, P. Bouyer, G.V. Shlyapnikov, and A. Aspect, Phys. Rev. Lett. **98**, 210401 (2007).

[104] T. Giamarchi and H.J. Schulz, Phys. Rev. B **37**, 325 (1988).

[105] M.P.A. Fisher, P.B. Weichman, G. Grinstein, and D.S. Fisher, Phys. Rev. B **40**, 546 (1989).

[106] H. Gimperlein, S. Wessel, J. Schmiedmayer, and L. Santos, Phys. Rev. Lett. **95**, 170401 (2005).

[107] A. De Martino, M. Thorwart, R. Egger, and R. Graham, Phys. Rev. Lett. **94**, 060402 (2005).

[108] V.W. Scarola and S. Das Sarma, Phys. Rev. A **73**, 041609(R) (2006).

[109] A.M. Rey, I.I. Satija, and C.W. Clark, Phys. Rev. A **73**, 063610 (2006).

[110] B. Horstmann, J.I. Cirac, and T. Roscilde, Phys. Rev. A **76**, 043625 (2007).

[111] G. Roux, T. Barthel, I.P. McCulloch, C. Kollath, U. Schollwöck, and T. Giamarchi, Phys. Rev. A **78**, 023628 (2008).

[112] X. Deng, R. Citro, A. Minguzzi, and E. Orignac, Phys. Rev. A, **78**, 013625 (2008).

[113] T. Roscilde, Phys. Rev. A **77**, 063605 (2008).

[114] G. Orso, A. Iucci, M.A. Cazalilla, and T. Giamarchi, Phys. Rev. A **80**, 033625 (2009).

[115] M. Mitchell, M. Segev, T.H. Coskun, and D.N. Christodoulides, Phys. Rev. Lett. **79**, 4990 (1997); M.I. Carvalho, T.H. Coskun, D.N. Christodoulides, M. Mitchell, and M. Segev, Phys. Rev. E **59**, 1193 (1999); H. Buljan, T. Schwartz, M. Segev, M. Soljačić, and D.N. Christodoulides, J. Opt. Soc. Am. B **21**, 397 (2004).

[116] P. Lugan, A. Aspect, and L. Sanchez-Palencia, D. Delande, B. Gremaud, C.A. Müller, C. Miniatura, Phys. Rev. A **80**, 023605 (2009).

[117] We utilize notation from Ref. [116] to denote the orders of the perturbation, however, the coefficients $\gamma^{(n)}$ here describe the decay of density, rather than the wave function as in [116], and they differ by a factor of 2.

[118] M. Naraschewski and R.J. Glauber, Phys. Rev. A **59**, 4595 (1999).

[119] L. Mandel and E. Wolf, *Optical Coherence and Quantum Optics* (Cambridge Press, New York, 1995).

List of Figures

108

110

111